General Disclaimer

One or more of the Following Statements may affect this Document

- This document has been reproduced from the best copy furnished by the organizational source. It is being released in the interest of making available as much information as possible.

- This document may contain data, which exceeds the sheet parameters. It was furnished in this condition by the organizational source and is the best copy available.

- This document may contain tone-on-tone or color graphs, charts and/or pictures, which have been reproduced in black and white.

- This document is paginated as submitted by the original source.

- Portions of this document are not fully legible due to the historical nature of some of the material. However, it is the best reproduction available from the original submission.

AEROJET GENERAL TIRE GENERAL

REPORT NO. RN-S-0211

AEC-NASA SPACE NUCLEAR PROPULSION OFFICE

NES/ETS-1 DUCT STRUCTURAL DYNAMICS

ROCKET ENGINE OPERATIONS – NUCLEAR

NERVA PROGRAM AUGUST 1965 CONTRACT SNP-1

AEROJET-GENERAL CORPORATION

A SUBSIDIARY OF THE GENERAL TIRE & RUBBER COMPANY

ABSTRACT

This report presents the final structural dynamics analysis of the Nuclear Exhaust System (NES) duct for the Engine Test Stand No. 1 (ETS-1) at NRDS. The duct assembly is designated SST-2, subsonic turn configuration. This report is submitted in fulfillment of Milestone No. 4 in Subtask 3.1 of the CY 1965 SNP-1 contract.

Using digital computer techniques, structural vibration modes and natural frequencies of the exhaust duct assembly were obtained. Dynamic stresses along the duct section under full scale nuclear (NERVA) engine operation were calculated. As a result of this analysis the structural dynamic integrity as well as the overall structural design stability has been proven to be adequate for the NES for ETS-1.

for W. D. Stinnett
Program Manager
REON

TABLE OF CONTENTS

BLANK PAGE

FIGURE LIST

TABLE LIST

NOMENCLATURE

The following notations have been generally used in this report. Symbols which occur only infrequently and are explained in immediate context have not been included in this list.

$R_{k,j}$	Redundant reaction at k for j^{th} loading condition
$m_{k,i}$	Moment at i^{th} spring of the redundant structure when unit load is applied at k^{th} redundant
$v_{k,i}$	Shear at i^{th} spring of the redundant structure when unit load is applied at k^{th} redundant
$p_{k,i}$	Axial force at i^{th} spring of the redundant structure when unit load is applied at k^{th} redundant
$M_{j,i}$	Moment at i^{th} spring of the redundant structure for j^{th} loading condition
$V_{j,i}$	Shear at i^{th} spring of the redundant structure for j^{th} loading condition
$P_{j,i}$	Axial force at i^{th} spring of the redundant structure for j^{th} loading condition
I_{max}	Number of springs
N_{max}	Number of elements
J_{max}	Number of load points (number of loads equal to two times J_{max})
E	Modulus of Elasticity
G	Shear modulus
k	Shape factor, ratio of specific heats
A	Gross section area
AP_i	Area of the i^{th} element resisting the axial force
AV_i	Area of the i^{th} element resisting the shear force
L_i, ℓ_i	Length of i^{th} element
R	Radius
R1	Radius of curvature of first curved portion
R2	Radius of curvature of second curved portion
I	Moment of inertia, impulse function
r1	Spring number at beginning of first curved portion
r2	Spring number at end of first curved portion
r3	Spring number at beginning of second curved portion

$r4$	Spring number at end of second curved portion
S_k, S_ℓ	Reaction at F of the redundant structure caused by a unit load at redundant k or ℓ
SRF_j	Reaction at F of the redundant structure for j^{th} loading
K_f	Spring constant at reaction F
$FP_{j,i}$	Axial force at i^{th} spring for j^{th} loading condition
$FM_{j,i}$	Bending moment at i^{th} spring for j^{th} loading condition
$FV_{j,i}$	Shear at i^{th} spring for j^{th} loading condition
GF, F	Flexibility matrix
$\overline{V}$	Volume
u	Transverse displacement, velocity of fluid flow
v	Longitudinal displacement
t	Time
M	Bending moment, mass, Mach number
s	Space coordinate
y	Centroidal distance
P	Force per unit volume
w	Distributed force
$F_j(t)$,$F_{2j}(t)$	Forcing function acting at j^{th} or $2j^{th}$ element at time t
C_k	Coefficient of sliding friction for k^{th} reaction (R_A, R_B, and R_E only)
Ma_j	Mass of j^{th} element
DL	Dead load
R_k	Force at k^{th} reaction under dynamic loading
$1_{k,j}$	Force at reaction k caused by j^{th} unit load
$r'_{k,n}$	Force at k^{th} reaction for unit acceleration of n^{th} mode
$p'_{n,i}$	Axial force at i^{th} spring for unit acceleration of n^{th} mode
$v'_{n,i}$	Shear at i^{th} spring for unit acceleration of n^{th} mode
$m'_{n,i}$	Bending moment at i^{th} spring for unit acceleration of n^{th} mode
P_i	Axial force at i^{th} spring under dynamic loading
M_i	Bending moment at i^{th} spring under dynamic loading
V_i, Q_i	Shear at i^{th} spring under dynamic loading
$F_m(t_m)$	Force in the model duct at model time t
$F_p(t_p)$	Force in the prototype duct at prototype time t

p	Pressure
$\overline{p}$	Average pressure
p_c	Motor chamber pressure
a_d, b_d	Constant
$\dot{m}_{12}$	Mass flow rate between stations 1 and 2
$\dot{m}_{st}$	Mass flow rate of steam
ℓ_{12}	Length between stations 1 and 2
Aw_{12}	Wetted area between stations 1 and 2
A_1	Cross section area at station 1
A_2	Cross section area at station 2
c_{f_i}	Coefficient of friction for station i
u_{st}	Velocity of steam flow
c_{p_i}	Specific heat at constant pressure for station i
T_i	Temperature at station i
T_{t_i}	Total (stagnation) temperature at station i
$\dot{Q}_{12}$	Heat input (removal) rate between stations 1 and 2
$\overline{p}_i$	Average pressure at station i
F_{LCF}	Longitudinal forcing function due to centrifugal force effects
F_{RCF}	Outward radial forcing function due to centrifugal force effects
$J_{i,j}$	Polar moment of inertia between the i^{th} and j^{th} elements
$\overline{U}$	Potential energy
$\overline{K}$	Kinetic energy
$\overline{W}$	External word done
f	Natural frequency (cps)
RF_n, RF_j	Reaction at F for n^{th} or j^{th} loading condition

Greek Letters

$\Delta_{k,\ell}$	Displacement at k^{th} redundant caused by unit load at ℓ^{th} redundant reaction
$\delta_{k,j}$	Displacement at k^{th} redundant reaction of redundant structure for j^{th} loading condition
ω	Frequency (radian per second)
σ	Stress
ε	Strain
ϕ	Angle
ρ	Mass density
η_n	Damping of n^{th} mode
$\phi_{n,j}$	Normalized deflection of n^{th} mode at j^{th} element
δ_i	Deflection of i^{th} element under dynamic loading
θ	Slope
$\bar{\rho}$	Average mass density

I. INTRODUCTION

This report presents the comprehensive structural dynamic analysis (in support of the final structural design concepts) performed on the NES duct for the ETS-1.

The approach and conclusions of the NES duct structural dynamic analysis have been divided into three phases: Phase One of the analysis determines the natural frequencies and mode shapes for the NES duct employing digital computer techniques. Phase Two develops the environmental forcing function simulating the actual nuclear engine operation. Phase Three takes the results obtained for the modes and frequencies of the duct system, and the environmental forces, and introduces them into a lumped parameter, dynamic response, digital computer program which determines the response of the duct.

Two methods, the lumped-parameter model and the quasi-closed form model, were employed to find the natural frequencies and mode shapes for the NES duct. The results obtained from the two methods were compared and verified. Since there was no appreciable difference in the first three mode frequencies between the two approaches, no attempt was tried to obtain more than three modes for the quasi-closed form method. As a result of this analytical check, the required degree of confidence in the frequency analysis has been achieved for Phase One of the NES duct dynamics program.

One of the most critical tasks in the overall dynamic analysis is to define the aerodynamic loading environment (forcing function) under the nuclear engine operation and its interaction with the duct structure. The state of the art at present is not advanced enough to predict the dynamic gas flow behavior, much less predict an accurate force-time history over the entire duct length. Consequently, two semi-empirical approaches-utilizing both the theoretical solution and test results from several duct scale models and the Kiwi reactor data-were undertaken. This combination of theoretical and experimental solutions will yield the most accurate forcing function profile short of testing the prototype duct.

BLANK PAGE

The final results of the dynamic response program obtained from Phase Three consist of maximum dynamic support reactions, moment, shear, axial force, and deflections along the duct. From the final design data, calculations of stresses and stress concentrations were made. The dynamic stresses were then superimposed by the static stresses obtained from the structural design calculations to ensure the overall structural integrity of the NES duct.

The analyses for the torsional vibration of the duct and the in-plane vibration of the truss are given in Section III-C-3,4. The intent of these analyses was to survey any other possible mode of vibration that might amplify the deterioration of the entire exhaust system.

The flow chart shown in Figure 1 outlines the channel of approaches to achieve the overall objective of the NES duct dynamics program.

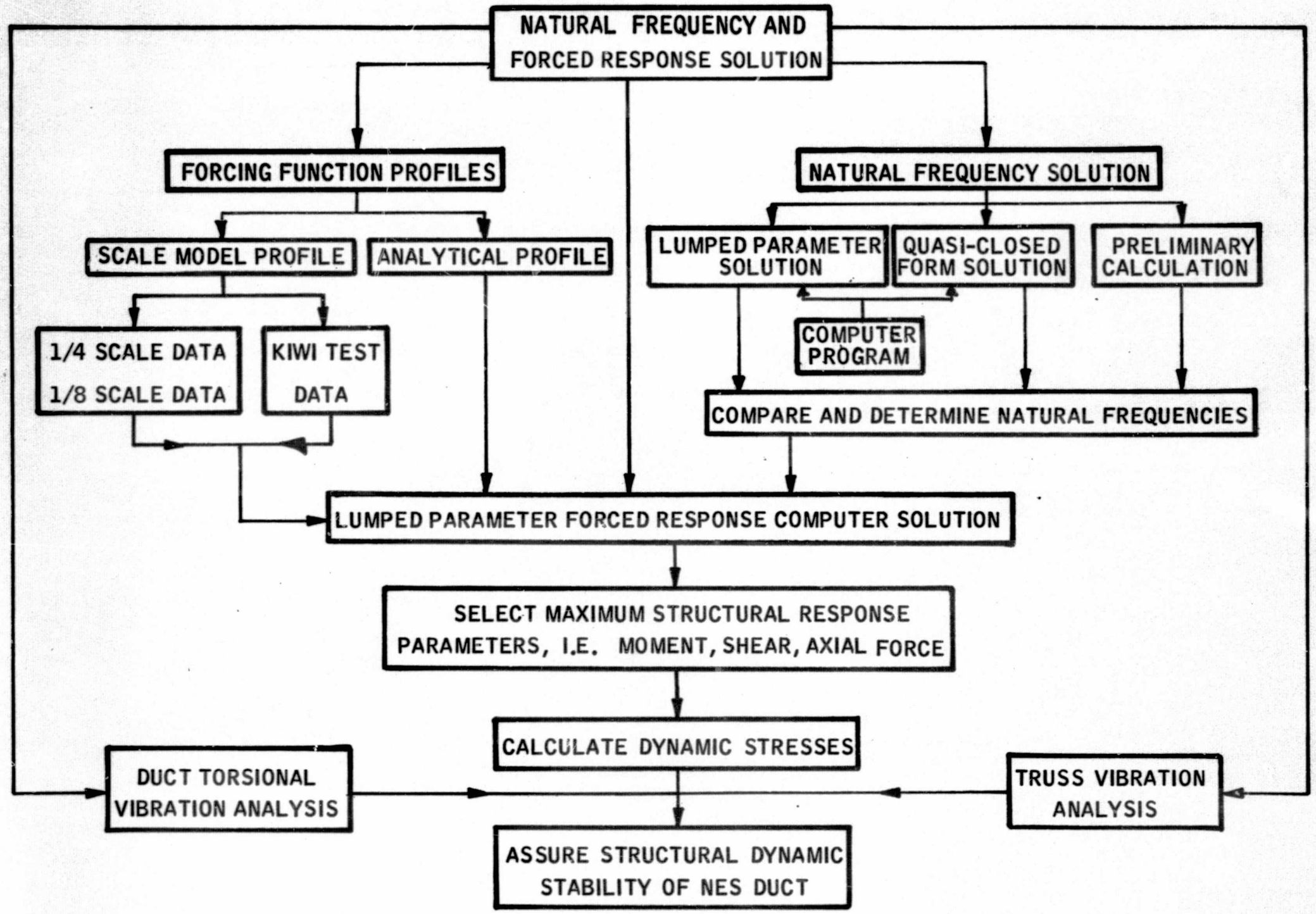

Figure 1

NES/ETS-1 Duct Structural Dynamics Program

"Page missing from available version"

II. SUMMARY

Structural dynamic analysis was performed on the NES duct. The natural frequencies of the duct for the first three modes were 30.6, 39.4, and 42.7 cps, respectively. The lowest duct torsional frequency was 64.0 cps.

For the in-plane vibration of the truss structure, decoupled from the duct, the first three modes were 6.66, 8.76, and 14.62 cps, respectively.

The critical stress sections of the duct occurred at the secondary ejector section. The maximum normal stress in this area occurs at station 996.0 with +0.05 margin of safety, and the maximum shear stress occurs at station 1076.6 with +3.30 margin of safety. For the NES duct, the dynamic stresses are extremely low in comparison with the static stresses; thus, the high magnitudes of normal stresses are attributed to the static loads. In short, no combined stress will be generated during full-scale engine operation that exceeds the given material strength allowables established in the structural design criteria.

"Page missing from available version"

III. TECHNICAL DISCUSSION

A. DESCRIPTION OF NUCLEAR EXHAUST SYSTEM DUCT

The exhaust assembly is primarily of welded construction and consists of the duct section and the truss support structure. Figure 2 shows the ETS-1 NES Exhaust Duct configuration.

1. Duct Section

The duct section is constructed of 347 stainless steel. It has a circular cross-section with an elbow section to deflect the engine exhaust flow through 90 degrees, and an additional angular deflector is provided at the exhaust outlet. The duct section assembly consists of three separate sections: the primary, or straight section, with transition cone; the subsonic 90 degree elbow section with off-set cone; and the horizontal, or secondary, ejector section with a 45 degree exit elbow section. The elbow section is welded to the secondary ejector section to form the lower duct assembly. A remotely operated clamp-type joint is provided at the severance plane located between the primary section and the lower duct assembly. The walls of the duct section are coolant channels whose configuration is as follows: The outer wall of the primary section consists of 195 formed angles welded to the inner skin plate to provide a water coolant flow path. The outer wall of the horizontal, secondary ejector, section consists of 150 formed angles also welded to the inner skin plate to provide a similar coolant flow path. The basic shell of the 90 degree elbow section of the secondary ejector consists of 230 formed tubes welded together to provide a coolant flow path.

An inlet and outlet manifold, in the form of a half torus, is welded to each duct section so as to provide a flow of water coolant through the wall passages.

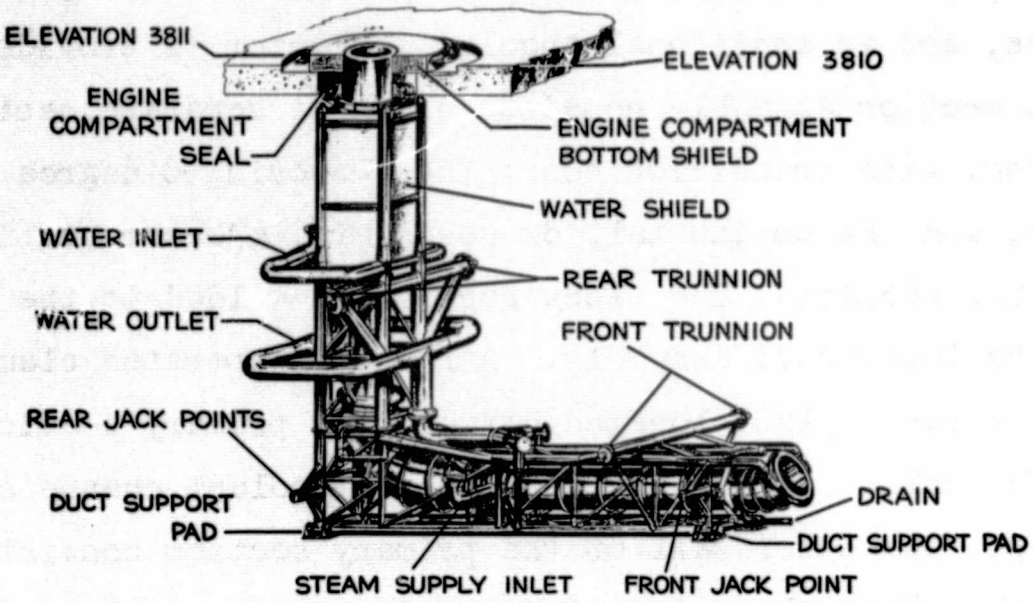

Figure 2

ETS-1 NES Exhaust Duct

2. Truss Support Structure

The truss structure is constructed of Type 304 stainless steel pipe. Longitudinal structural truss members are used to transfer the structural loads from the duct to the ETS-1 concrete vault walls. The truss also has a severance plane which is located approximately at the same place as the duct severance plane. Each of the four columns of the truss assembly uses bolted flanges, located at the severance plane, to permit separation during assembly or disassembly. One front and one rear trunnion is provided on each side of the truss to support the duct assembly within the duct vault. These trunnions are connected to the main truss members by means of butterfly trusses.

3. Secondary Steam Ejector

The secondary steam ejector is located on the downstream end of the elbow section and includes a stream plenum manifold. Also, a steam manifold (in the form of a torus) encircles the outside periphery of the duct at the downstream end of the offset cone. The steam ejector will provide a partial vacuum in the duct and engine compartment prior to engine firing and will assist in the purging operation. However, the primary purpose will be to provide for safety by preventing air backflowing into the duct and mixing with hydrogen during engine operation or malfunction.

4. Water Radiation Shield

The water-filled radiation shield is located at the upstream end of the upper duct-truss assembly to shield the walls of the ETS-1 vault which are not otherwise protected by the compartment shield. The shield is a water tank surrounding the duct and is welded to the truss members.

5. Upper Duct Seal and Bellow

The upper duct seal provides a sealed connection between the duct inlet and the bottom shield of the engine compartment.

The seal includes the following:

a. An annular nitrogen pressurized bellow to allow for relative motion between the duct and the engine compartment.

b. A Marman-type clamp for remotely connecting the seal and the duct inlet.

6. Other Structural Support Components

In addition to the truss support structure, the duct proper is supported by the following structural members:

a. Stiffeners

Ring-type stiffeners are welded around the outside of each duct section. These stiffeners add rigidity to the structure and enable the skin to resist buckling induced by external pressure.

b. Sliding Supports

Two pairs of sliding supports are located on the horizontal portion of the secondary ejector and one pair on the vertical primary section of the duct. These supports, which transmit transverse duct loads into the truss, allow thermal freedom of movement along both axes of the duct away from the fixed hinge.

c. Fixed Hinge

The fixed hinge on the 90 degree elbow section is free to rotate about its axis and is designed to transmit duct axial loads into the truss. A network of rings and gussets is attached to the hinge. The network is referred to as the saddle and is covered with a membrane to provide an internal water cavity adjacent to the tubes. This cavity will provide a backup shield in the vulnerable portion of the elbow.

B. STRUCTURAL DESIGN CRITERIA

1. General Requirements

The following requirements are outlined for use in the structural design of the ETS-1, NES duct:

a. Limit Loads

The limit loads for the duct assembly shall be defined as the most critical combination of the loads for the design condition under consideration. Each design condition shall include all factors which can influence the structural design and typically include hydrostatic pressure, gas dynamic pressure, nuclear heating, vibration, ground handling, and dead weight of the structure.

b. Factor of Safety

Material allowable shall be divided by the appropriate factor of safety to obtain the design yield or ultimate stress. The factors shall be as follows:

Yield safety factor	2
Ultimate safety factor	4

The governing safety factor shall be dependent on whether the structural strength is more critical in yield or ultimate.

c. Proof Pressure

The cooling system of the completed duct assembly, including headers, manifolds, and coolant passages, shall be capable of withstanding a hydrostatic pressure of 360 psig $\pm$ 15 psi for at least 15 minutes. There shall be no permanent deformation, failure, or leakage permitted.

d. Pressure Factor

The pressure factor used to obtain the proof pressure shall be 1.5. This value is obtained by dividing the proof pressure by the maximum stagnation working pressure.

e. Margin of Safety

The margin of safety shall be defined as $\frac{1}{R} - 1$ where R is the ratio of design load (or stress) to the allowable load (or stress) of the material.

f. Support Truss

The support truss shall be designed for the following loads:

(1) All duct loads specified in the loads section that are transmitted to the truss at the duct supports

(2) All inertia loads caused by the weight of the exhaust assembly, coolant, and water shield (these loads are transmitted through the trunnions to the walls of the ETS-1 vault)

(3) Transportation and handling shocks and vibrations applied to the exhaust assembly or truss

(4) The coolant pressures specified in the loads section.

2. Design Conditions

a. Loads

The exhaust duct is connected to the truss structure by a five-point support system (Figure 3). A fixed hinge point is located at the center

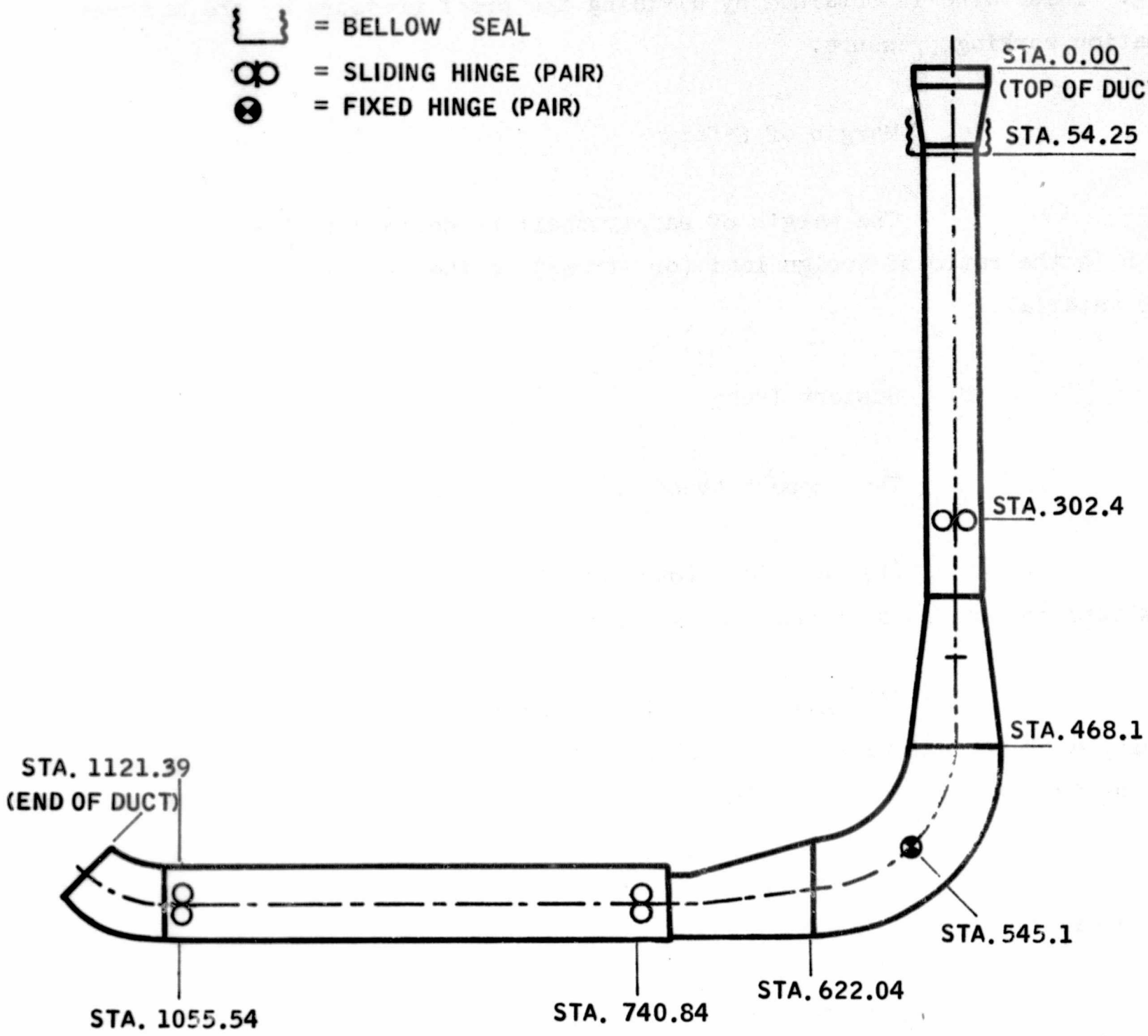

Figure 3

NES Duct Supports and Stationing for Structural Evaluations

of the 90 degree elbow section, and three sliding supports are provided that allow axial movement but restrain lateral movement. In addition, a bellow spring-type support is located near the top of the duct. This feature allows the duct to expand during engine operation and minimizes thermal stresses. The distribution of loads imposed on the duct is determined for the various supports by utilizing the moment-distribution method. These loads are determined for each loading condition, then are superimposed to obtain the governing case for any point on the duct structure. The loads under consideration are:

(1) Dead weight
(2) Skin friction
(3) Normal load caused by dynamic gas pressure (engine)
(4) Ejector thrust
(5) Jacking
(6) Temperature gradients
(7) Dynamic load

References 1 and 2 cover load conditions (1) to (6) and contain the complete analysis of the internal moments, forces, and static stresses along the duct. The dynamic load (condition (7)) is contained in this report. The calculated static stresses obtained from References 1 and 2 were superimposed onto the dynamic stresses to obtain the final stresses profile for the NES duct (See Subsection III-C-2-d).

b. Coolant Pressure and Heat Transfer Data

Both the heat transfer coefficient on the gas side and the duct wall static pressure were obtained by scale model testing. All other information was determined by the design requirements, that is, heat transfer, aerodynamic, or stress requirements.

The maximum values for temperature conditions in both the rectangular and the tubular channels were used in all structural calculations. A design coolant pressure of 250 psi was used in conjunction with other applied loads, and a proof condition of 360 psi was set for the proposed structural acceptance test.

3. Allowable Material Stress

The material chosen for the duct structure is Type 347 stainless steel, and for the truss structure is Type 304 stainless steel. For purposes of design, in accordance with Section III-B-1, an ambient allowable of 15,000 psi was set for maximum combined normal stresses and 8,000 psi for maximum shear stresses. These allowables are modified relative to temperature effects.

C. DYNAMIC ANALYSIS

The overall purpose of the structural dynamics program for the NES/ETS-1 Duct is to ensure its structural integrity under the environment of a nuclear engine operation.

The first step for such an analysis is to obtain the governing equations of motion and the resulting natural frequencies of the duct. This is followed by a determination of the externally and/or internally applied forcing functions and the subsequent dynamic response of the duct to these forcing functions. From the results of these calculations the displacements, velocities, accelerations, bending, shear and axial stresses at any section along the center line of the duct can be found. The following analysis has established that interaction between the duct and its supporting truss is negligible, so that each can be handled separately. This assumption is valid since the truss vibration mode frequencies are sufficiently low to be decoupled from the duct modes. Computation of the truss vibration modes will be given in Subsection III-C-4.

In the following paragraphs two entirely different approaches will be employed to find the solution and the results will be checked against each other. These two methods of approaches are:

1. the lumped parameter model
2. quasi-closed form model

1. Natural Frequency Solution

a. Lumped Parameter Model

The lumped-parameter method is widely used in calculating eigenvalue-eigenvector problems such as the evaluations of the natural frequencies of the NES duct. (The definition and meaning of the terms eigenvalue-eigenvector and lumped-parameter method are defined in the Appendix). Essentially, it is a

force-deflection calculation which results in a set of influence coefficients; these in turn, when multiplied by the mass of each section, form the mass flexibility matrix. The latter is then analyzed on an eigenvalue-eigenvector digital computer program and the outcome is the natural frequencies and mode shapes.

To account for the variation in the moment of inertias, axial and shear areas, and variable masses, the NES duct is subdivided into 50 sections (each section will have two degrees of freedom, see Figure 4 and Table I). The analysis takes into account in-plane bending flexibility, in-plane shear flexibility, and longitudinal flexibility. Structural analysis of the three-degree indeterminate structure involves the evaluation of the three redundant reactions and the determination of influence coefficients for unit loads applied at each of the "N" sections.

The three redundant reactions are given in the following matrix equation. (For development of these equations as well as the following equations, see Reference 3).

$$\left[R_{k,j}\right] = \left[\Delta_{k,\ell}\right]^{-1} \left[\delta_{k,j}\right] \tag{1.1}$$

where

$$\Delta_{k,\ell} = \sum_{i=1}^{I_{max}} \left[(m_{k,i})\,(m_{\ell,i})\,(EI_i) + (v_{k,i})\,(v_{\ell,i})\,(AG_i) + (p_{k,i})\,(p_{\ell,i})\,(AE_i)\right]$$

$$+ \sum_{i=r1}^{r2} \left[(p_{k,i})\,(m_{\ell,i})\,\left(\frac{AE_i}{R1}\right) + (m_{k,i})\,(p_{\ell,i})\,\left(\frac{AE_i}{R1}\right) + (m_{k,i})\,(m_{\ell,i})\,\frac{AE_i}{(R1)^2}\right]$$

$$+ \sum_{i=r3}^{r4} \left[(p_{k,i})\,(m_{\ell,i})\,\left(\frac{AE_i}{R2}\right) + (m_{k,i})\,(p_{\ell,i})\,\left(\frac{AE_i}{R2}\right) + (m_{k,i})\,(m_{\ell,i})\,\left(\frac{AE_i}{(R2)^2}\right)\right]$$

$$+ (S_k)\,(S_\ell)/K_f \tag{1.2}$$

TABLE I

LUMPED PARAMETER MODEL DESCRIPTION

ELEMENT NO.	DUCT STATION	REMARKS	ELEMENT NO.	DUCT STATION	REMARKS
1	1111.8		26	545.1	Fixed Hinge
2	1095.8		27	528.0	
3	1083.0		28	510.9	
4	1070.2		29	493.8	
5	1055.54	Sliding Hinge	30	476.7	
6	1031.1		31	461.1	
7	1005.5		32	444.7	
8	976.7		33	421.9	
9	937.7		34	397.6	
10	898.5		35	375.6	
11	859.2		36	351.2	
12	820.1		37	322.1	
13	790.9		38	302.4	Sliding Hinge
14	763.0		39	286.6	
15	740.84	Sliding Hinge	40	262.8	
16	726.8		41	238.8	
17	708.8		42	214.8	
18	692.8		43	190.8	
19	673.9		44	166.8	
20	652.9		45	142.8	
21	632.2		46	118.59	
22	613.5		47	99.59	
23	596.4		48	87.59	
24	579.3		49	54.25	Bellow Seal
25	562.2		50	12.9	

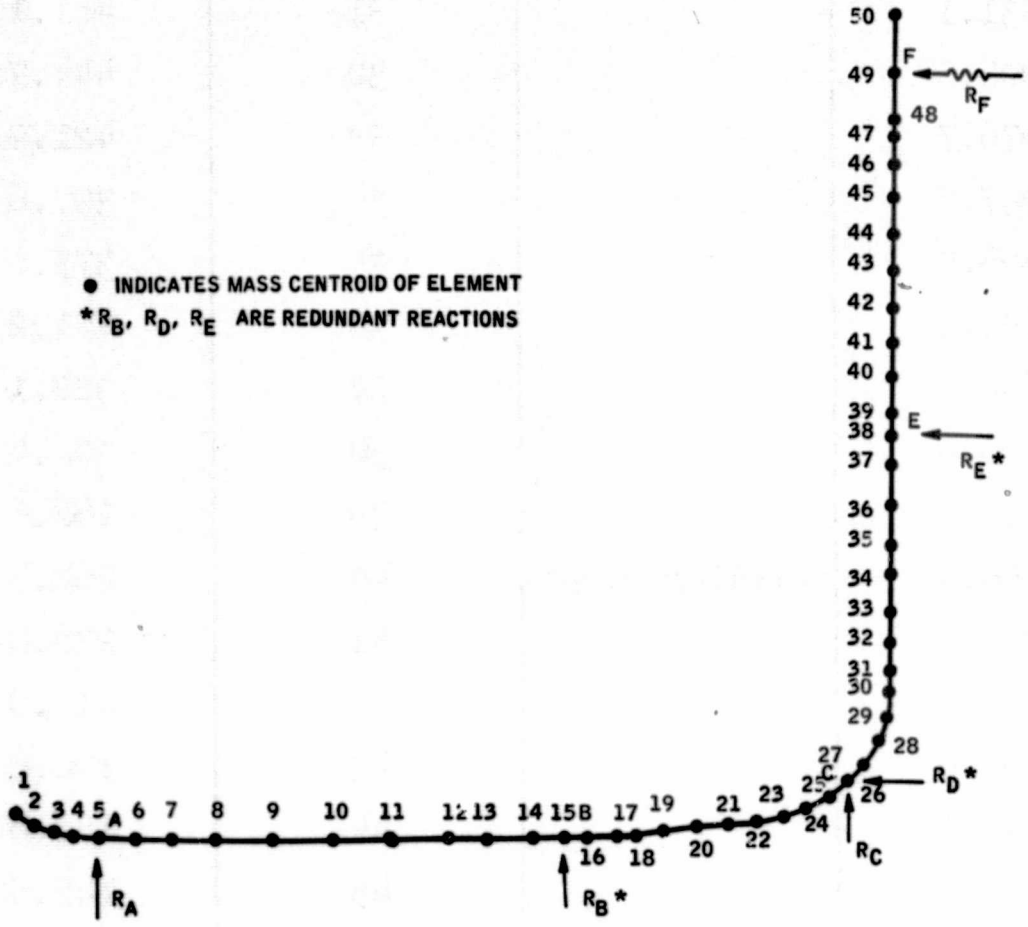

Figure 4
Lumped Parameter Model of NES Duct

$$\delta_{k,j} = \sum_{i=1}^{I_{max}} \left[(M_{j,i})\,(m_{k,i})\,(EI_i) + (V_{j,i})\,(v_{k,i})\,(AG_i) + (P_{j,i})\,(p_{k,i})\,(AE_i) \right]$$

$$+ \sum_{i=r1}^{r2} \left[(P_{j,i})\,(m_{k,i})\,\left(\frac{AE_i}{R1}\right) + (M_{j,i})\,(p_{k,i})\,\left(\frac{AE_i}{R1}\right) + (M_{j,i})\,(m_{j,i})\,\frac{AE_i}{(R1)^2} \right]$$

$$+ \sum_{i=r3}^{r4} \left[(P_{j,i})\,(m_{k,i})\,\left(\frac{AE_i}{R2}\right) + (M_{j,i})\,(p_{k,i})\,\left(\frac{AE_i}{R2}\right) + (M_{j,i})\,(m_{j,i})\,\frac{AE_i}{(R2)^2} \right]$$

$$+ (S_k)\,(SRF_j)/K_f \qquad (1.3)$$

and

$$\left.\begin{aligned} AE_i &= \frac{1}{2E}\left(\frac{L_i}{AP_i} + \frac{L_{i-1}}{AP_{i-1}}\right) \\ EI_i &= \frac{1}{2E}\left(\frac{L_i}{I_i} + \frac{L_{i-1}}{I_{i-1}}\right) \\ AG_i &= \frac{k}{2G}\left(\frac{L_i}{AV_i} + \frac{L_{i-1}}{AV_{i-1}}\right) \end{aligned}\right\} \quad \text{For } 1 < i < I_{max}$$

$$AE_i = EI_i = AG_i = 0 \quad \text{For } i = 1,\ I_{max}$$

The final forces and moments at the ith spring due to jth loading are given by:

$$\left.\begin{aligned} FP_{j,i} &= P_{j,i} - \sum_{k=1}^{3} (R_{k,j})\,(p_{k,i}) \\ FV_{j,i} &= V_{j,i} - \sum_{k=1}^{3} (R_{k,j})\,(v_{k,i}) \\ FM_{j,i} &= M_{j,i} - \sum_{k=1}^{3} (R_{k,j})\,(m_{k,i}) \end{aligned}\right\} \text{For } \begin{matrix} 1 \le i \le I_{max} \\ 1 \le j \le 2J_{max} \end{matrix} \qquad (1.4)$$

Finally, the flexibility matrix is given by:

$$1 \le n,j \le 2\,N_{max}$$

$$GF_{n,j} = \sum_{i=1}^{I_{max}} \Big[(FM_{n,i})\,(FM_{j,i})\,(EI_i) + (FV_{n,i})\,(FV_{j,i})\,(AG_i) + (FP_{n,i})\,(FP_{j,i})\,(AE_i)\Big] + \sum_{i=r1}^{r2} \Big[(FP_{n,i})\,(FM_{j,i})\,\left(\frac{AE_i}{R1}\right) + (FM_{n,i})\,(FP_{j,i})\,\left(\frac{AE_i}{R1}\right) + (FM_{n,i})\,(FM_{j,i})\,\frac{AE_i}{(R1)^2}\Big] + \sum_{i=r3}^{r4} \Big[(FP_{n,i})\,(FM_{j,i})\,\left(\frac{AE_i}{R2}\right) + (FM_{n,i})\,(FP_{j,i})\,\left(\frac{AE_i}{R2}\right) + (FM_{n,i})\,(FM_{j,i})\,\frac{AE_i}{(R2)^2}\Big] + (RF_n)\,(RF_j)/K_f \qquad (1.5)$$

The diagonal mass matrix can be found from the geometry and properties of the sections. In matrix form:

$$M_{n,j} = \begin{bmatrix} M_{11} & & & & & & \\ & M_{12} & & & & & \\ & & M_{21} & & & & \\ & & & M_{22} & & & \\ & & & & \ddots & & \\ & & & & & M_{n1} & \\ & & & & & & M_{n2} \end{bmatrix} \tag{1.6}$$

where M_{11}, M_{21}, ..., M_{n1} represent the lateral masses and M_{12}, M_{22}, ..., M_{n2} represent the longitudinal masses.

The equation of motion in the absence of any forcing function can be written in the form:

$$\left[\frac{1}{\omega^2} - (GF)\, M \right] X = 0 \tag{1.7}$$

Substituting (1.5) and (1.6) into (1.7) and using the Aerojet developed eigenvalue - eigenvector digital computer program, the natural frequency ω and the mode shape X can be obtained. The results are shown in Subsection III-C-1-c.

b. Quasi-Closed Form Model

In this approach, the governing equations of motion for the NES duct are obtained from a modified Hamiltonian principle as an initial step in solving the overall duct dynamics problem. In general, the motion of the duct is dependent upon the types of forcing functions to which it is subjected. This may require the duct to bend in one or more planes, twist about its longitudinal axis,

and translate longitudinally. As is the case of the lumped parameter method, this analysis will consider only single-plane bending and longitudinal translation. Schematically the duct with coordinate orientation is represented as shown in Figure 5.

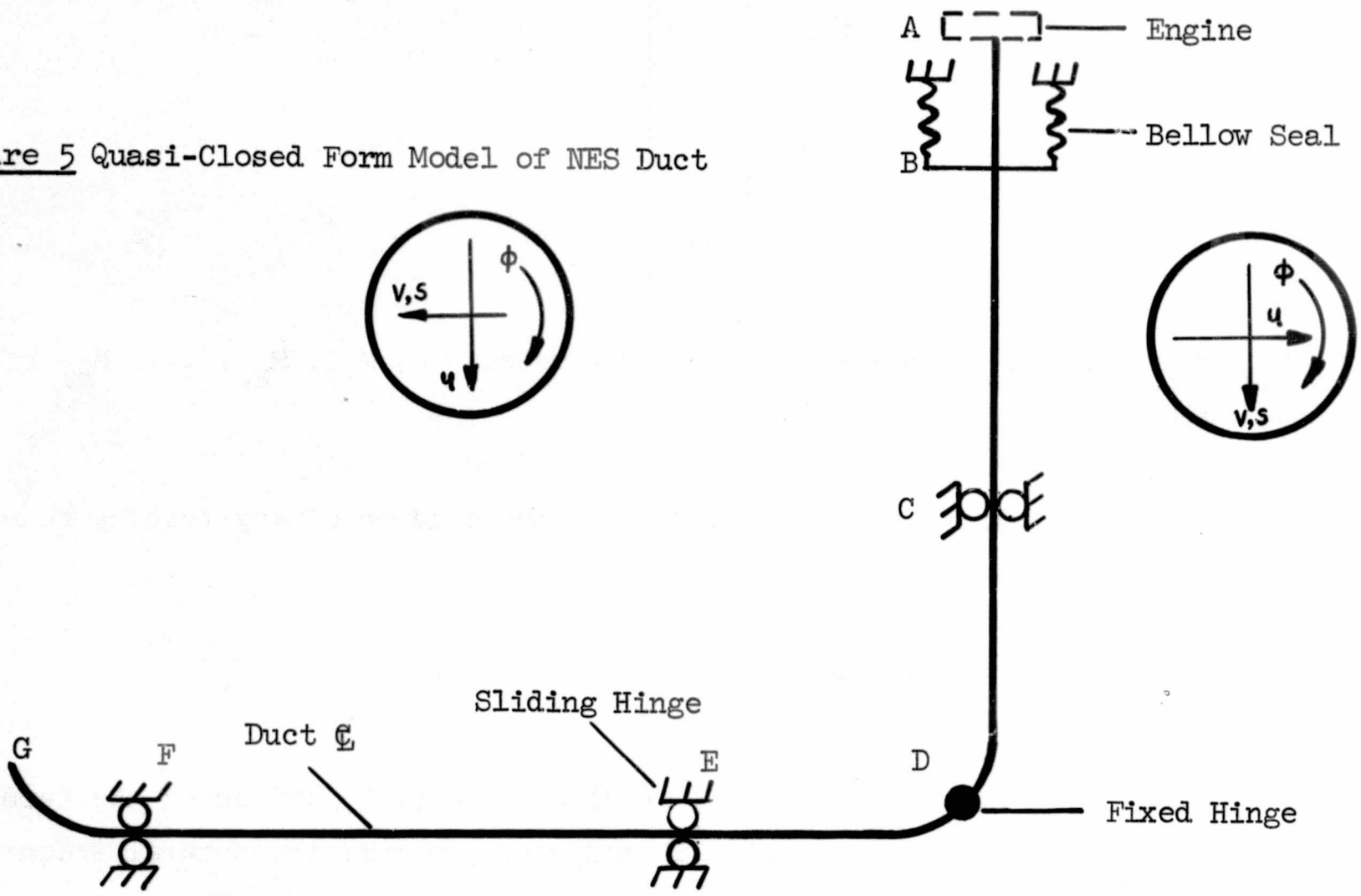

Figure 5 Quasi-Closed Form Model of NES Duct

The displacements "u" and "v" are taken normal and tangential to the duct center line, respectively.

The mathematical formulation of the Hamiltonian principle can be expressed by:

$$\int_{t_o}^{t_1} (d\bar{U} - d\bar{K})\, dt = \int_{t_o}^{t_1} d\bar{W}\, dt \qquad (2.1)$$

This equation states that the variation of the potential and kinetic energy of a system taken between fixed initial and final values (t_o and t_1) for time "t" must equal the variation of work done by the external forces over the same time interval. Requirements for specific expressions dictate that the variations be expressed in a form compatible with the dependent variables sought. The dependent variables sought are "u", the transverse displacement and "v", the longitudinal displacement.

The potential variation is the variation of the strain energy of bending and axial stresses, which may be expressed as:

$$\bar{dU} = \oint_{\bar{V}} \sigma d\ \varepsilon\ \bar{dV} \qquad (2.2)$$

The bending and axial stresses can be written in terms of the displacements as follows:

Bending

$$M = EI\ \frac{\partial^2 u}{\partial s^2}\ ,\ \sigma = \frac{My}{I} = Ey\ \frac{\partial^2 u}{\partial s^2}\ ,\ \varepsilon = \frac{\sigma}{E} = y\ \frac{\partial^2 u}{\partial s^2}\ ,\ d\varepsilon = y\ \frac{\partial^2 (\Delta u)}{\partial s^2} \qquad (2.3)$$

Axial

$$\varepsilon = \frac{\partial v}{\partial s}\ ,\ \sigma = E\varepsilon = E\ \frac{\partial v}{\partial s}\ ,\ d\varepsilon = \frac{\partial (\Delta v)}{\partial s} \qquad (2.4)$$

for straight duct segments, and:

Bending

$$M = \frac{EI}{R^2}\left(\frac{\partial^2 u}{\partial \phi^2} + u\right),\ \sigma = \frac{Ey}{R^2}\left(\frac{\partial^2 u}{\partial \phi^2} + u\right),\ \varepsilon = \frac{y}{R^2}\left(\frac{\partial^2 u}{\partial \phi^2} + u\right),\ d\varepsilon = \frac{y}{R^2}\,\Delta\left(\frac{\partial^2 u}{\partial \phi^2} + u\right)$$

(2.5)

Axial

$$\varepsilon = \frac{1}{R}\left(u + \frac{\partial v}{\partial \phi}\right), \quad \sigma = \frac{E}{R}\left(u + \frac{\partial v}{\partial \phi}\right), \quad d\varepsilon = \frac{1}{R}\,\Delta\left(u + \frac{\partial v}{\partial \phi}\right) \tag{2.6}$$

for curved duct segments.

Substituting equations (2.3), (2.4) and (2.5), (2.6) into equation (2.1) obtain:

$$d\bar{U} = \int_0^{\ell} EI \; \frac{\partial^2 u}{\partial s^2} \; \frac{\partial^2 (\Delta u)}{\partial s^2} \, ds + \int_0^{\ell} \frac{\partial v}{\partial s} \; \frac{\partial (\Delta v)}{\partial s} \, ds \tag{2.7}$$

and:

$$d\bar{U} = \int_0^{\phi} \left[\frac{EI}{R^3} \left(\frac{\partial^2 u}{\partial \phi^2} + u\right) \Delta \left(\frac{\partial^2 u}{\partial \phi^2} + u\right) + \frac{EA}{R}\left(u + \frac{\partial v}{\partial \phi}\right) \Delta \left(u + \frac{\partial v}{\partial \phi}\right) \right] d\phi \tag{2.8}$$

for straight and curved duct segments, respectively.

Similarly, the variation of kinetic energy and external work done can also be expressed in terms of the displacements as follows:

$$d\bar{K} = \int_0^{\ell} \rho A \left\{ \left[\frac{\partial u}{\partial t} + \frac{\partial}{\partial t}\left(\frac{\partial^2 u}{\partial s^2}\right) \right] \frac{\partial \Delta u}{\partial t} + \left[\frac{\partial v}{\partial t} \; \frac{\partial \Delta v}{\partial t} \right] \right\} ds \tag{2.9}$$

$$d\bar{W} = \int_0^{\ell} PA \, ds \, \Delta v + \int_0^{\ell} w \, ds \, \Delta u \tag{2.10}$$

for straight duct segments, and:

$$d\bar{K} = \int_0^{\phi} \rho A \left\{ \left[\frac{\partial u}{\partial t} + \frac{1}{R} \; \frac{\partial}{\partial t}\left(\frac{\partial^2 u}{\partial \phi^2}\right) \right] \frac{\partial \Delta u}{\partial t} + \frac{\partial v}{\partial t} \; \frac{\partial \Delta v}{\partial t} \right\} R \, d\phi \tag{2.11}$$

$$\bar{dW} = \int_0^{\phi} PAR\, d\phi \Delta v + \int_0^{\phi} w R\, d\phi\, \Delta u \qquad (2.12)$$

for curved duct segments.

Substituting equations (2.7), (2.9) and (2.10), or (2.8), (2.11) and (2.12) into equation (2.1) with the constraint requirements that Δu and Δv must vanish at $t = t_o$ and t_1, give:

$$EI \frac{\partial^4 u}{\partial s^4} + \rho A \frac{\partial^2 u}{\partial t^2} = 0 \qquad (2.13)$$

$$EA \frac{\partial^2 v}{\partial s^2} - \rho A \frac{\partial^2 v}{\partial t^2} = 0 \qquad (2.14)$$

and:

$$\frac{EI}{R^3}\left(\frac{\partial^4 u}{\partial \phi^4} + 2\frac{\partial^2 u}{\partial \phi^2} + u\right) + \frac{EA}{R}\left(\frac{\partial v}{\partial \phi} + u\right) + \rho AR \frac{\partial^2 u}{\partial t^2} = 0 \qquad (2.15)$$

$$\frac{EA}{R}\left(\frac{\partial^2 v}{\partial \phi^2} + \frac{\partial u}{\partial \phi}\right) - \rho AR \frac{\partial^2 v}{\partial t^2} = 0 \qquad (2.16)$$

for transverse and longitudinal motion of straight and curved duct segments, respectively.

Equations (2.13) through (2.16) are the governing equations of motion for the NES duct in the absence of forcing functions and subjected to the appropriate boundary conditions on moments, shears, slopes, and deflections. The rotary inertia and shear inertia terms are neglected in the previous equations since their contributions are small, especially for lower frequencies or when the duct is subdivided into nodal cross sections of rather than short lengths.

The equations of motion, equations (2.13) to (2.16), are solved by the Laplace Transformation method. For any two consecutive segments of the duct configuration, the following equations are obtained (see Reference 4 for the complete solution to this problem):

$$v_{r+1}\left[\frac{EA_{r+1}}{\ell_{r+1}} D_1(\sigma_{r+1})\right] + v_r\left[\frac{EA_{r+1}}{\ell_{r+1}} R_1(\sigma_{r+1}) + \frac{EA_r}{\ell_r} R_1(\sigma_r)\right]$$

$$+ v_{r-1}\left[\frac{EA_r}{\ell_r} D_1(\sigma_r)\right] = 0 \qquad (2.17)$$

$$\theta_{r+1}\left[\frac{EI_{r+1}}{\ell_{r+1}} H_2(\beta_{r+1})\right] + \theta_r\left[-\frac{EI_{r+1}}{\ell_{r+1}} H_1(\beta_{r+1}) + \frac{EI_r}{\ell_r} H_1(\beta_r)\right]$$

$$- \theta_{r-1}\left[\frac{EI_r}{\ell_r} H_2(\beta_r)\right] + u_{r+1}\left[\frac{EI_{r+1}}{\ell^2_{r+1}} F_2(\beta_{r+1})\right] + u_r\left[-\frac{EI_{r+1}}{\ell^2_{r+1}} F_1(\beta_{r+1})\right.$$

$$\left. + \frac{EI_r}{\ell_r^2} F_1(\beta_r)\right] - u_{r-1}\left[\frac{EI_r}{\ell_r^2} F_2(\beta_r)\right] = 0 \qquad (2.18)$$

$$- \theta_{r+1}\left[\frac{EI_{r+1}}{\ell^2_{r+1}} F_2(\beta_{r+1})\right] + \theta_r\left[\frac{EI_{r+1}}{\ell^2_{r+1}} F_1(\beta_{r+1}) + \frac{EI_r}{\ell_r^2} F_1(\beta_r)\right]$$

$$- \theta_{r-1}\left[\frac{EI_r}{\ell_r^2} F_2(\beta_r)\right] + u_{r+1}\left[\frac{EI_{r+1}}{\ell^3_{r+1}} K_2(\beta_{r+1})\right] + u_r\left[\frac{EI_{r+1}}{\ell^3_{r+1}} K_1(\beta_{r+1})\right.$$

$$\left. + \frac{EI_r}{\ell_r^3} K_1(\beta_r)\right] + u_{r-1}\left[\frac{EI_r}{\ell_r^3} K_2(\beta_r)\right] = 0 \qquad (2.19)$$

for straight duct segments, and:

$$v_{r+1}\left[\frac{EA_{r+1}}{R}N_1(\kappa_{r+1})\right] + v_r\left[\frac{EA_{r+1}}{R}T_1(\kappa_{r+1}) + \frac{EA_r}{R}T_1(\kappa_r)\right]$$
$$+ v_{r-1}\left[\frac{EA_r}{R}N_1(\kappa_r)\right| = 0 \qquad (2.20)$$

$$-\theta_{r+1}\left[\frac{EI_{r+1}}{R}h_2(\alpha_{r+1})\right] + \theta_r\left[\frac{EI_{r+1}}{R}h_1(\alpha_{r+1}) - \frac{EI_r}{R}h_1(\alpha_r)\right]$$
$$+\theta_{r-1}\left[\frac{EI_r}{R}h_2(\alpha_r)\right]$$
$$-u_{r+1}\left[\frac{EI_{r+1}}{R^2}f_2(\alpha_{r+1})\right] + u_r\left[\frac{EI_{r+1}}{R^2}f_1(\alpha_{r+1}) - \frac{EI_r}{R^2}f_1(\alpha_r)\right]$$
$$+u_{r-1}\left[\frac{EI_r}{R^2}f_2(\alpha_r)\right] = 0 \qquad (2.21)$$

$$\theta_{r+1}\left[\frac{EI_{r+1}}{R^2}f_2(\alpha_{r+1})\right] - \theta_r\left[\frac{EI_{r+1}}{R^2}f_1(\alpha_{r+1}) + \frac{EI_r}{R^2}f_1(\alpha_r)\right]$$
$$+\theta_{r-1}\left[\frac{EI_r}{R^2}f_2(\alpha_r)\right] - u_{r+1}\left[\frac{EI_{r+1}}{R^3}k_2(\alpha_{r+1})\right]$$
$$-u_r\left[\frac{EI_{r+1}}{R^3}k_1(\alpha_{r+1}) + \frac{EI_r}{R^3}k_1(\alpha_r)\right] - u_{r-1}\left[\frac{EI_r}{R^3}k_2(\alpha_r)\right] = 0 \qquad (2.22)$$

for curved duct segments, where Table II gives the definitions for the symbolic terms

In the foregoing equations, "r" represents any element on the duct segment, r-1 and r+1 are elements located just before and after "r". Equations (2.17) and (2.20) are for forced equilibrium, whereas equations (2.18) and (2.21) are for moment equilibrium and equations (2.19) and (2.22) are for shear equilibrium. These equations will be modified and used in the forced response solution. The

TABLE II

DEFINITIONS FOR SYMBOLIC TERMS

SYMBOL	TERM	SYMBOL	FUNCTION
π	$\frac{EA}{\ell} R_1(\sigma)$	$R_1(\sigma)$	$\sigma \ell \cot \sigma \ell$
Λ	$\frac{EA}{\ell} D_1(\sigma)$	$D_1(\sigma)$	$\sigma \ell \operatorname{cosec} \sigma \ell$
Σ	$\frac{EA}{R} N_1(\kappa)$	$N_1(\kappa)$	$\kappa \operatorname{cosec} \kappa \phi_r$
I	$\frac{EA}{R} T_1(\kappa)$	$T_1(\kappa)$	$\kappa \cot \kappa \phi_r$
χ	$\frac{EI}{\ell^2} F_1(\beta)$	$F_1(\beta)$	$\beta^2 \left(\frac{\sin \beta \sinh \beta}{1-\cos \beta \cosh \beta}\right)$
ψ	$\frac{EI}{\ell^2} F_2(\beta)$	$F_2(\beta)$	$\beta^2 \left(\frac{\cos \beta - \cosh \beta}{1-\cos \beta \cosh \beta}\right)$
η	$\frac{EI}{\ell^3} K_1(\beta)$	$K_1(\beta)$	$\beta^3 \left(\frac{\cos \beta \sinh \beta + \sin \beta \cosh \beta}{1-\cos \beta \cosh \beta}\right)$
ν	$\frac{EI}{\ell^3} K_2(\beta)$	$K_2(\beta)$	$\beta^3 \left(\frac{\sin \beta + \sinh \beta}{1-\cos \beta \cosh \beta}\right)$
ε	$\frac{EI}{\ell} H_1(\beta)$	$H_1(\beta)$	$\beta \left(\frac{\sin \beta \cosh \beta - \cos \beta \sinh \beta}{1-\cos \beta \cosh \beta}\right)$
φ	$\frac{EI}{\ell} H_2(\beta)$	$H_2(\beta)$	$\beta \left(\frac{\sin \beta - \sinh \beta}{1-\cos \beta \cosh \beta}\right)$
μ	$\frac{EI}{R} h_2(\alpha)$	$h_2(\alpha)$	$\frac{\alpha(a \operatorname{cosec} a\phi_r - b \operatorname{cosec} b\phi_r)}{1-ab(\operatorname{cosec} a\phi_r \operatorname{cosec} b\phi_r - \cot a\phi_r \cot b\phi_r)}$
γ	$\frac{EI}{R} h_1(\alpha)$	$h_1(\alpha)$	$\frac{\alpha(a \cot a\phi_r - b \cot b\phi_r)}{1-ab(\operatorname{cosec} a\phi_r \operatorname{cosec} b\phi_r - \cot a\phi_r \cot b\phi_r)}$
δ	$\frac{EI}{R^2} f_2(\alpha)$	$f_2(\alpha)$	$\frac{\alpha^2 \left(\frac{ab}{\alpha} \cot b\phi_r \operatorname{cosec} a\phi_r - \frac{ab}{\alpha} \cot a\phi_r \operatorname{cosec} b\phi_r\right)}{1-ab(\operatorname{cosec} a\phi_r \operatorname{cosec} b\phi_r - \cot a\phi_r \cot b\phi_r)}$
λ	$\frac{EI}{R^2} f_1(\alpha)$	$f_1(\alpha)$	$\frac{\alpha^2}{1-ab(\operatorname{cosec} a\phi_r \operatorname{cosec} b\phi_r - \cot a\phi_r \cot b\phi_r)}$

TABLE II (cont.)

SYMBOL	TERM	SYMBOL	FUNCTION
Ω	$\frac{EI}{R^3} k_1(\alpha)$	$k_1(\alpha)$	$\frac{ab\alpha\,(b\cot a\phi_r - a\cot b\phi_r)}{1-ab\,(\operatorname{cosec} a\phi_r \operatorname{cosec} b\phi_r - \cot a\phi_r \cot b\phi_r)}$
ξ	$\frac{EI}{R^3} k_2(\alpha)$	$k_2(\alpha)$	$\frac{ab\alpha\,(b\operatorname{cosec} a\phi_r - a\operatorname{cosec} b\phi_r)}{1-ab(\operatorname{cosec} a\phi_r \operatorname{cosec} b\phi_r - \cot a\phi_r \cot b\phi_r)}$

$\kappa = \frac{\omega R}{c}$ $\quad \sigma = \frac{\omega}{c}$ $\quad c = \sqrt{\frac{EA_E}{\rho A \rho}}$ $\quad d = \sqrt{\frac{EI}{\rho A \rho}}$

$a = \sqrt{1-\alpha}$ $\quad b = \sqrt{1+\alpha}$ $\quad \alpha = \frac{\omega R^2}{d}$ $\quad \beta = \ell\sqrt{\frac{\omega}{d}}$

When $\alpha \geq 1$, let $a = iA$

Where $A = \sqrt{\alpha - 1}$

Then $\cot a\phi_r = -i \coth A\phi_r$

$\operatorname{cosec} a\phi_r = -i \operatorname{cosech} A\phi_r$

Where A_E = Effective cross-section area

$A\rho$ = Total cross-section area

ϕ_r = Angle for r element of curved duct segment

boundary conditions and discontinuities in spatial coordinates dictate modifications to these basic equations. Thus for example at the top of the duct (r=0), the conditions of zero force, moment, and shear at point "0" yield:

$$-v_o\left[\frac{EA_1}{\ell_1}\ R_1(\sigma_1)\right] - v_1\left[\frac{EA_1}{\ell_1}\ D_1(\sigma_1)\right] = 0 \tag{2.23}$$

$$\theta_o\left[\frac{EI_1}{\ell_1}\ H_1(\beta_1)\right] - \theta_1\left[\frac{EI_1}{\ell}\ H_2(\beta_1)\right] + u_o\left[\frac{EI_1}{\ell_1^2}\ F_1(\beta_1)\right]$$
$$- u_1\left[\frac{EI_1}{\ell_1^2}\ F_2(\beta_1)\right] = 0 \tag{2.24}$$

$$- \theta_o\left[\frac{EI_1}{\ell_1^2}\ F_1(\beta_1)\right] + \theta_1\left[\frac{EI_1}{\ell_1^2}\ F_2(\beta_1)\right] - u_o\left[\frac{EI_1}{\ell_1^3}\ K_1(\beta_1)\right]$$
$$- u_1\left[\frac{EI_1}{\ell_1^3}\ K_2(\beta_1)\right] = 0 \tag{2.25}$$

When a straight span intersects a curved span at the left boundary when proceeding along the duct, the applicable equations are:

$$v_{r+1}\left[\frac{EA_{r+1}}{R}\ N_1(\kappa_{r+1})\right] + V_r\left[\frac{EA_{r+1}}{R}\ T_1(\kappa_{r+1}) + \frac{EA_r}{\ell_r}\ R_1(\sigma_r)\right]$$
$$+ v_{r-1}\left[\frac{EA_r}{\ell_r}\ D_1(\sigma_r)\right] = 0 \tag{2.26}$$

$$- \theta_{r+1}\left[\frac{EI_{r+1}}{R}\ h_2(\alpha_{r+1})\right] + \theta_r\left[\frac{EI_{r+1}}{R}\ h_1(\alpha_{r+1}) + \frac{EI_r}{\ell_r}\ H_1(\beta_r)\right]$$
$$- \theta_{r-1}\left[\frac{EI_r}{\ell_r}\ H_2(\beta_r)\right] - u_{r+1}\left[\frac{EI_{r+1}}{R^2}\ f_2(\alpha_{r+1})\right] + u_r\left[\frac{EI_{r+1}}{R^2}\ f_1(\alpha_{r+1})\right.$$
$$\left. + \frac{EI_r}{\ell_r^2}\ F_1(\beta_r)\right] - u_{r-1}\left[\frac{EI_r}{\ell_r^2}\ F_2(\beta_r)\right] = 0 \tag{2.27}$$

and:

$$\theta_{r+1}\left[\frac{EI_{r+1}}{R^2} f_2(\alpha_{r+1})\right] - \theta_r\left[\frac{EI_{r+1}}{R^2} f_1(\alpha_{r+1}) - \frac{EI_r}{\ell_r^2} F_1(\beta_r)\right]$$

$$+ \theta_{r-1}\left[\frac{EI_r}{\ell_r^2} F_2(\beta_r)\right] - u_{r+1}\left[\frac{EI_{r+1}}{R^3} k_2(\alpha_{r+1})\right]$$

$$- u_r\left[\frac{EI_{r+1}}{R^3} k_1(\alpha_{r+1}) - \frac{EI_r}{\ell_r^3} K_1(\beta_r)\right] + u_{r-1}\left[\frac{EI_r}{\ell_r^3} K_2(\beta_r)\right] = 0 \quad (2.28)$$

The foregoing equations define the transverse and longitudinal motion of the duct with any number of subdivisions "r". In general the slopes, transverse displacements and longitudinal displacements are arbitrary and assume values which are not identically zero; hence the vanishing of the determinant of the coefficients matrix furnishes the natural frequencies.

For the NES duct configuration, 22 segments were used (see Figure 6). The applicable input data are presented in Reference 4. The natural frequencies are obtained from an evaluation of the determinant by the direct application of the Myklestad approach to the Bauachiewicz-Cholesky-Crout determinant evaluation. This determinant can be represented as follows::

$$D = \begin{Vmatrix} a_{11} & a_{12} & \cdots & a_{1n} \\ a_{21} & a_{22} & \cdots & a_{2n} \\ a_{31} & a_{32} & \cdots & a_{3n} \\ & & & \\ a_{m1} & a_{m2} & \cdots & a_{mn} \end{Vmatrix} = 0$$

where $m = n = 64$, and a_{ij} is the deplacement coefficient.

The results for the first three modes obtained from the computer output are presented in Subsection III-C-1-c of this report.

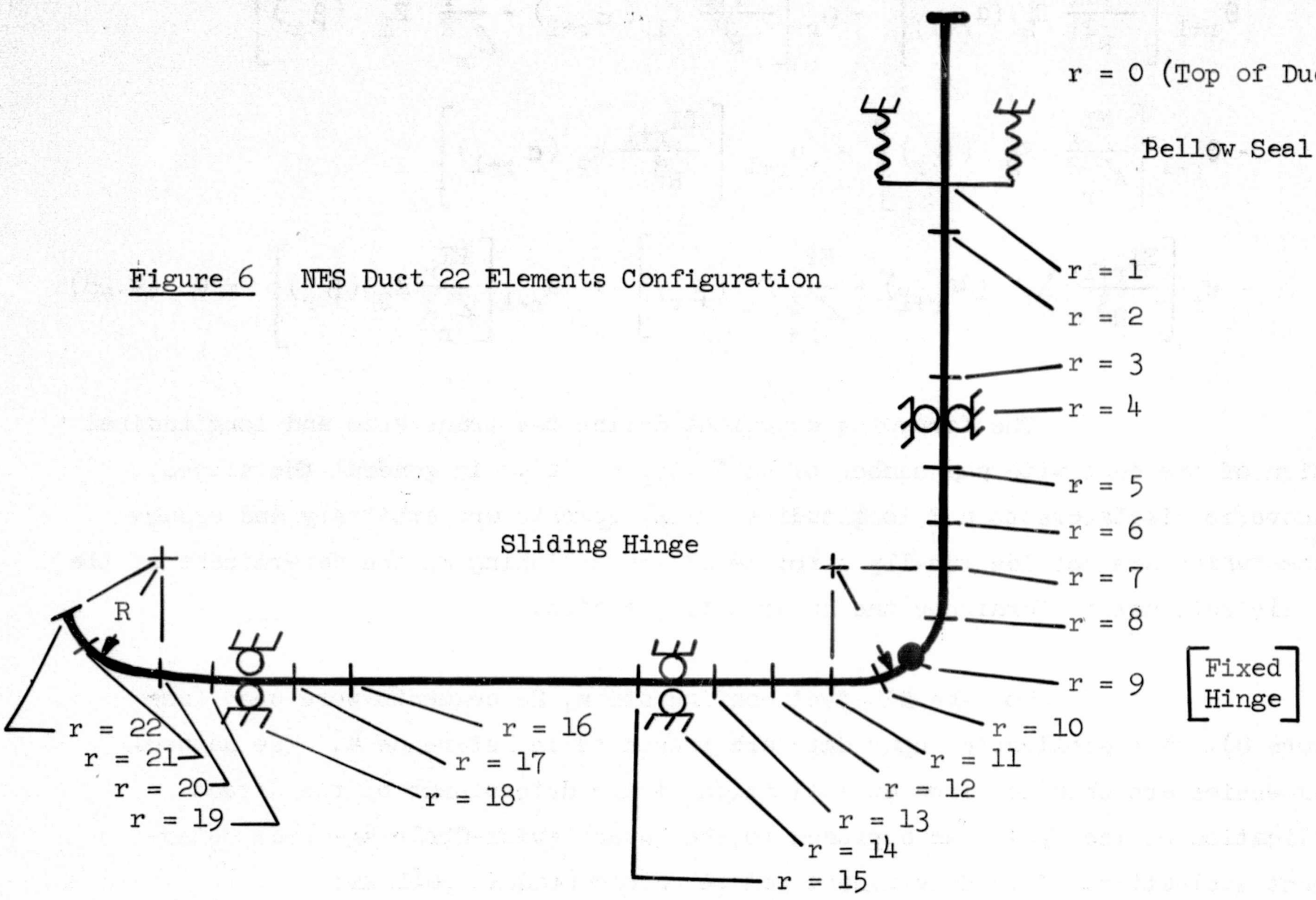

Figure 6 NES Duct 22 Elements Configuration

c. Natural Frequencies

The natural frequencies obtained from the two previous methods are presented in Table III. The first three modes checked very closely, although they were developed by two entirely different approaches. In Table III, the first six modes by the first method are given, whereas three modes are given for the second method. The values obtained from the latter method is for verification of the lumped-parameter method.

TABLE III

NATURAL FREQUENCIES FOR LUMPED-PARAMETER AND QUASI-CLOSED FORM MODELS

Natural Frequency Mode	Lumped Parameter Model	Quasi-Closed Form Model
1	30.6 cps	33.7 cps
2	39.4	37.0
3	42.7	48.3
4	45.9	--
5	53.2	--
6	62.9	--

Presented in Figures 7 to 12 are the mode shapes for the first six natural modes of vibration of the NES duct using the lumped parameter model.

2. Forced Response Solution

a. Lumped Parameter Model

Normal modes and existing solutions for a single degree of freedom system can be used in obtaining transient, or steady-state, response to sinusoidal and random forces for the multi-degree system, lumped parameter model of the duct. For the n^{th} mode an equation-of-motion of the following form (Reference 5)

$$\ddot{q}_n + 2\eta_n \dot{q}_n + \omega_n^2 q_n = \frac{1}{g_n} \sum_{j=1}^{2Jmax} \left[F_j(t) \left(\phi_{n,j} \right) \right] \qquad (3.1)$$

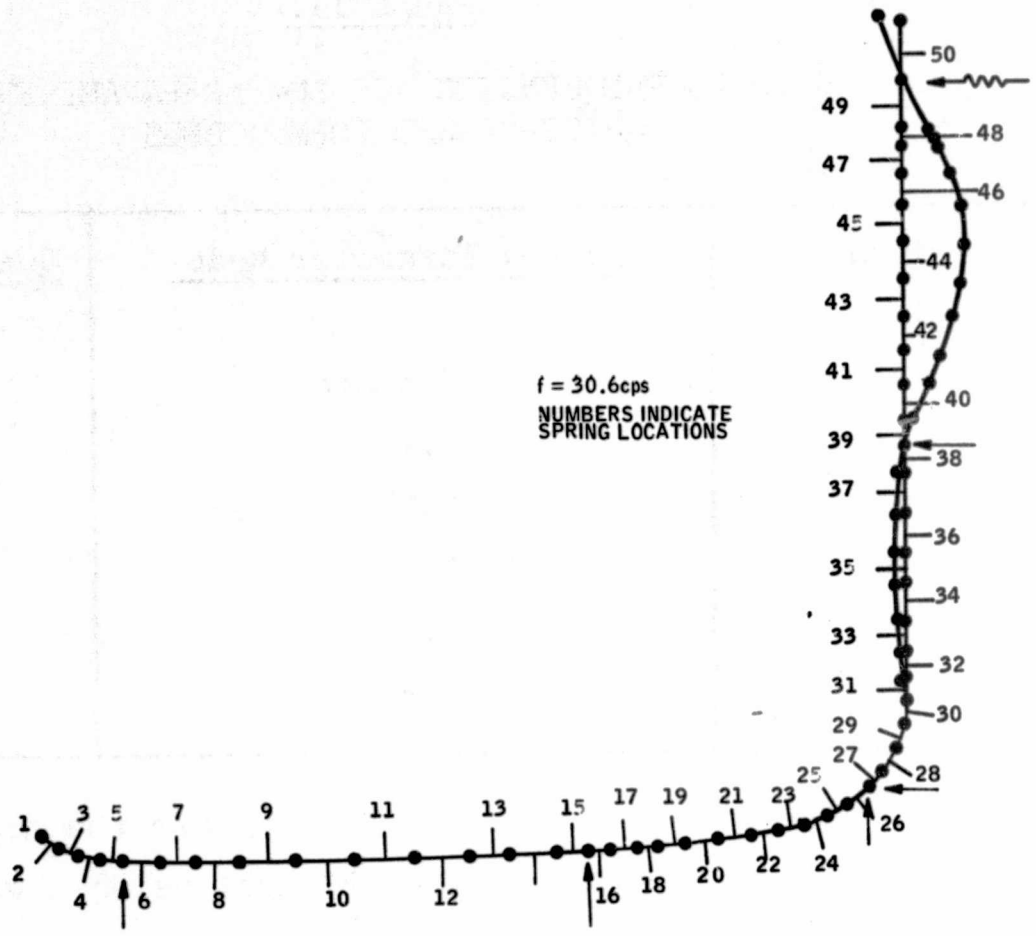

Figure 7

First Mode Shape of Vibration of the NES Duct

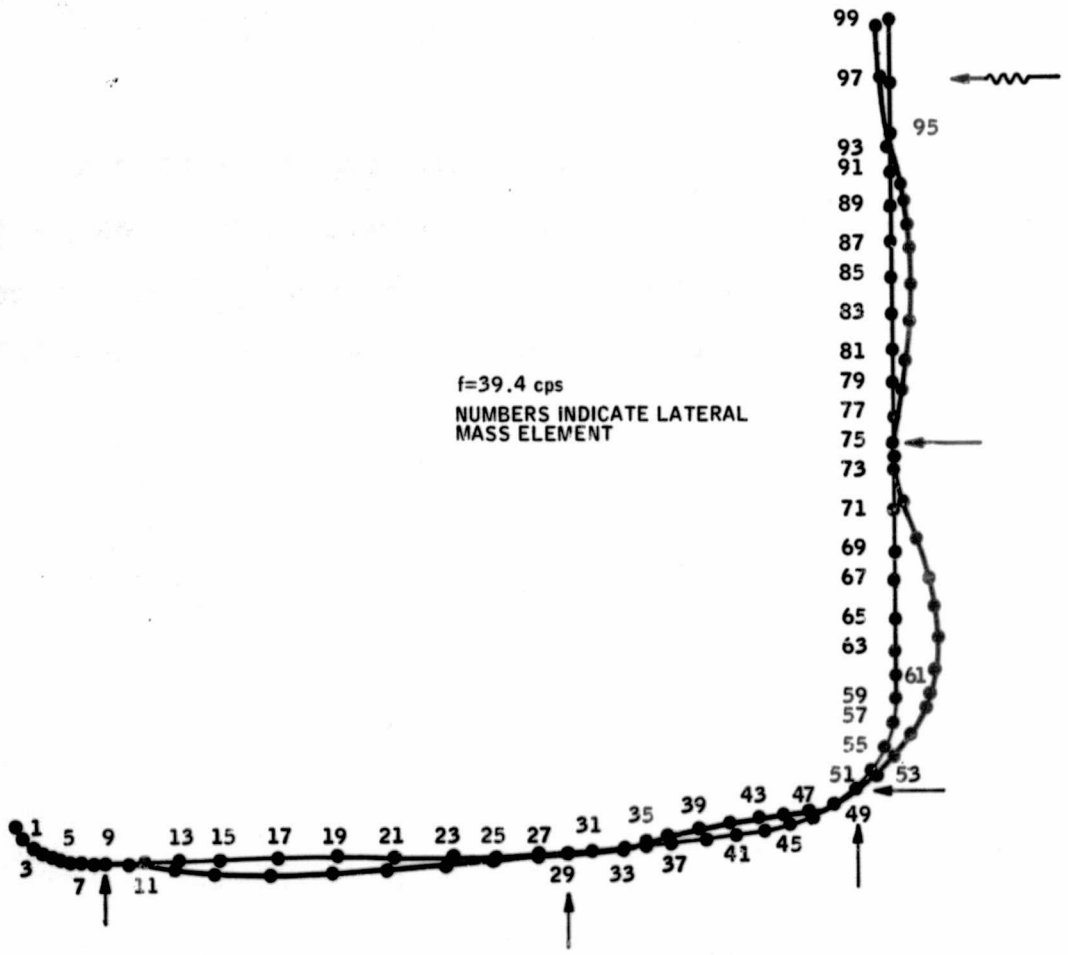

Figure 8

Second Mode Shape of Vibration of the NES Duct

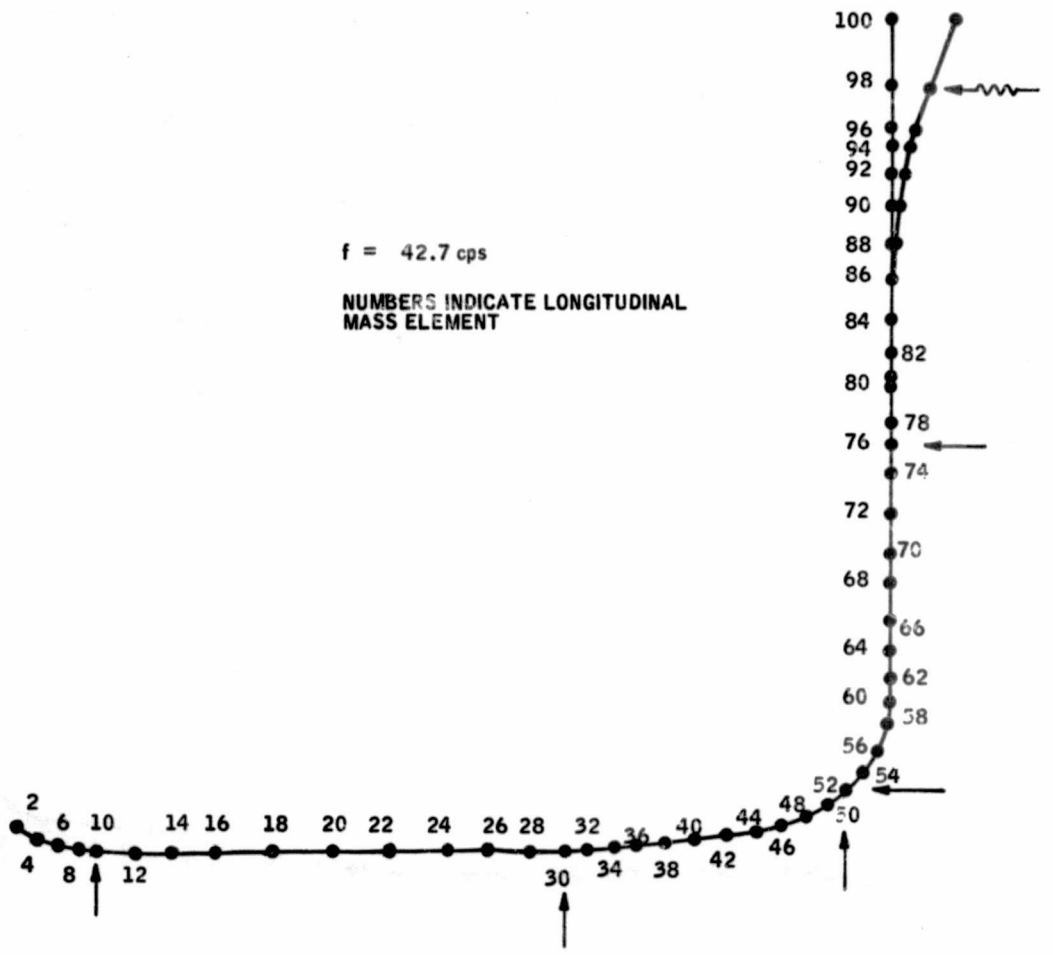

Figure 9

Third Mode Shape of Vibration of the NES Duct

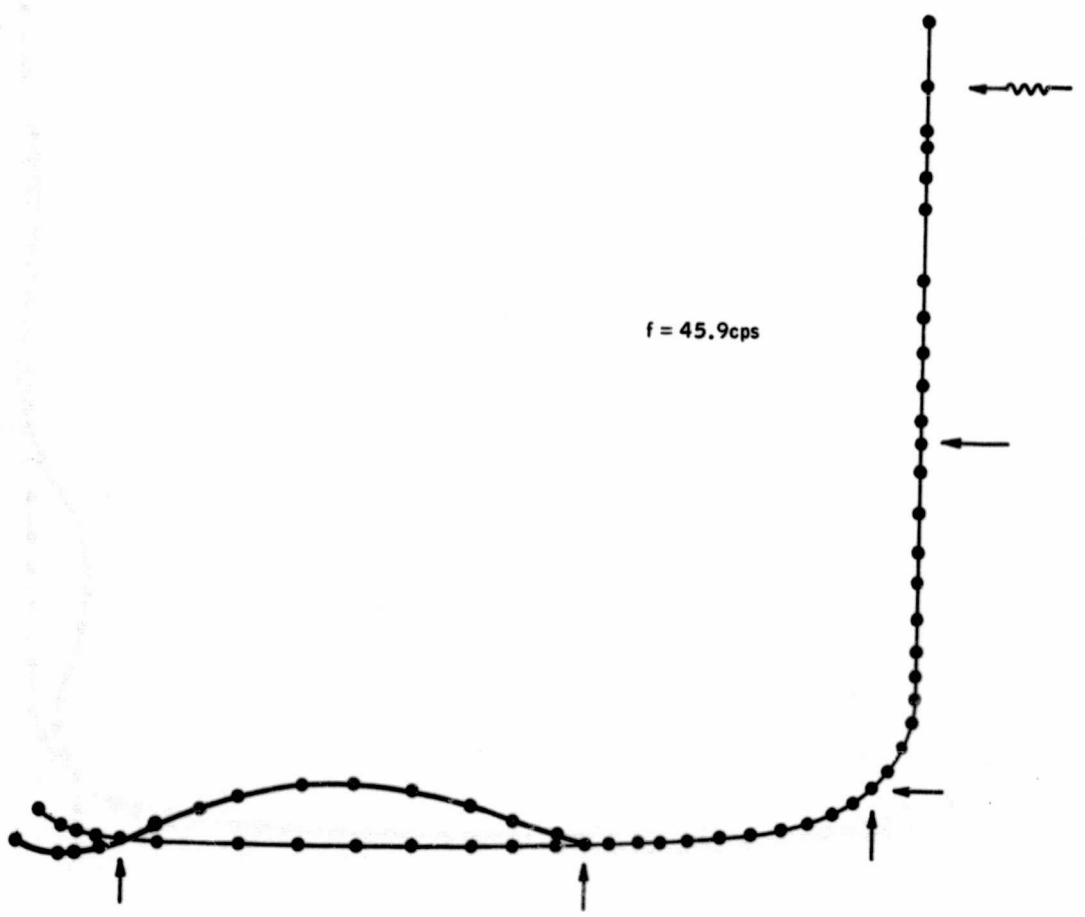

Figure 10

Fourth Mode Shape of Vibration of the NES Duct

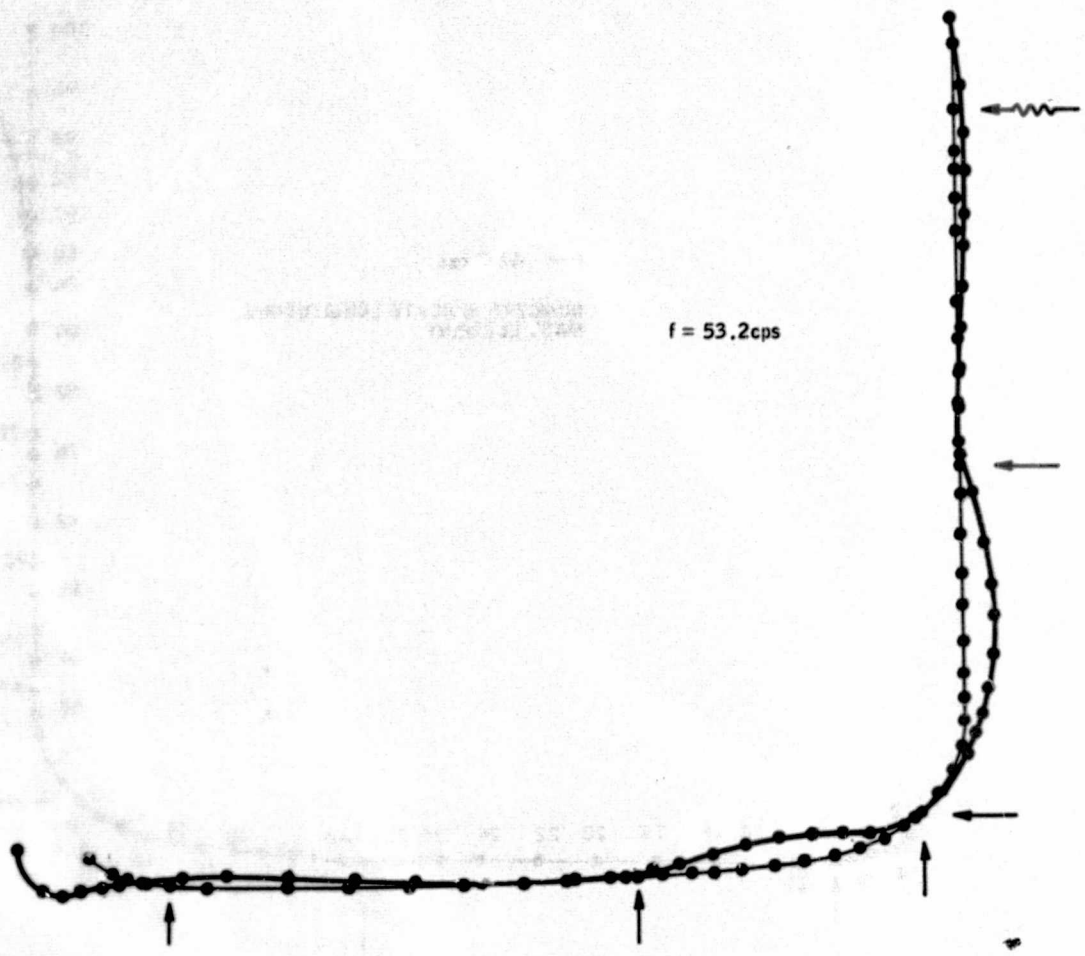

Figure 11

Fifth Mode Shape of Vibration of the NES Duct

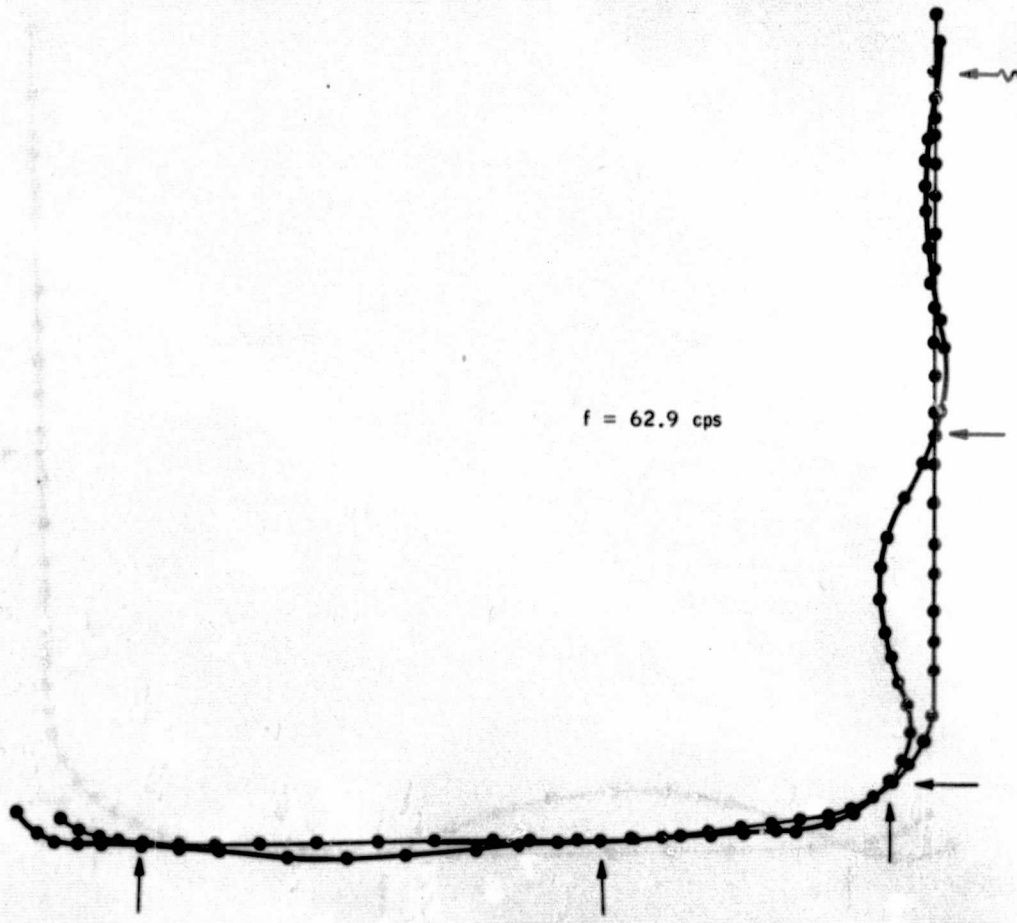

Figure 12

Sixth Mode Shape of Vibration of the NES Duct

will apply; where the coordinate q_n is a generalized displacement, indicative of the entire duct response in a particular n^{th} mode, and the generalized mass g_n is given by

$$g_n = \sum_{j=1}^{2Jmax} (Ma_j)\ (\phi_{n,\,j})^2$$

The forcing function will be modified at three locations (namely the three sliding hinges) as follows:

$$F_{2j}(t) = F_{2j}(t) - C_k\ R'_k\ (t-1)\ \left\{\pm\left[\sum_{n=1}^{Mmax} (\phi_{n,\,2j})\ (\dot{q}_n)\right.\right. \qquad (3.2)$$

where $R'_k = R_k + DL$

Aside from the forcing functions and the modal damping, the modal influence coefficients for unit acceleration can be obtained from the results of the flexibility matrix and the eigenvalue - eigenvector computer programs (see Sub-section III-C-1-a). They can be represented as follows:

$$r'_{k,\,n} = \sum_{j=1}^{2Jmax} (Ma_j)\ (\phi_{n,\,j})\ \ (I_{k,\,j})$$

$$p'_{n,\,i} = \sum_{j=1}^{2Jmax} (Ma_j)\ (\phi_{n,\,j})\ \ (F\,P_{j,\,i}) \qquad (3.3)$$

$$v'_{n,\,i} = \sum_{j=1}^{2Jmax} (Ma_j)\ (\phi_{n,\,j})\ \ (F\,V_{j,\,i})$$

$$m'_{n,\,i} = \sum_{j=1}^{2Jmax} (Ma_j)\ (\phi_{n,\,j})\ \ (F\,M_{j,\,i})$$

The displacements, reactions, axial forces, bending moments, and shears for any section of the duct will be determined by solving the set of equations of the type shown by Equation (3.1) simultaneously, adding the responses, and using the following relationships:

$$\delta_i = \sum_{j=1}^{2Jmax} \left[F_j(t) \right] \left[G\, F_{i,j} \right] - \sum_{n=1}^{Mmax} (\phi_{n,i})(q_n) \tag{3.4}$$

$$R_k = \sum_{j=1}^{2Jmax} \left[F_j(t) \right] \left[I_{k,j} \right] - \sum_{n=1}^{Mmax} (r'_{k,n})(\ddot{q}_n) \tag{3.5}$$

$$P_i = \sum_{j=1}^{2Jmax} \left[F_j(t) \right] \left[F\, P_{j,i} \right] - \sum_{n=1}^{Mmax} (p'_{n,i})(\ddot{q}_n) \tag{3.6}$$

$$M_i = \sum_{j=1}^{2Jmax} \left[F_j(t) \right] \left[F\, M_{j,i} \right] - \sum_{n=1}^{Mmax} (m'_{n,i})(\ddot{q}_n) \tag{3.7}$$

$$V_i = \sum_{j=1}^{2Jmax} \left[F_j(t) \right] \left[F\, V_{j,i} \right] - \sum_{n=1}^{Mmax} (v'_{n,i})(\ddot{q}_n) \tag{3.8}$$

Where the number of values for "i" may vary from 1 to 2Jmax.

The foregoing values are printed out at each time increment of the computer output giving a complete time history of the response of the system.

b. Quasi-Closed Form Model

The natural frequencies of the NES duct for the combined longitudinal and transverse motion using the Quasi-Closed Form Model were obtained in Subsection III-C-1-b. The se of equations (2.17, 2.18, 2.19) and (2.20, 2.21, 2.22) used to compute the natural frequencies arises from a consideration of the axial force, moment, and shear acting at any element "r" on the duct. In the presence of forcing functions of the following form:

$$P(t) = Pe^{i\omega t} \qquad \text{(axial)}$$
$$M(t) = Me^{i\omega t} \qquad \text{(moment)}$$
$$Q(t) = Qe^{i\omega t} \qquad \text{(shear)}$$

the previous equations may be modified to read:

$$\Lambda_r v_{r-1} + \left[\pi_r + \pi_{r+1}\right] v_r + \Lambda_{r+1} v_{r+1} = \pm P(t) \tag{4.1}$$

$$-\varphi_r \theta_{r-1} + \left[\varepsilon_r - \varepsilon_{r+1}\right]\theta_r + \varphi_{r+1}\theta_{r+1} - \Psi_r u_{r-1} + \left[\chi_r - \chi_{r+1}\right]$$

$$+ \Psi_{r+1} u_{r+1} = \pm M(t) \tag{4.2}$$

$$-\Psi_r \theta_{r-1} + \left[\chi_r + \chi_{r+1}\right]\theta_r - \Psi_{r+1}\theta_{r+1} + \nu_r u_{r-1}$$

$$+\left[\eta_r + \eta_{r+1}\right] u_r + \nu_{r+1} u_{r+1} = \pm Q(t) \tag{4.3}$$

for straight duct segments and:

$$\Sigma_r v_{r-1} + \left[I_r + I_{r+1}\right] v_r + \Sigma_{r+1} v_{r+1} = \pm P(t) \tag{4.4}$$

$$\mu_r \theta_{r-1} - \left[\gamma_r - \gamma_{r+1}\right]\theta_r - \mu_{r+1}\theta_{r+1} + \delta_r u_{r-1}$$

$$-\left[\lambda_r - \lambda_{r+1}\right] u_r - \delta_{r+1} u_{r+1} = \pm M(t) \tag{4.5}$$

$$\delta_r \theta_{r-1} - \left[\lambda_r + \lambda_{r+1}\right]\theta_r + \delta_{r+1}\theta_{r+1} - \xi_r u_{r-1}$$

$$-\left[\Omega_r + \Omega_{r+1}\right] u_r - \xi_{r+1} u_{r+1} = \pm Q(t) \tag{4.6}$$

for curved duct segments, where the notation for the symbolic form is employed. (see Table II).

In general, the application of the above procedure yields a system of simultaneous equations with the longitudinal displacements, slopes, and transverse displacements as the three unknowns. By specifying the forcing functions and taking into account the boundary conditions this system of simultaneous equations is formulated into matrix form for computer solution of the three unknown displacements. This matrix formulation is represented as follows:

$$\begin{bmatrix} a_{11} & a_{12} & \cdots & a_{1h} & \cdots & a_{1n} \\ a_{21} & a_{22} & \cdots & a_{2h} & \cdots & a_{2n} \\ \cdots & \cdots & \cdots & \cdots & \cdots & \cdots \\ a_{i1} & a_{i2} & \cdots & a_{ih} & \cdots & a_{in} \\ \cdots & \cdots & \cdots & \cdots & \cdots & \cdots \\ a_{m1} & a_{m2} & \cdots & a_{mh} & \cdots & a_{mn} \end{bmatrix} \begin{bmatrix} b_1 \\ b_2 \\ \vdots \\ b_h \\ \vdots \\ b_n \end{bmatrix} = \begin{bmatrix} c_1 \\ c_2 \\ \vdots \\ c_i \\ \vdots \\ c_m \end{bmatrix} \qquad (4.7)$$

where a_{mn} represents the matrix of the coefficients whose values are obtained from the structural properties of the duct; b_n represents the matrix of the longitudinal displacements (v), slope (θ) and transverse displacements (u); and c_m represents the matrix of the three types of forcing functions (that is axial force, moment, and shear).

With the displacements (u & v) and slopes (θ) determined the axial forces, moments and shear acting at any element " r " are found by utilizing the following equations (Reference 6):

$$P_r = -\pi_{r+1}\ v_r - \Lambda_{r+1}\ v_{r+1} \tag{4.8}$$

$$M_r = \varepsilon_{r+1}\ \theta_r + \chi_{r+1}\ u_r - \varphi_{r+1}\ \theta_{r+1} - \psi_{r+1}\ u_{r+1} \tag{4.9}$$

$$Q_r = -\chi_{r+1}\ \theta_r - \eta_{r+1}\ u_r + \psi_{r+1}\ \theta_{r+1} - \nu_{r+1}\ u_{r+1} \tag{4.10}$$

for straight duct segments and

$$P_r = -I_{r+1}\ v_r - \Sigma_{r+1}\ v_{r+1} \tag{4.11}$$

$$M_r = -\gamma_{r+1}\ \theta_r - \lambda_{r+1}\ u_r + \mu_{r+1}\ \theta_{r+1} + \delta_{r+1}\ u_{r+1} \tag{4.12}$$

$$Q_r = \lambda_{r+1}\ \theta_r + \Omega_{r+1}\ u_r - \delta_{r+1}\ \theta_{r+1} + \xi_{r+1}\ u_{r+1} \tag{4.13}$$

for curved duct segments.

This system of equations is also formulated in the following matrix form for computer solution:

$$\begin{bmatrix} d_1 \\ d_2 \\ \cdot \\ \cdot \\ \cdot \\ \cdot \\ d_i \\ \cdot \\ \cdot \\ \cdot \\ \cdot \\ d_m \end{bmatrix} = \begin{bmatrix} e_{11} & e_{12} \cdots e_{1h} \cdots e_{1n} \\ e_{21} & e_{22} \cdots e_{2h} \cdots e_{2n} \\ - & - & - & - & - & - & - & - & - & - \\ - & - & - & - & - & - & - & - & - & - \\ e_{i1} & e_{i2} \cdots e_{ih} \cdots e_{in} \\ - & - & - & - & - & - & - & - & - & - \\ - & - & - & - & - & - & - & - & - & - \\ e_{m1} & e_{m2} \cdots e_{mh} \cdots e_{mn} \end{bmatrix} \begin{bmatrix} b_1 \\ b_2 \\ \cdot \\ \cdot \\ \cdot \\ \cdot \\ b_i \\ \cdot \\ \cdot \\ \cdot \\ \cdot \\ b_n \end{bmatrix} \qquad (4.14)$$

where d_m represents the matrix of the axial force, moment and shear, e_{mn} represents the matrix of the coefficients and b_n represents the deflections and slopes matrix obtained from (4.7).

The subdivisions of the NES duct into 22 segments and the formulations of the displacements and forced matrices are both shown in Reference 6.

c. Forcing Function Profile

The dynamic response equations for the NES duct have been developed previously. Calculations of the forcing functions are presented in this section. For the duct structure these forces are attributed to the accelerations (change in velocity and direction) in the gas flow. Methods based on scale model flow tests and by analytical procedure are developed and analyzed. Fluctuating forces are determined such that they can be applied directly to the model developed in the structural dynamics analysis program.

(1) Scale Model Profile

The development of the gas dynamic forces through scale model tests and test data obtained from previous Kiwi reactor operation (Reference 7) represented an extensive test program conducted by the personnel at Aerojet Von Karman Center. As a result of these tests, the duct forcing functions were established and subsequently verified by the gas dynamic theories. Using this approach, force fluctuations acting along the center line of the duct can be predicted as a function of the motor chamber pressure fluctuations.

The dynamic similarity between two different flows around geometrically similar bodies can be shown by the fundamental equations of fluid dynamics. These fundamentals are the equation of state, equation of continuity (conservation of mass), momentum equation and the energy equation. By writing these equations in non-dimensional form they become identical for different flow systems, if the non-dimensional parameters in the equations are maintained equally. The most important dimensionless parameters in fluid dynamics are the Mach number, Reynolds number, Prandtl number and the ratio of specific heats. For isentropic flow, where the viscous and heat conduction effects are relatively unimportant, similarity in Mach number and specific heat ratio are the most important parameter which need be considered. In the one-eighth and one-quarter scale duct model gas dynamics tests conducted by Aerojet, Mach number and specific heat ratio similarity were maintained.

Thus, the flow in the models and in the prototype duct was similar. The magnitude of the forces resulting from pressure for the model and prototype are related by the following equation:

$$F_m(t_m) = (\frac{1}{n})^2 F_p(t_p) \tag{5.1}$$

where $\frac{1}{n^2}$ is the Jacobian of the prototype to model transformation.

The duct system has been divided into fifty elements, as shown in Figure 4. In certain of these elements the gas undergoes a change either in direction of flow or in velocity because of the geometry of that section. The force acting on each of these elements is equal to the difference between the input and output vector impulse functions. The impulse function is given by the following equation:

$$I = pA\ (1 + kM^2) \tag{5.2}$$

By using equation (5.2) together with the known geometry of the duct the force at any section of the duct can be found as a function of the fluctuation pressure at that section. The sections in which the geometry leads to a net force are given in Table IV. For each of these sections, the pressure to force coefficient and the angle at which this force acts are also given. Thus, the pressure to force coefficients given in Table IV convert any element pressure fluctuation into a force fluctuation acting on that element.

The pressure fluctuation in each element may be related to the motor chamber pressure fluctuation. For each element the input and output pressure was determined as a linear function of the chamber pressure according to the following equation:

$$p_d = a_d + b_d p_c \tag{5.3}$$

TABLE IV

FORCE COEFFIENTS BASED ON GEOMETRY AND PRESSURE FLUCTUATION

ELEMENT NUMBER	DIA. INLET INCHES	ANGLE INLET DEGREES	MACH NUMBER INLET	DIA. OUTLET INCHES	ANGLE OUTLET DEGREES	MACH NUMBER OUTLET	AREA DIFFERENCE INCHES	ANGLE OF FORCE	FORCE COEFFICIENT OF p_d LBS/PSI	FORCE COEFFICIENT OF p_c LBS/PSI	FORCE FOR $p_c = \pm 10$ PSI LBS
Contract											
50	50	90	M > 1	46.2	90	M > 1	287	--	--	--	--
49	46.2	90	M > 1	39.0	90	M > 1	482	--	--	--	--
Expansion		Longitudinal Force									
35	39.0	90	1.0	45.2	90	.85	410	90	+330	+8.9	+89
34	45.2	90	.85	51.3	90	.70	462	90	+300	+8.1	81
33	51.3	90	.70	58.8	90	.52	648	90	+160	+4.3	43
32	58.8	90	.52	64.1	90	.39	512	90	+280	+7.6	76
31	64.1	90	.39	68.0	90	.30	404	90	+140	+3.8	38
Elbow (90°)		Radial Force									
30	68.2	90	.25	68.2	80	.25	0	175	636	17.2	172
29	68.2	80	.25	68.2	70	.25	0	165	636	17.2	172
28	68.2	70	.20	68.2	60	.20	0	155	636	17.2	172
27	68.2	60	.20	68.2	50	.20	0	145	636	17.2	172
26	68.2	50	.20	68.2	40	.20	0	135	636	17.2	172
25	68.2	40	.20	68.2	30	.20	0	125	636	17.2	172
24	68.2	30	.20	68.2	20	.20	0	115	636	17.2	172
23	68.2	20	.25	68.2	10	.25	0	105	636	17.2	172
22	68.2	10	.25	68.2	0	.25	0	95	636	17.2	172
Contract		Longitudinal Force									
21	68.6	0	.25	62.3	0	.25	645	0	-703	-19.0	190
20	62.3	0	.25	55.9	0	.30	590	0	-650	-17.5	175
19	55.9	0	.30	49.6	0	.50	526	0	-160	-4.3	43
18	49.6	0	.50	44.4	0	.80	481	0	+340	+9.2	±92
Secondary Chamber		Longitudinal Force									
18								0	$75p_{sc}$	$75p_{sc}$	+750
16								0	$75p_{sc}$	$75p_{sc}$	−750
45° Turn		Radial Force									
4	50.5	0	--	50.5	10	--	0	85	350	28	280
3	50.5	10	--	50.5	20	--	0	75	350	28	280
2	50.5	20	--	50.5	30	--	0	65	350	28	280
1	50.5	30	--	50.5	45	--	0	52.5	520	41.5	415

The fluctuating components of these pressures were given by the equation:

$$p_d' = b_d p_c' \tag{5.4}$$

During numerous scale model tests with hot nitrogen and hydrogen gases, measurements were made of pressure fluctuation along the scale model ducts and of chamber pressure fluctuations. These experimental data, together with the Kiwi reactor test data, were studied in detail. The results of these studies will be incorporated into the model scale law and into the pressure-to-force coefficients given by Table IV in order to obtain the fluctuating force acting on the elements of the duct. The forcing functions thus developed for the NES duct would be too time dependent and too numerous for their values to be reproduced here (see Reference 8 for the complete history of the forcing functions). Figure 13 shows the gas dynamic scale model test setup.

(2) Analytical Profile

The approach selected for the analysis is based on the determination of the average values of the flow field of the exhaust gas and steam at discreet points in the NES ducts. The conservation equations of gases (energy, mass and momentum) for the successive stations are solved in terms of the preceding station. The results of this analysis indicate that the basic chamber pressure frequencies are preserved, but phase shifts and amplitude changes are introduced and vary throughout the duct profile. A forcing function for the NES duct is then derived which is based on the average time dependent pressure and an "average" friction force between the stations.

The modified conservation equations for non-stationary duct flow with heat and mass addition can be written as:

$$-\frac{1}{2}\ell_{12} A_2 \frac{\partial \rho_2}{\partial t} + \rho_2 u_2 A_2 = \frac{1}{2}\ell_{12} A_1 \frac{\partial \rho_1}{\partial t} + \rho_1 u_1 A_1 + \dot{m}_{12} \tag{6.1}$$

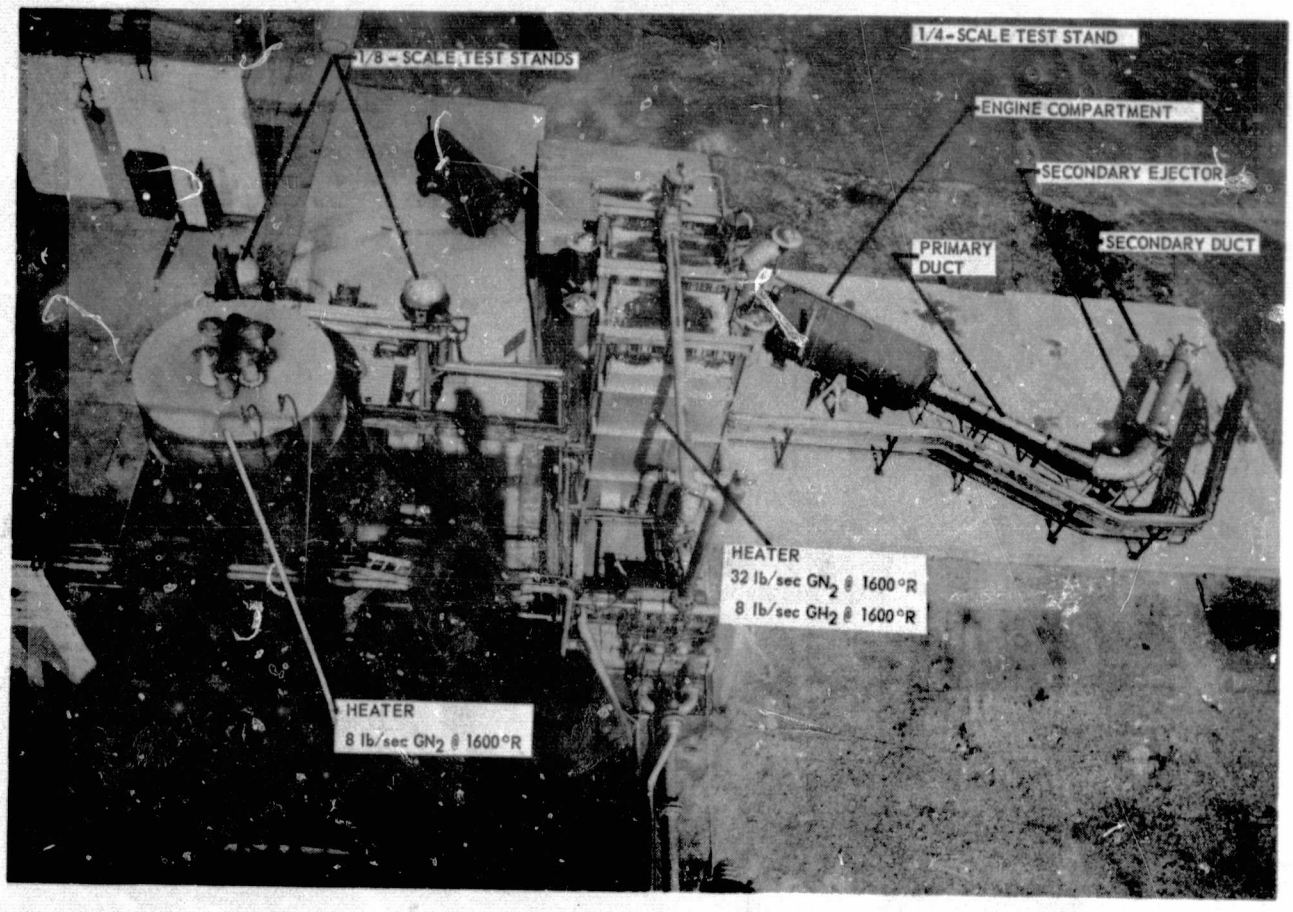

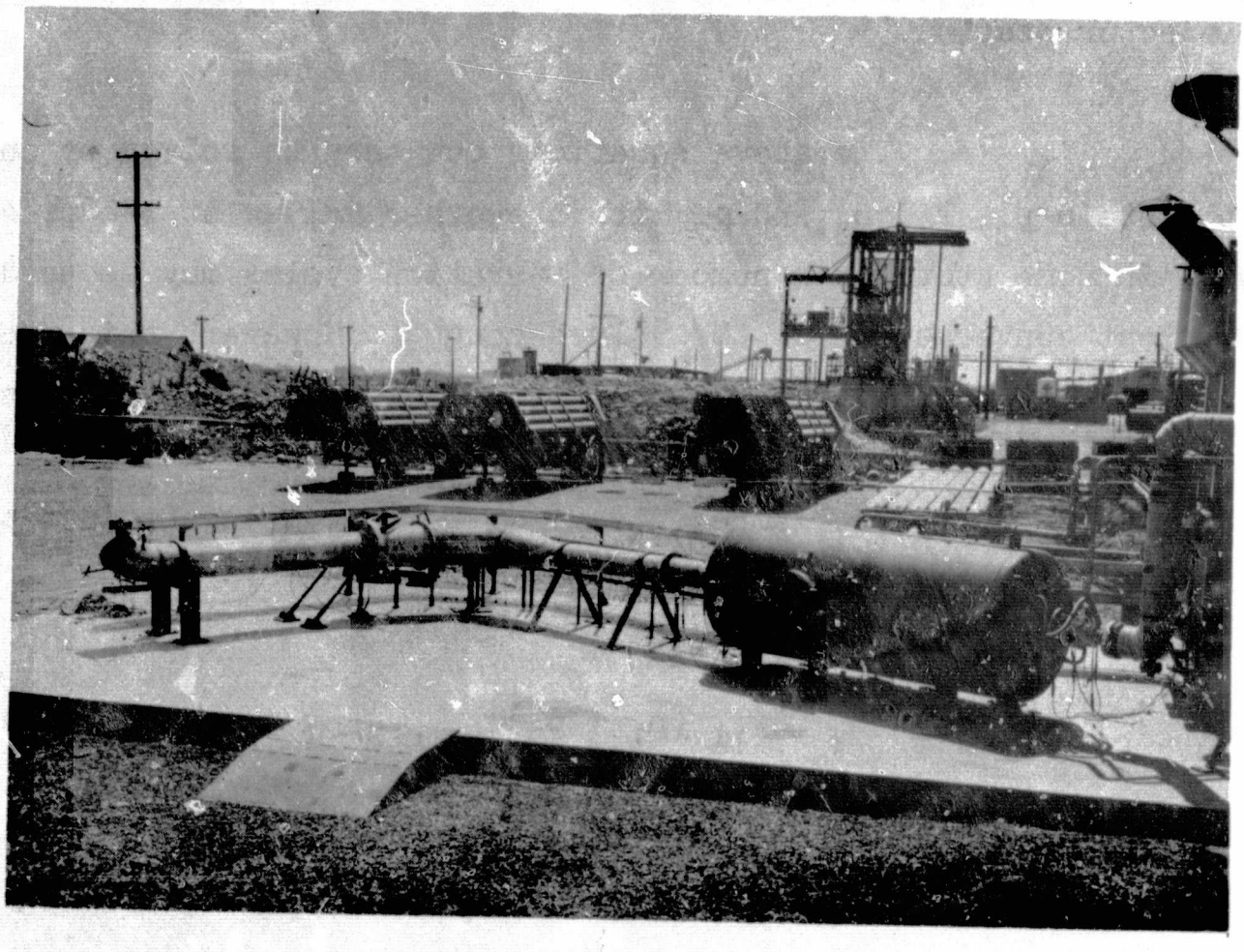

Figure 13

Gas Dynamic Scale Model Test Setup

$$- \tfrac{1}{2} \ell_{12} A_2 u_2 \frac{\partial \rho_2}{\partial t} + \rho_2 u_2^2 A_2 + \tfrac{1}{2} p_2 (A_1 + A_2) + \tfrac{1}{2} \left(\frac{\ell_{12}}{r_c}\right) \rho_2 A_2 u_2^2 =$$

$$\tfrac{1}{2} \ell_{12} A_1 u_1 \frac{\partial \rho_1}{\partial t} - \tfrac{1}{2} \left(\frac{\ell_{12}}{r_c}\right) \rho_1 A_1 u_1^2 + \rho_1 u_1^2 A_1 + \tfrac{1}{2} p_1 (A_1 + A_2) - \tfrac{1}{4} A w_{12}$$

$$(c_{f_1} \rho_1 u_1^2 + c_{f_2} \rho_2 u_2^2) + \dot{m}_{st} \Delta u_{st} \qquad (6.2)$$

$$\rho_2 u_2 A_2 C_{p_2} T_{t_2} - \tfrac{1}{2} \ell_{12} A_2 T_{t_2} C_{p_2} \frac{\partial \rho_2}{\partial t} + \tfrac{1}{2} \ell_{12} A_2 \frac{\partial \rho_2}{\partial t} + \tfrac{1}{4} \left(\frac{\ell_{12}}{r_c}\right) \rho_2 A_2 u_2^3 =$$

$$\rho_1 u_1 A_1 C_{p_1} T_{t_1} - \tfrac{1}{4} \left(\frac{\ell_{12}}{r_c}\right) \rho_1 A_1 u_1^3 + \tfrac{1}{2} \ell_{12} A_1 T_{t_1} C_{p_1} \frac{\partial \rho_1}{\partial t} - \tfrac{1}{2} \ell_{12} A_1 \frac{\partial \rho_1}{\partial t} - \dot{Q}_{12} A w_{12} \qquad (6.3)$$

$$p_i = \bar{p}_i \left[1 + E_i \sin (\omega t + \phi_i) \right] \qquad (6.4)$$

for mass, momentum, energy and state equations, where $\dot{m}_{st}$ and u_{st} are zero except at the steam injector station.

The above equations can then be solved by an iteration technique to obtain p_2, T_2, u_2 and ρ_2 with the other values at the preceding station being known. In some stations a number of iteration cycles may be needed in order to obtain sufficient convergence for the values sought. However, this presents no problem since the iteration procedure will be formulated for computer solution.

The lumped steady state forces at any duct section normal to, and parallel with, the duct walls respectively are:

$$F_N = \tfrac{1}{2} A w_{12} (\bar{p}_1 + \bar{p}_2) \qquad (6.5)$$

$$F_p = \tfrac{1}{4} A w_{12} \left[c_{f_1} \bar{\rho}_1 u_1^2 + c_{f_2} \bar{\rho}_2 u_2^2 \right] \qquad (6.6)$$

Then, the lumped steady state forces for the same duct sections normal to, and parallel with, the duct center line are:

$$F_R = F_p \sin\theta + F_N \cos\theta \tag{6.7}$$

$$F_L = F_p \cos\theta - F_N \sin\theta \tag{6.8}$$

where the angle θ denotes the slope of the duct wall and is defined by the following equation.

$$\theta = \tan^{-1}\left[\frac{\sqrt{\frac{A_2}{\pi}} - \sqrt{\frac{A_1}{\pi}}}{\ell_{12}}\right] \tag{6.9}$$

In curved sections of the duct, additional lumped forces due to centrifugal force effects must be included. These are given by:

$$F_{LCF} = \left[\bar{\rho}_1 u_1^2 A_1 - \bar{\rho}_2 u_2^2 A_2\right] \cos\frac{\phi}{2} \tag{6.10}$$

$$F_{RCF} = \left[\bar{\rho}_1 u_1^2 A_1 + \bar{\rho}_2 u_2^2 A_2\right] \sin\frac{\phi}{2} \tag{6.11}$$

From equations (6.1, 6.2, 6.3) one may now solve for the transient relative amplitude E_2 and phase angle ϕ_2 as functions of ω, ϕ_1, and the steady state values (Reference 9). Given E_2 and ϕ_2, transient force amplitudes equivalent to F_R, F_L, F_{LCF} and F_{RCF} are then obtained from the previous formulas (Equations 6.5 through 6.10), using $\bar{p}_1 E_1$ and $\bar{p}_2 E_2$ instead of $\bar{p}_1$ and $\bar{p}_2$, and noting that transient density amplitudes are obtained from the transient pressure amplitudes by the perfect gas equation of state. The forcing function thus determined is to be incorporated into the dynamic response analysis. The geometry as well as the input data and the output forcing functions for the NES duct are shown in Tables V through VII.

TABLE V

GEOMETRY AND INPUT

Station (in.)	Cross Section Area ($in.^2$)	Prior Span Length (in.)	Wetted Area ($in.^2$)	$\overline{Q}/A_w$ (Btu w/sec $in.^2$)	Duct Radius at Curvature (in.)	
8.00	2063					
52.30	1182	44.30	6328	.55	∞	
62.40	1182	10.10	1231	.30	∞	
90.32	1182	27.92	3403	.25	∞	
306.40	1182	216.08	26336	.43	∞	
364.62	1182	58.22	7096	.53	shock here	
468.10	3621	103.48	17517	.55	∞	
493.00	3621	24.90	5327	.75	98.0	First Bend
590.00	3621	97.00	20752	.90	98.0	
622.09	3621	32.09	6865	.82	98.0	
703.69-	1555	81.60	14433	.77	Steam Injector	
703.69+	2124					
736.84	2124	33.15	5211	.65	∞	
1015.04	2124	278.20	45448	.48	∞	
1063.82	2124	48.78	7969	.52	∞	
1104.39	2124	40.57	6628	.65	73.3	Second Bend
1121.39	2124	17.00	2777	.75	73.3	

TABLE VI

STEADY-STATE AND FIRST NATURAL FREQUENCY RESULTS

Station (in.)	$\bar{p}$ (psi)	M	$\bar{\rho}$ (slugs/ft^3)	T (°R)	u (fps)	Transient Pressure Amplitude (psi)	
8.00	2.500	2.860	5.789×10^{-6}	2520	26234	.3549	
52.30	5.960	2.334	1.126×10^{-5}	3088	23537	.8462	
62.40	6.008	2.321	1.130×10^{-5}	3103	23457	.8531	
90.32	6.088	2.300	1.136×10^{-5}	3126	23325	.8644	
306.40	6.229	2.259	1.152×10^{-5}	3155	23003	.8845	
364.62-	6.322	2.234	1.161×10^{-5}	3177	22827	.8977	Shock here
364.62+	36.72	.4946	4.199×10^{-5}	5103	6312	5.214	
468.10	40.68	.1475	4.550×10^{-5}	5217	1902	5.776	
493.00	40.38	.1483	4.532×10^{-5}	5198	1909	5.734	First Bend
590.00	39.21	.1515	4.470×10^{-5}	5118	1935	5.568	
622.09	38.81	.1526	4.448×10^{-5}	5092	1945	5.512	
703.69	36.45	.3743	4.263×10^{-5}	4989	4726	5.178	Steam Injection
736.84	43.50	.1718	6.853×10^{-4}	2356	584	5.999	
1015.04	43.58	.1666	7.246×10^{-4}	2233	552	6.011	
1063.82	43.60	.1656	7.326×10^{-4}	2209	546	6.013	
1104.39	42.74	.1676	7.289×10^{-4}	2176	549	5.895	Second Bend
1121.39	42.38	.1684	7.279×10^{-4}	2161	550	5.845	

TABLE VII

FORCING FUNCTION FOR FIRST MODE

Station (in.)	F_{Lt} (lb)	F_{Rt} (lb)	F_{LCFt} (lb)	F_{RCFt} (lb)	
8.00					
52.30	565	3758	-	-	
62.40	16	1046	-	-	
90.32	27	2922	-	-	
306.40	76	23029	-	-	
364.62-	39	6322	-	-	Shock here
364.62+			-	-	
468.10	-13391	95318	-	-	
493.00	2	30656	-2	149	First Bend
590.00	5	117260	-7	564	
622.09	3	38030	-3	195	
703.69	10958	76354	-	-	Steam Injection
736.84	21	29122	-	-	
1015.04	2	272917	-	-	
1063.82	1	47907	-	-	
1104.39	1	39461	-2	244	Second Bend
1121.39	.6	16301	-.6	104	

d. Forced Response Results

The NES duct dynamic environmental forces indicated by the scale model tests and by analysis (Subsection III-C-2-c) are incorporated into the dynamic response equations (Subsection III-C-2-a) by use of a digital computer program developed for the lumped parameter model. The two computer solutions were compared and the larger of the forced response parameters were selected. Results of this analysis, using the first six natural modes, are summarized in Table VIII. In this table the maximum bending moment, axial force, and shear at various sections of the duct are given (Figure 14). For stations of the duct not given in Table VIII, adequate values can be obtained by using linear interpolation. (Figures 15 through 17 show the locations of the critical dynamic bending moment, axial force, and shear.) For a complete time and space distribution of the structural response parameters, the complete computer output should be referred to (References 8 and 10). Knowing the forces and moments at the duct station, the maximum normal and shear stresses can be computed from the relationships:

$$f_{nd} = \frac{Mc}{I} + \frac{P}{A_p}$$

$$f_{vd} = \frac{Q}{A_v}$$

These values are shown in column 2 of Tables IX and X, respectively. For the completeness of the report and to verify that the NES duct is within the design limit the static load stresses are also given in column 3 of Tables IX and X. The total (dynamic plus static) stress is then compared with the allowable ambient stress (15,000 psi for normal and 8,000 psi for shear) and the margin of safety is computed and is shown in column 5. Figures 18 and 19 show the locations of the critical-normal and critical shear stresses.

It can be seen that no stresses will be generated during full-scale operation that exceed the given strength allowables established by the duct structural design criteria.

TABLE VIII

MAXIMUM FORCES AND MOMENTS IN NES DUCT

DUCT STATION*	MOMENT, M (IN.-LBS)	AXIAL FORCE, P (LBS)	SHEAR, Q (LBS)
25.9	14000	1755	1065
82.4	106000	8981	2177
92.6	126000	9426	1859
130.6	176000	9754	778
178.8	170000	10103	1118
226.8	85000	10416	2652
274.8	88000	10726	3553
306.4	166000	10696	3785
364.6	100000	10958	3599
408.6	226000	16626	3174
454.2	321000	22898	1719
485.2	292000	25683	5772
519.4	160000	22496	14934
587.9	312000	12581	6598
622.04	264000	13027	6711
663.0	478000	7628	6250
702.8	675000	7755	4935
736.8	789000	7780	3458
781.2	274000	5472	12625
839.6	415000	5326	9695
918.1	877000	5027	5027
996.0	778000	4643	5016
1047.2	523000	4227	7348
1076.6	258000	2454	9767
1121.39	0	0	0

*Duct station is measured along center line of the duct. Station 0.0 corresponds to the top of the duct.

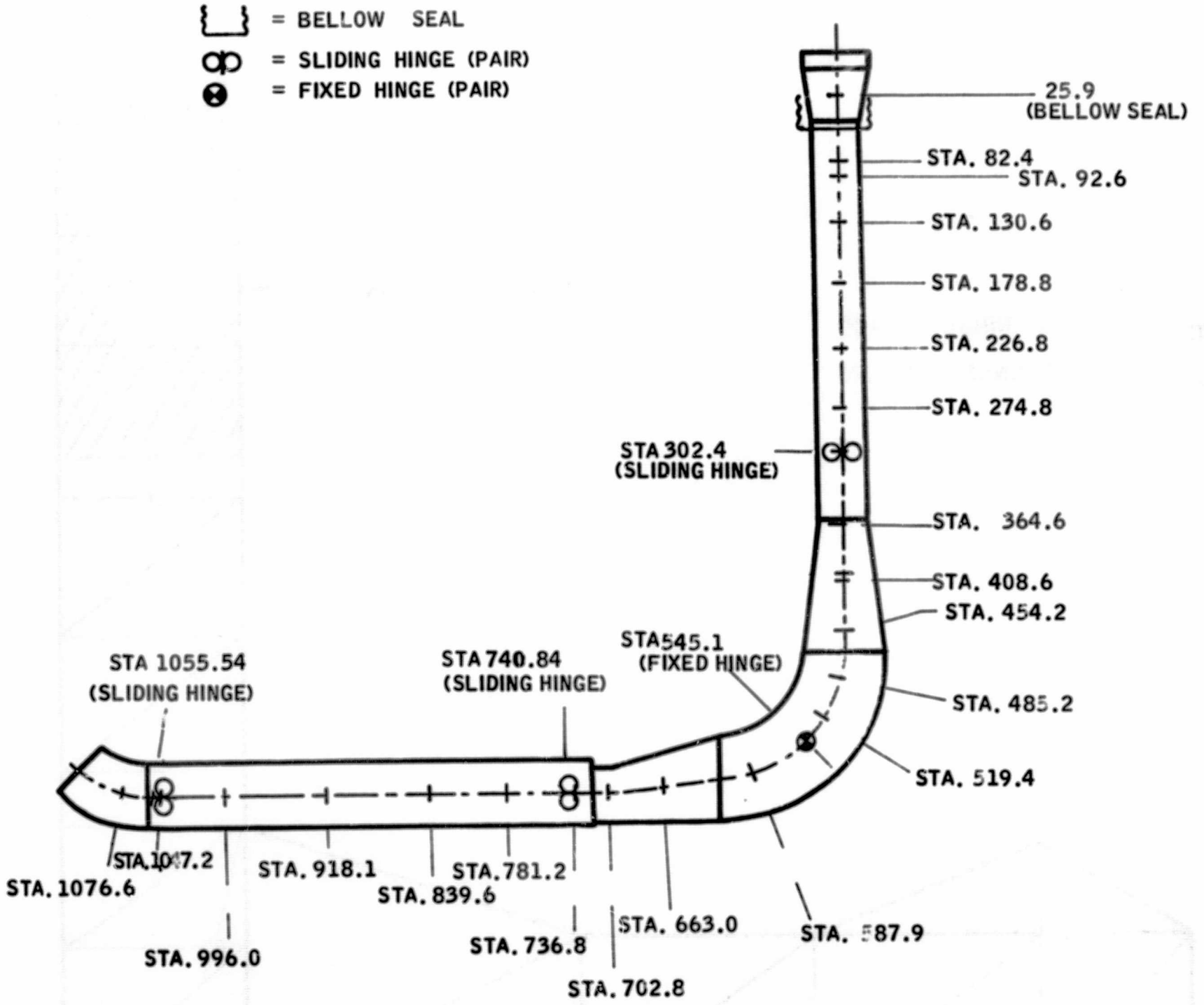

Figure 14

NES Duct Stationing for Stress Calculations

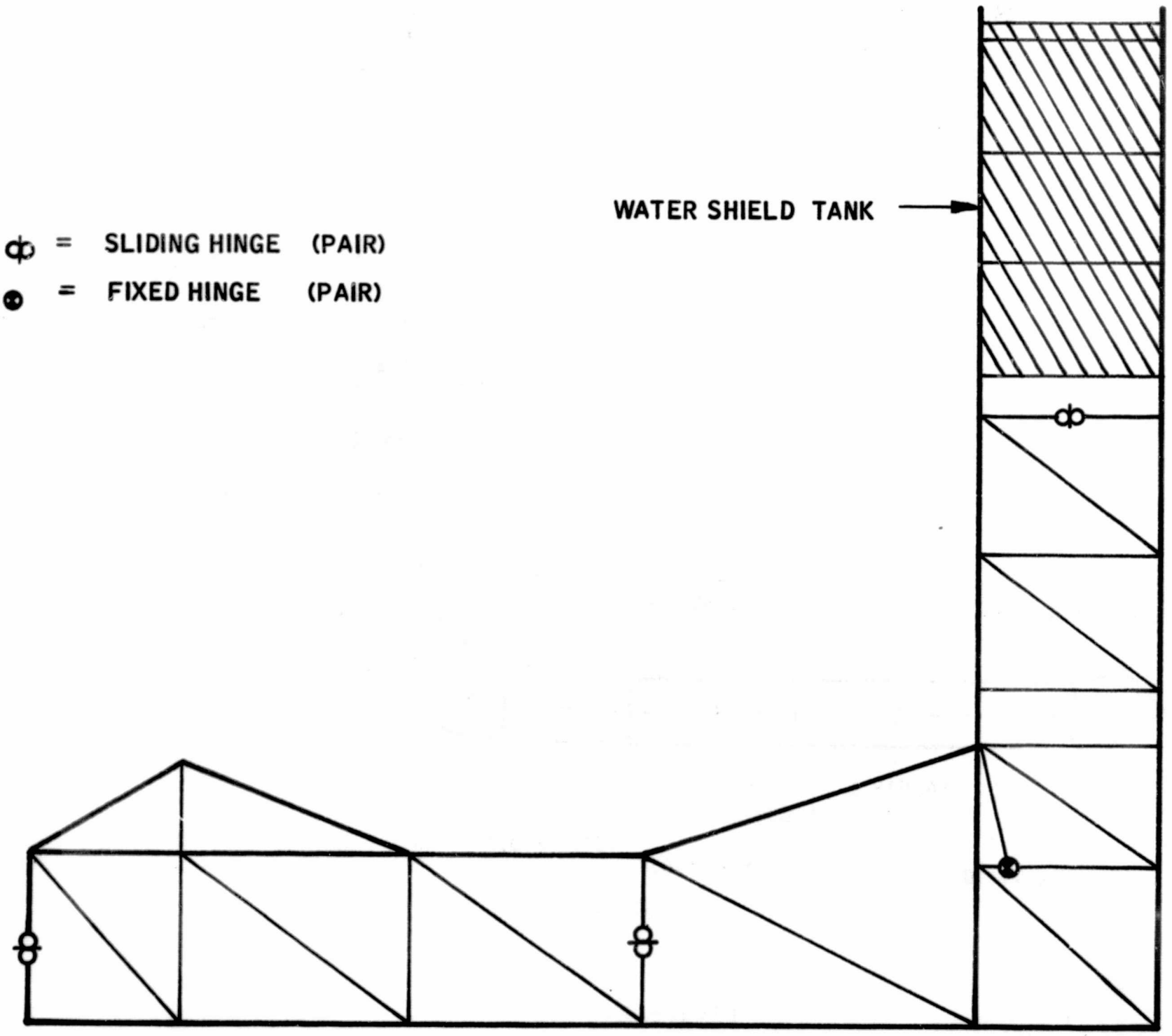

Figure 15

Locations of Critical Dynamic Bending Moment in NES Duct

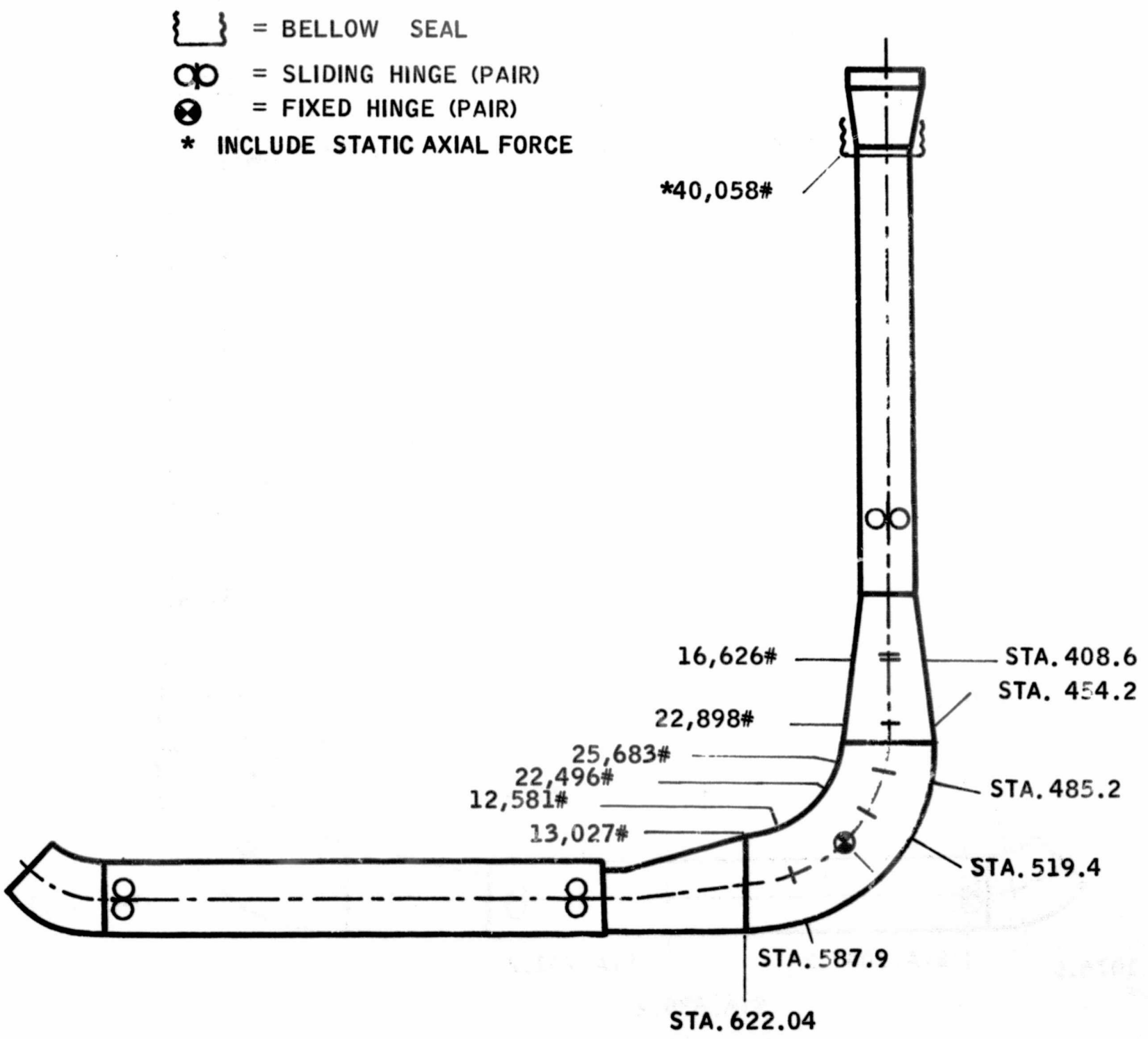

Figure 16

Locations of Critical Dynamic Axial Force in NES Duct

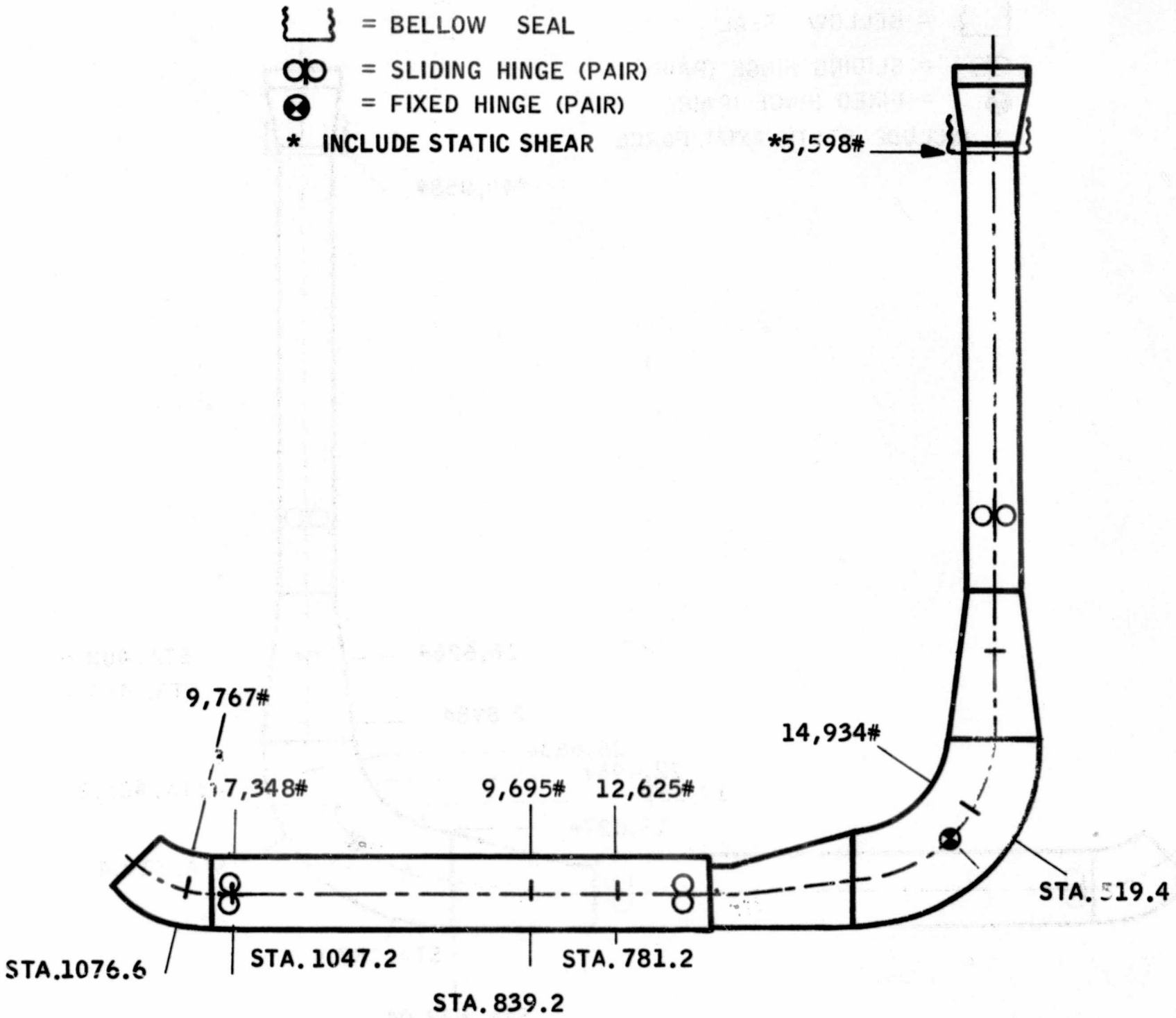

Figure 17

Locations of Critical Dynamic Shear in NES Duct

TABLE IX

MAXIMUM NORMAL STRESS IN NES DUCT

Allowable Normal Stress = 15,000 psi

1	2	3 **	4 = 2 + 3	5
DUCT STATION	DYNAMIC NORMAL STRESS, f_{nd} (psi)	STATIC NORMAL STRESS, f_{ns} (psi)	TOTAL NORMAL STRESS, f_n (psi)	MARGIN OF SAFETY
25.9	25	3307	3332	3.50
82.4	130	3437	3567	3.21
92.3	199	3466	3665	3.09
130.6	606	4391	4997	2.00
178.8	600	4833	5433	1.76
226.8	416	5295	5711	1.63
274.8	430	5734	6164	1.43
306.4	309	4453	4762	2.15
364.6	462	5709	6171	1.43
408.6	724	12748	13472	0.11
454.2	281	10205	10486	0.43
485.2	298	2347	2645	4.67
519.4	181	2218	2399	5.25
587.9	173	2001	2174	5.90
622.04	159	1682	1841	7.15
663.0	699	2549	3248	3.62
702.8	470	1016	1486	9.09
736.8	539	10061	10600	0.42
781.2	572	11917	12489	0.20
839.6	843	11598	12441	0.21
918.1	1641	12103	13744	0.09
996.0	1459	12819	14278	0.05
1047.2	551	11324	11875	0.26
1076.6	281	10207	10488	0.43
1121.39	0	8830	8830	0.70

**From Reference 2

TABLE X

MAXIMUM SHEAR STRESS IN NES DUCT
Allowable Shear Stress = 8,000 psi

1	2	3 **	4 = 2 + 3	5
DUCT STATION	DYNAMIC SHEAR STRESS, f_{vd} (psi)	STATIC SHEAR STRESS, f_{vs} (psi)	TOTAL SHEAR STRESS, f_v (psi)	MARGIN OF SAFETY
25.9	12	0	12	Very Large
82.4	24	44	68	" "
92.6	21	44	65	" "
130.6	32	165	197	39.6
178.8	46	165	211	36.9
226.8	110	165	275	28.1
274.8	147	165	312	24.6
306.4	44	291	335	22.9
364.6	149	1051	1200	5.7
408.6	108	994	1102	6.3
454.2	8	118	126	62.4
485.2	53	218	271	28.5
519.4	138	259	397	19.1
587.9	61	254	315	24.4
622.04	62	326	388	19.6
663.0	171	983	1154	5.9
702.8	25	191	216	36.0
736.8	17	220	237	32.7
781.2	403	244	647	11.4
839.6	310	207	517	14.5
918.1	161	156	317	24.2
996.0	160	201	361	21.2
1047.2	[illegible]	234	469	16.1
1076.6	312	1570	1882	3.3
1121.39	0	0	0	∞

= BELLOW SEAL

= SLIDING HINGE (PAIR)

= FIXED HINGE (PAIR)

ALLOWABLE NORMAL STRESS = 15,000PSI

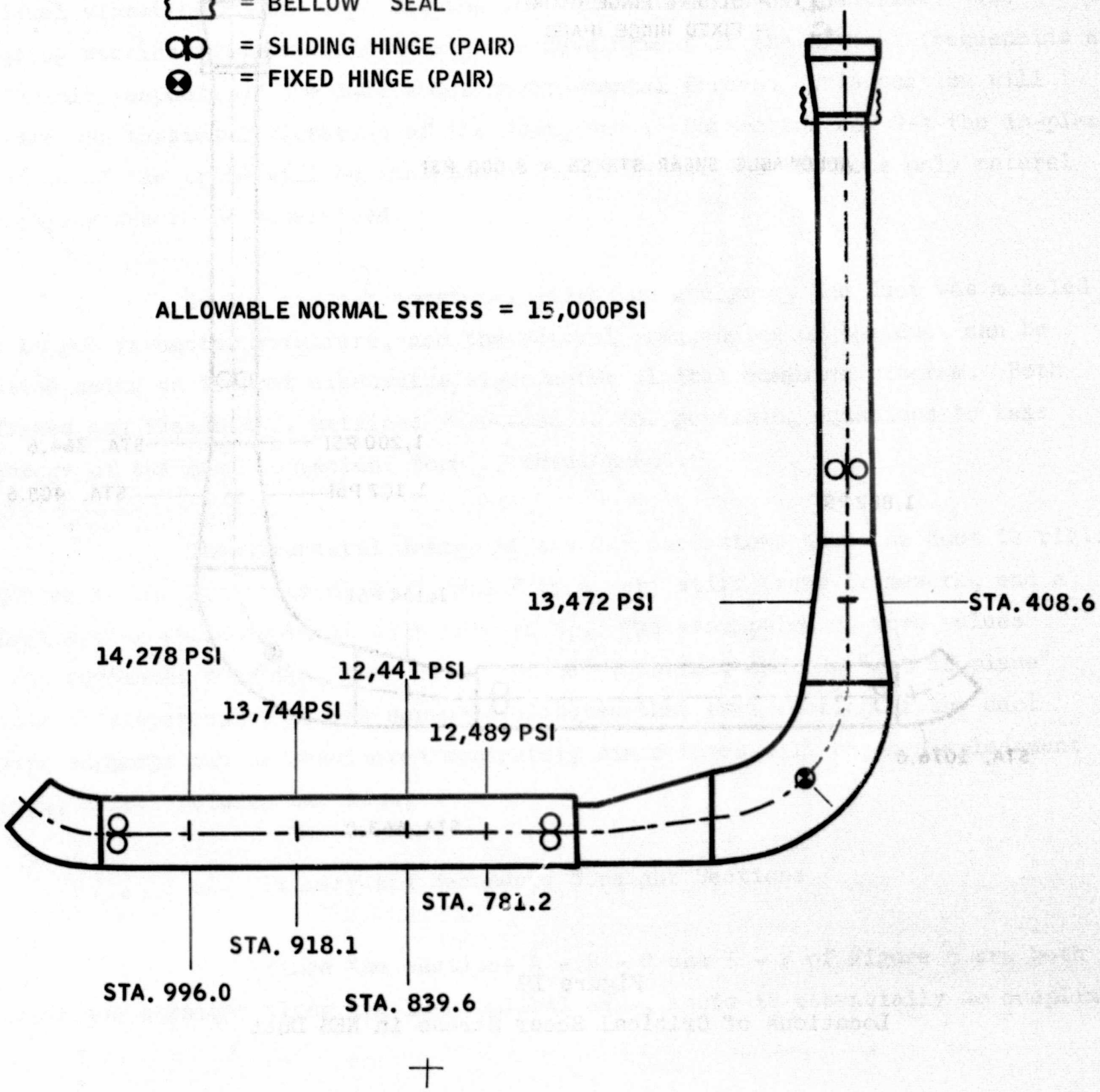

Figure 18

Locations of Critical Normal Stress in NES Duct

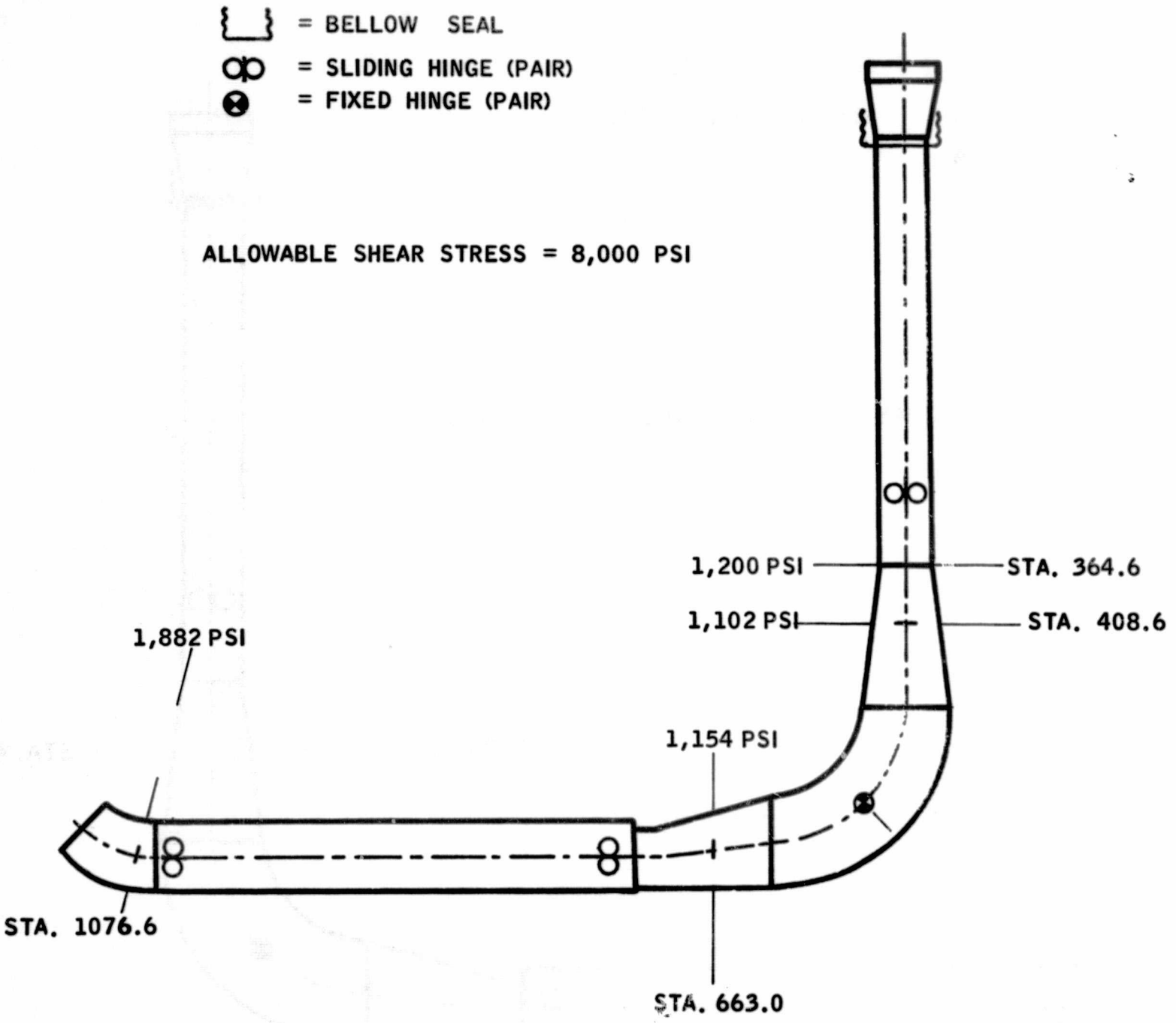

Figure 19

Locations of Critical Shear Stress in NES Duct

3. Duct Torsional Vibration Analysis

A gross development of the dynamic analysis to ensure the structural adequacy of the NES duct-truss system under the environment of nuclear engine operation should not only include the in-plane longitudinal and transverse bending vibration of the duct, but should also include other types of vibration such as the torsional vibration of the duct and the in-plane vibration of the truss. The foregoing sections discussed in detail the development of the natural frequencies and the dynamic response of the duct under environmental forces. This section will consider the torsional vibration of the duct, and in Subsection III-C-4 the in-plane vibration of the truss will be analyzed. In the latter two sections only natural frequencies are to be determined.

In the present torsional vibration analysis, the duct was modeled as a lumped parameter structure, and the natural frequencies of the duct can be obtained using an Aerojet eigenvalue/eigenvector digital computer program. Both stiffness and flexibility matrices were used i. the governing equations to take advantage of the most convenient form of development.

The structural design of the NES duct shows that the duct is rigidly supported at the locations C, D, E, and F by a very stiff truss framework, and a bellows spring attached to it at B (Figure 5). The assumption of zero values for the torsional rotation, the "out of plane" rotation, and the "out of plane" horizontal displacement at the supports dictates that each section of the duct between supports can be considered separately since there will be no displacement coupling effect between sections.

a. Primary and Secondary Straight Sections

Since the sections A - B - C and E - F of Figure 5 are both circular and straight along the longitudinal axis, there is essentially no coupling

between torsional vibrations and any other mode of vibration. The equation of motion for the $i^{\underline{th}}$ mass of an undamped free vibration can be expressed as

$$M_i \ddot{\theta}_i + S_{i,j} \theta_i = 0$$

where the elements in the stiffness matrix $S_{i,j}$ are defined as the force at the $j^{\underline{th}}$ mass when the structure is loaded in a manner such that all masses are restrained against translation except the $i^{\underline{th}}$ mass, which is given a unit rotation. These matrix elements are given by:

$$S_{i,j} = \frac{G J_{i,j}}{L_{i,j}} \quad , j = i - 1, i + 1$$

$$S_{i,j} = 0 \quad , j < i - 1 \text{ and } j > i + 1$$

$$S_{i,i} = -(S_{i,j-1} + S_{i,j+1})$$

where $J_{i,j}$ and $L_{i,j}$ are the polar moment of inertia and distance between the $i^{\underline{th}}$ and $j^{\underline{th}}$ mass, respectively.

b. Curved Sections

For the curves sections C - D, D - E, and F - G of the duct, the torsional vibrations will be coupled with the out-of-plane or horizontal vibrations, since a torsional moment applied at any location along the axis of the duct will cause a torque and an out-of-plane bending moment at the supports.

In each of the curved sections, the duct is statically indeterminate to the third degree. By applying the usual basic structural theory, the three redundant forces and moments can be found. Once the redundant reactions are known the elements in the flexibility matrix can be calculated. The flexibility matrix rather than the stiffness matrix is used in the equilibrium equation because of the nature of the problem. In the calculation of these displacement influence

coefficients the torsional, bending, and shear strain energies are included; and in the dynamic analysis the torsional and horizontal inertia forces alone are considered, as the rotary inertia can be neglected. For the evaluations of the indeterminate problem and the derivation of the displacement influence coefficients refer to Reference 11.

For undamped free vibration the final equation of equilibrium can be given in matrix form as:

$$X = \omega^2 FMX$$

where X is the displacement vector in terms of the angle of twist (θ) and the horizontal displacement (u), and M is the diagonal mass matrix containing both horizontal (J_t) and polar (M_t) moment-of-inertia mass elements. The form of this matrix is:

$$\begin{bmatrix} M_1 & & & & & & & \\ & J_1 & & & & & & \\ & & M_2 & & & & & \\ & & & J_2 & & & & \\ & & & & - & & & \\ & & & & & - & & \\ & & & & & & M_t & \\ & & & & & & & J_t \end{bmatrix}$$

c. Results

The natural frequencies for the straight and curves sections of the NES duct under torsional vibration were obtained from the eigenvalue/ eigenvector computer program and are summarized below:

Natural Frequency Mode \ Section	A - B - C	C - D	D - E	E - F	F - G
1st	101 cps	64 cps	64 cps	126 cps	114 cps
2nd	167	133	139	246	185
3rd	316	147	178	362	400
4th	362	233	207	474	450

d. Conclusions

The gas dynamic forces from the engine will not excite torsional moments directly onto the duct; furthermore, the duct has a high torsional rigidity due to its stiff structural members and the attached stiff-truss-framework. Therefore, torsional modes (although present) will have a negligible effect on the overall dynamic program.

4. Truss Frame Analysis

a. Method of Analysis

The gas dynamic forces are primarily in the plane of the duct (as in the case of the duct analysis) and, therefore, in the plane of the truss, major vibration will consist of the in-plane motions. It is thus, possible to analyze the significant vibration problems by considering the truss as a planar frame. Futhermore, the assumption of a no-coupling effect between the truss and the duct greatly simplifies the computation. This assumption is valid since the truss frequencies are low compared to the duct frequencies; thus, the duct will behave as an additional mass attached to the truss, whose flexibility does not grossly affect the truss frequencies.

To expedite the computation of the truss stiffness data for free vibration analysis the truss joints are conservatively being treated as pin-connected. This reduction of the truss frame to a statically determinant structure

greatly reduces the complexity of determining the stiffness influence coefficients. For a pin connected truss the stiffness coefficient of any joint is a function only of members framing into that joint, with half the total panel mass preperties located at each joint. Thus, knowing the geometry and member preperties, the stiffness matrix can be obtained by algebraic calculations. The water shield tank at the upper truss assembly forms a rigid diaphragm deck and can be approximated by a three bar frame. Figure 20 shows the actural truss structure, and Figure 21 shows a schematic idealized representation of the truss with joint numbers and coordinates orientation. Four dummy diagonal members were introduced at joints 12-18, 16-17, 21-24 and 22-23 in order to define a pin-connected configuration. Calculations for these equivalent dummy diagonal member cross sections were made based on the force-deflection characteristics of the truss members. The usual strain energy technique and Castigliano's Theorem were employed. The equation for the deflection is given by:

$$\Delta_{\text{at p}} = \int_0^{\ell} \frac{M}{EI} \frac{\partial M}{\partial P} ds + \int_0^{\ell} \frac{kV}{AG} \frac{\partial V}{\partial p} ds$$

Knowing the deflection characteristics, the cross section of the dummy diagonal members can be obtained based on the relationship:

$$\Delta = \frac{P\ell}{AE}$$

The stiffness representation of the truss assembly is in the form of a set of influence coefficients at each joint. The calculation of these coefficients was based on the work done by the axial forces of the truss members and not by bending, except at the butterfly trusses where bending must be included in the calculations.

= BELLOW SEAL

= SLIDING HINGE (PAIR)

= FIXED HINGE (PAIR)

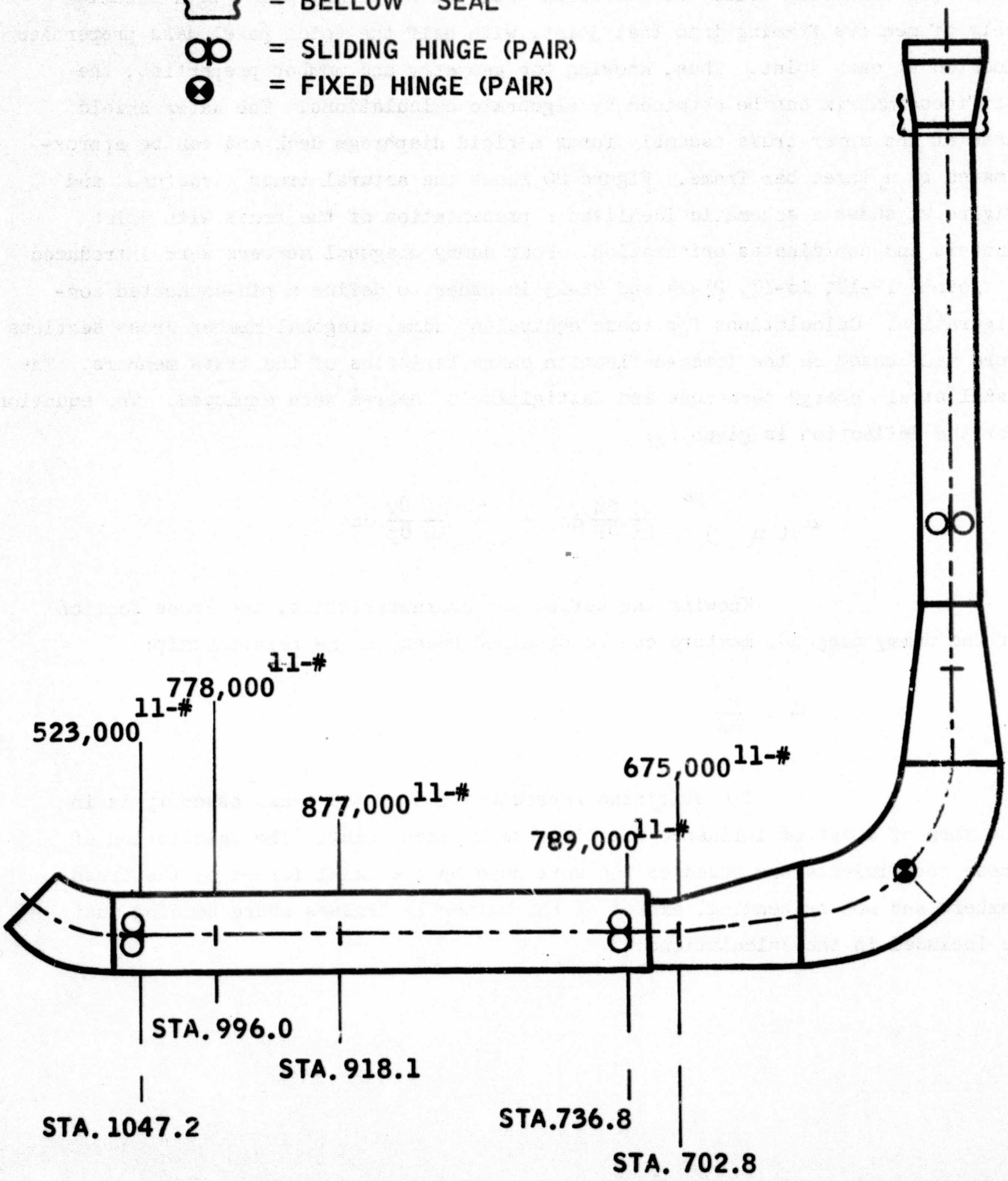

Figure 20

Actual Truss Structure

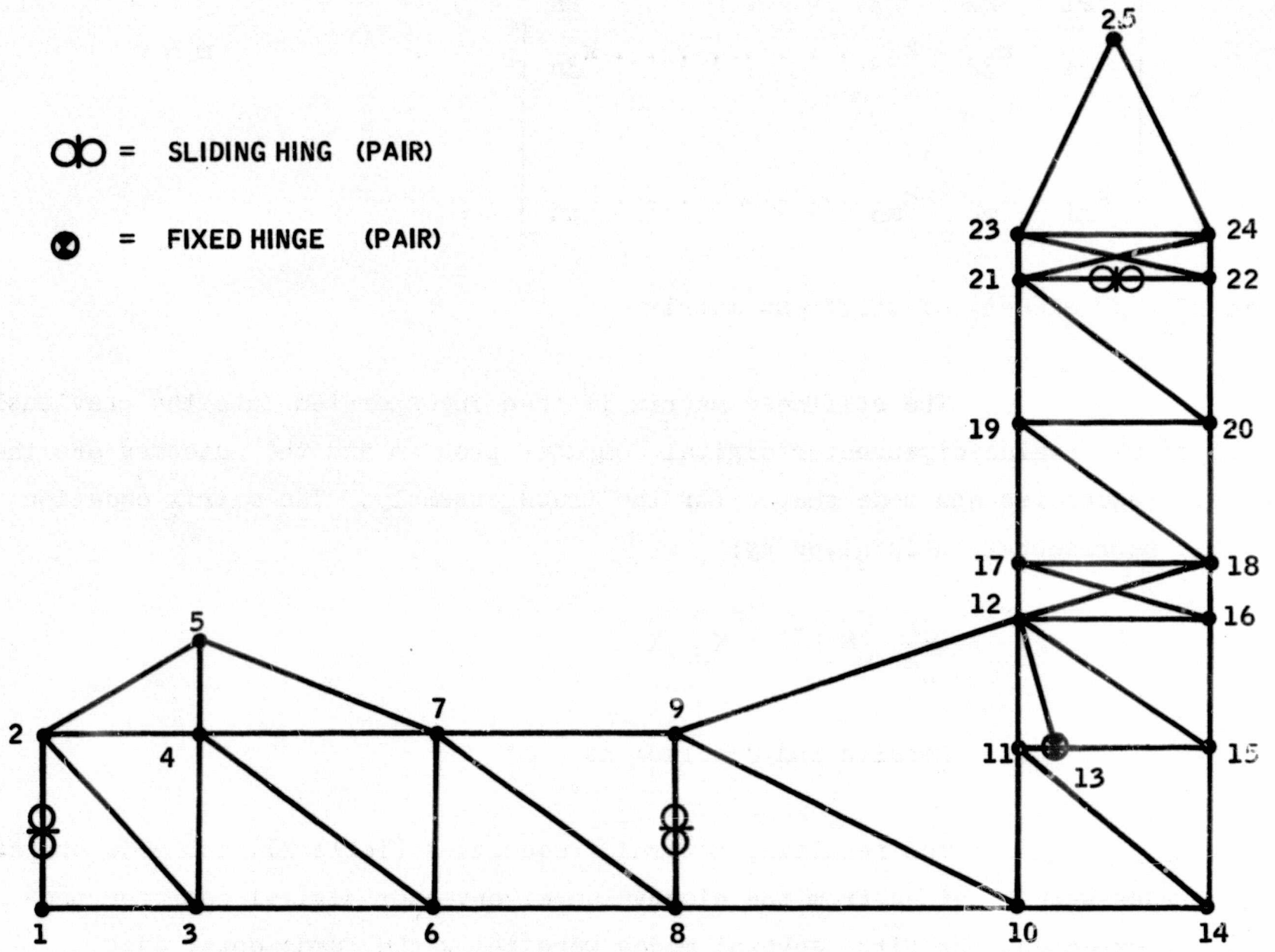

Figure 21

Idealized Representation of Truss for Plane Frame Analysis

The final stiffness matrix is given by (see Reference 12):

$$K = \begin{bmatrix} k_{11} & k_{12} & k_{13} \cdots\cdots\cdots k_{1n} \\ k_{21} & k_{22} & k_{23} \cdots\cdots\cdots k_{2n} \\ k_{31} & k_{32} & k_{33} \cdots\cdots\cdots k_{3n} \\ \\ \\ k_{m1} & k_{m2} & k_{m3} \cdots\cdots\cdots k_{mn} \end{bmatrix} \qquad m = n$$

where k_{ij} = element of stiffness matrix

The stiffness matrix is then incorporated into the previously developed eigenvalue/eigenvector digital computer program and the outcomes are the natural frequencies and mode shapes for the truss assembly. The matrix equation for this representation is given by:

$$X = \frac{1}{\omega^2} \left[M\right]^{-1} \left[K\right] X$$

b. Results and Conclusions

The resulting natural frequencies (Table XI) and mode shapes of the truss were obtained from the eigenvalue/eigenvector digital computer program. As expected, the first several modes were below the fundamental duct frequency. The complete modal data are presented in Table XII through XVI, and the mode shapes are plotted in Figures 22 through 31. Major response of the truss occurs at the fifth mode frequency of 20.7 cps. The first duct natural frequency having appreciable displacement in the region of the truss exhibiting high response is the fourth duct mode of 45.9 cps. Because of this wide difference in frequencies true dynamic coupling between the duct and truss need not be considered when estimating response. Thus, the duct will follow the slower vibration of the truss as well as vibrating in its own modes. Any dynamic coupling that does tend to take place will be a dissipating rather than an enhancing effect.

TABLE XI

NATURAL FREQUENCY OF TRUSS FRAME

MODE NO.	NATURAL FREQUENCY (cps)
1	6.66
2	8.76
3	14.62
4	16.55
5	20.69
6	22.60
7	28.68
8	31.23
9	44.39
10	49.94

TABLE XII

FIRST AND SECOND MODAL DATA OF TRUSS

	Mode No. 1 Omega 41.84 radians/sec. Frequency 6.66 cps M = 147.21 lb. sec.^{2}/in.		Mode No. 2 Omega 55.04 radians/sec. Frequency 8.76 cps M = 211.79 lb. sec.^{2}/in.	
NJ	Q (x)	Q (y)	Q (x)	Q (y)
1	-.488	.127	.860	-.270
2	-.311	.127	.553	-.269
3	-.447	-.003	.856	.023
4	-.314	-.008	.558	.047
5	-.225	-.008	.355	.047
6	-.441	-.193	.837	.527
7	-.323	-.197	.598	.548
8	-.426	-.243	.771	.707
9	-.364	-.227	.709	.685
10	-.452	-.162	.703	.182
11	-.486	-.141	.995	.138
12	-.392	-.090	.915	.070
13	-.492	-.127	1.000	.106
14	-.514	-.330	.763	.005
15	-.528	-.372	.963	.044
16	-.400	-.420	.902	.058
17	-.318	-.078	.863	.062
18	-.324	-.441	.843	.062
19	-.068	-.047	.718	.043
20	-.085	-.504	.642	.035
21	.232	-.032	.502	.052
22	.199	-.576	.417	-.038
23	.381	-.027	.528	.060
24	.385	-.596	.537	-.056
25	1.000	-.315	.694	0

Q (x) = x Displacement amplitude
Q (y) = y Displacement amplitude
NJ = Joint number
M = Generalized mass

TABLE XIII

THIRD AND FOURTH MODAL DATA OF TRUSS

	Mode No. 3 Omega 91.85 radians/sec. Frequency 14.62 cps M = 67.29 lb. sec.^{2}/in.		Mode No. 4 Omega 103.99 radians/sec. Frequency 16.55 cps M = 167.03 lb. sec.^{2}/in.	
NJ	Q (x)	Q (y)	Q (x)	Q (y)
1	-.076	-.297	.149	-.208
2	-.370	-.293	-.065	-.205
3	-.075	.010	.147	.022
4	-.357	.033	-.055	.053
5	-.561	.032	-.219	.051
6	-.091	.501	.122	.432
7	-.297	.520	.009	.457
8	-.150	1.000	.040	.664
9	-.272	.997	.080	.650
10	-.385	.277	-.174	-.434
11	-.344	.230	-.012	-.481
12	-.123	.202	.383	-.522
13	-.346	.189	-.011	-1.000
14	-.410	.102	-.170	-.652
15	-.292	.088	.111	-.636
16	-.123	.100	.363	-.566
17	-.097	.185	.323	-.500
18	-.095	.105	.295	-.536
19	-.059	.141	.226	-.434
20	-.051	.117	.131	-.488
21	-.005	.153	-.088	-.527
22	-.001	.133	-.109	-.490
23	.007	.156	-.188	-.548
24	.005	.138	-.176	-.493
25	.030	.154	-.304	-.552

TABLE XIV

FIFTH AND SIXTH MODAL DATA OF TRUSS

	Mode No. 5 Omega 130.00 radians/sec. Frequency 20.69 cps M = 22.67 lb. sec.^{2}/in.		Mode No. 6 Omega 142.01 radians/sec. Frequency 22.60 cps M = 181.18 lb. sec.^{2}/in.	
NJ	Q (x)	Q (y)	Q (x)	Q (y)
1	.385	-1.000	-.329	.408
2	-.162	-.976	-.137	.396
3	.375	-.216	-.319	.100
4	-.079	-.263	-.171	.119
5	-.598	-.258	.032	.117
6	.211	-.071	-.225	.119
7	-.020	-.112	-.193	.132
8	.119	-.118	-.154	.335
9	-.015	-.136	-.223	.321
10	.080	-.009	-.116	.107
11	.003	-.014	.536	.068
12	-.070	-.010	-.274	-.027
13	.002	.026	.545	.658
14	.069	.029	-.005	-.287
15	-.019	.018	.189	-.200
16	-.077	.001	-.380	-.282
17	-.094	-.009	-.560	-.060
18	-.097	-.007	-.642	-.323
19	-.115	-.007	-.934	-.135
20	-.107	-.034	-1.000	-.568
21	-.065	-.006	-.790	-.219
22	-.053	-.055	-.688	-.819
23	-.048	-.006	-.685	-.242
24	-.048	-.062	-.677	-.901
25	.013	-.037	-.012	-.635

TABLE XV

SEVENTH AND EIGHTH MODAL DATA OF TRUSS

	Mode No. 7 Omega 180.22 radians/sec. Frequency 28.68 cps M = 80.50 lb. sec.^{2}/in.		Mode No. 8 Omega 196.20 radians/sec. Frequency 31.23 cps M = 53.40 lb. sec.^{2}/in.	
NJ	Q (x)	Q (y)	Q (x)	Q (y)
1	.694	.228	-1.000	-.139
2	.663	.218	-.883	-.131
3	.659	.081	-.941	-.074
4	.587	.085	-.792	-.080
5	.768	.081	-.955	-.075
6	.637	.177	-.845	-.207
7	.457	.176	-.632	-.210
8	.573	.128	-.677	-.001
9	.336	.075	-.489	.040
10	.476	.057	-.417	.054
11	-.025	.030	.395	.041
12	-.030	.032	-.117	-.088
13	-.029	-.378	.413	-.240
14	.457	.491	-.221	-.146
15	.078	.437	.242	.010
16	-.118	.426	-.145	.058
17	-.436	.063	-.231	-.057
18	-.500	.409	-.240	.076
19	-1.000	.145	-.295	.027
20	-.886	.195	-.210	.098
21	-.466	.315	.005	.123
22	-.336	.072	.039	.174
23	-.230	.353	.078	.145
24	-.258	.035	.061	.199
25	.235	.238	.062	.216

TABLE XVI

NINTH AND TENTH MODAL DATA OF TRUSS

	Mode No. 9 Omega 278.89 radians/sec. Frequency 44.39 cps M = 107.37 lb. sec.^{2}/in.		Mode No. 10 Omega 313.80 radians/sec. Frequency 49.94 cps M = 10.12 lb. sec.^{2}/in.	
NJ	Q (x)	Q (y)	Q (x)	Q (y)
1	-.487	-.077	.156	-.003
2	-.326	-.068	-.112	-.002
3	-.430	-.042	.133	.266
4	-.243	-.021	-.062	.452
5	-.400	-.015	-.459	.466
6	-.344	-.097	.051	1.000
7	-.073	-.076	.153	.977
8	-.241	-.149	-.195	-.078
9	.144	-.063	.088	-.126
10	-.057	.231	-.090	-.095
11	-.069	.270	.007	-.051
12	.553	.306	.016	-.020
13	-.071	-.076	.008	.010
14	-.086	.204	-.010	-.145
15	.141	.168	-.015	-.117
16	.711	.214	.003	-.093
17	.997	.319	-.007	-.016
18	.988	.237	-.019	-.082
19	.888	.306	-.016	-.004
20	.230	.215	-.031	-.041
21	-.959	.415	-.009	.012
22	-1.000	-.207	-.009	-.001
23	-.948	.490	-.006	.017
24	-.994	-.343	-.011	.011
25	.215	.135	.002	.003

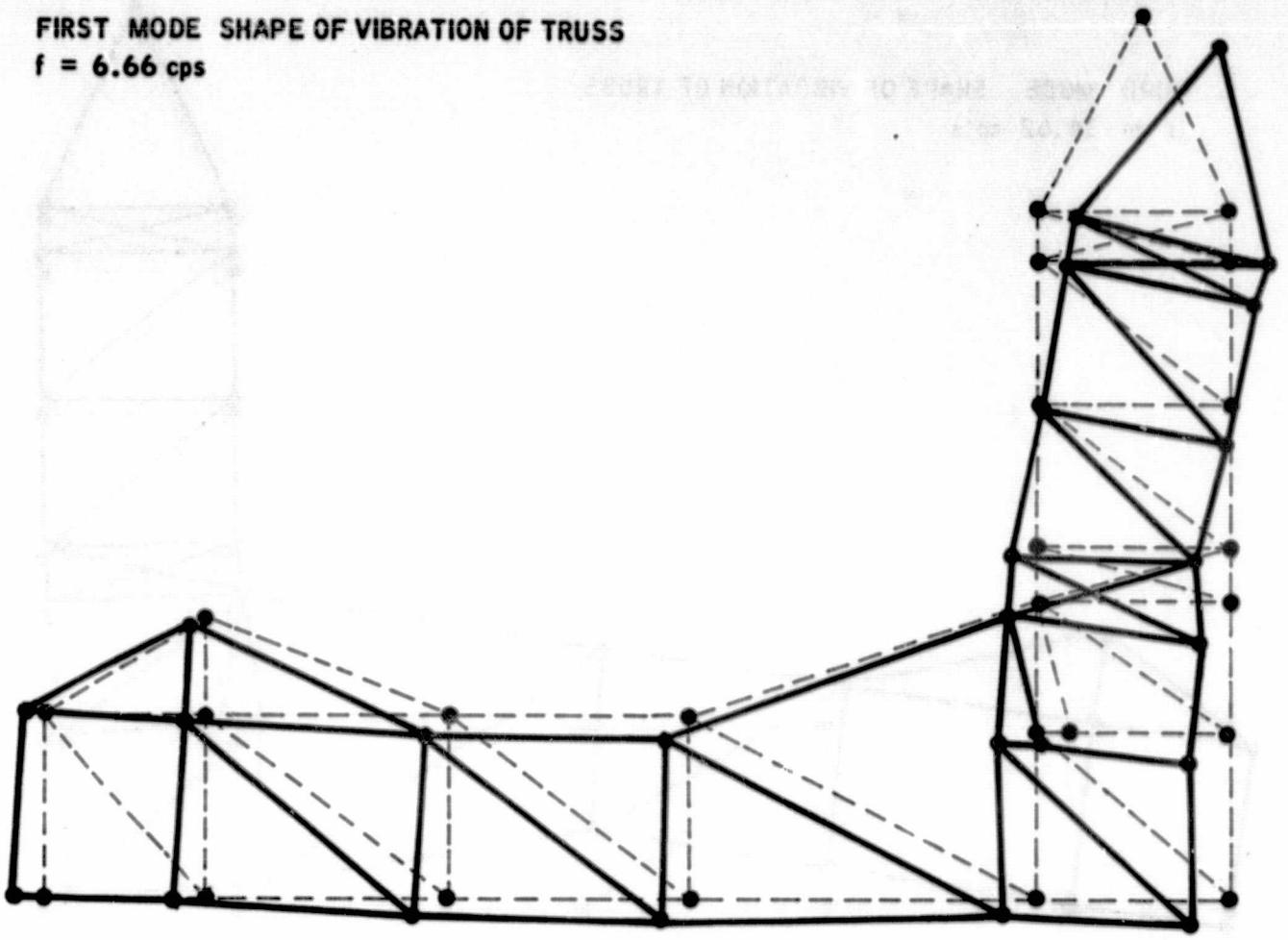

Figure 22

First Mode Shape of Vibration of Truss

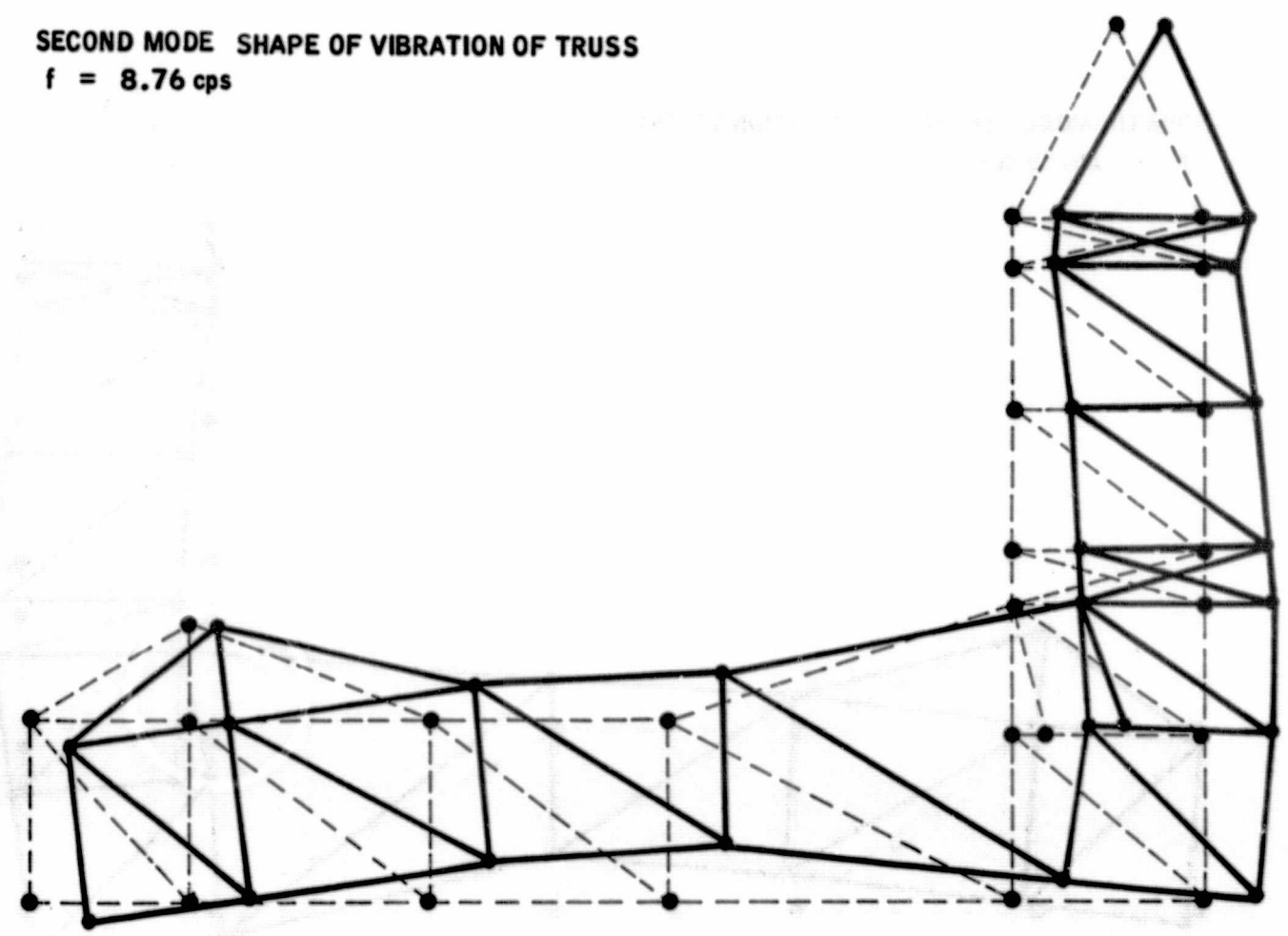

Figure 23

Second Mode Shape of Vibration of Truss

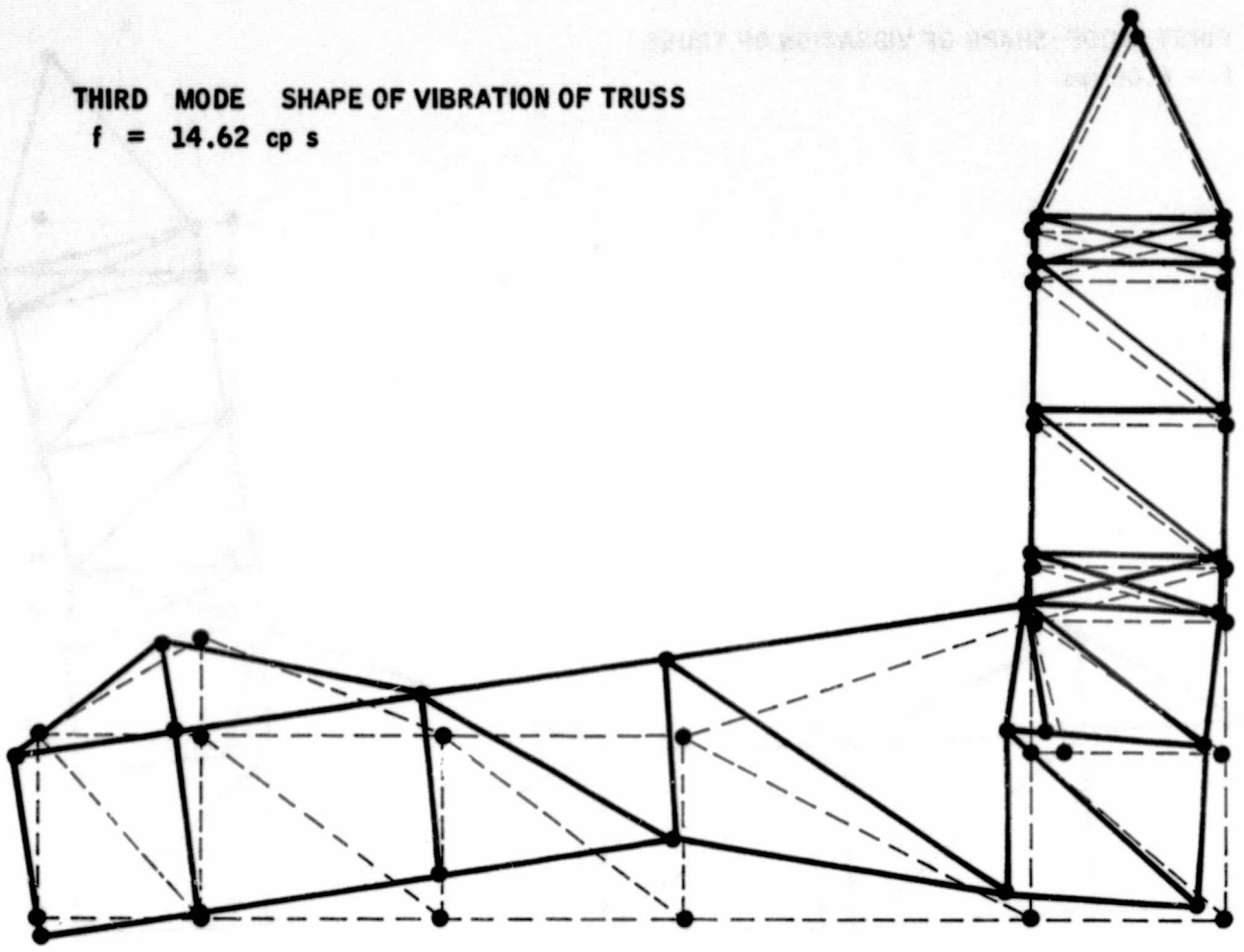

Figure 24

Third Mode Shape of Vibration of Truss

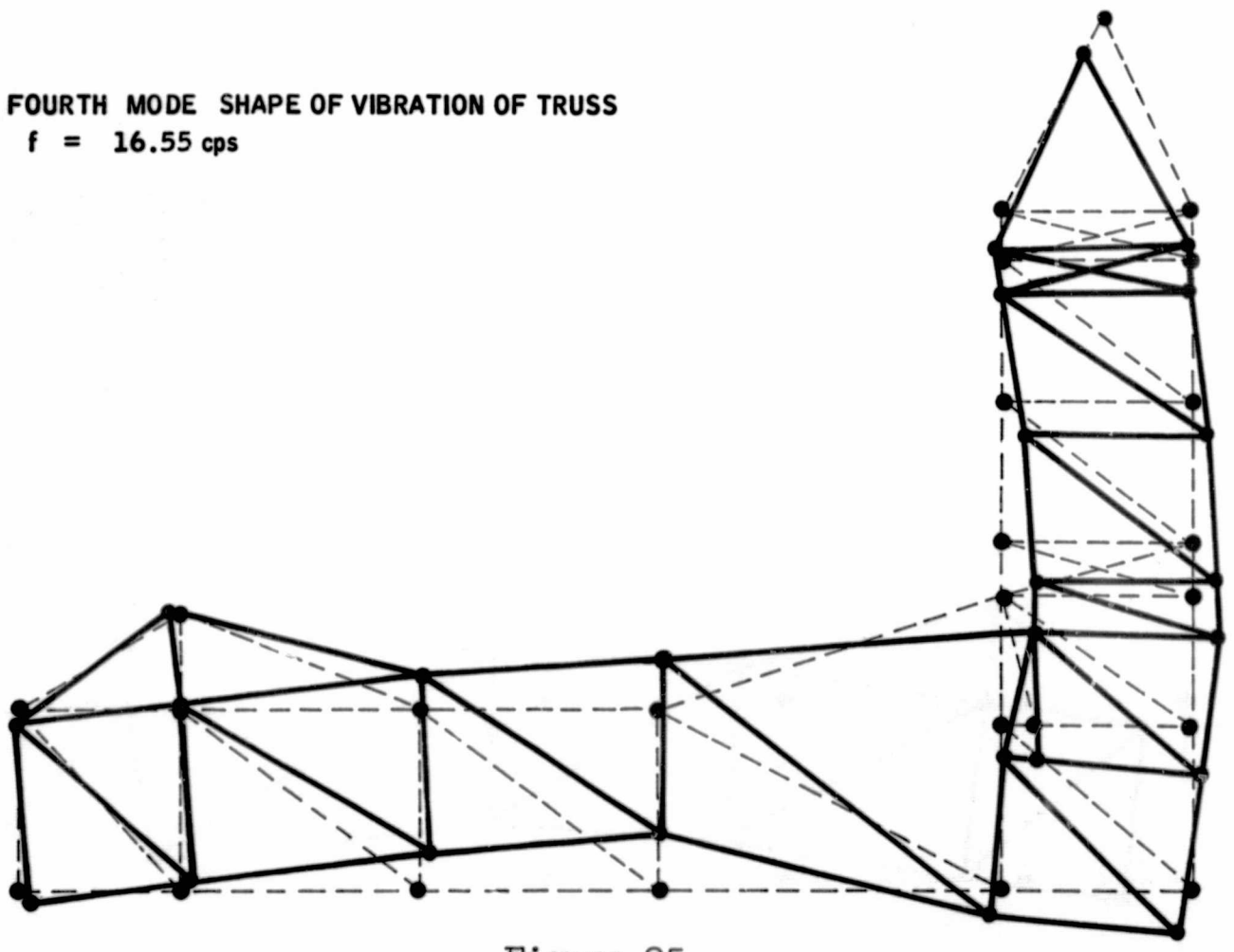

Figure 25

Fourth Mode Shape of Vibration of Truss

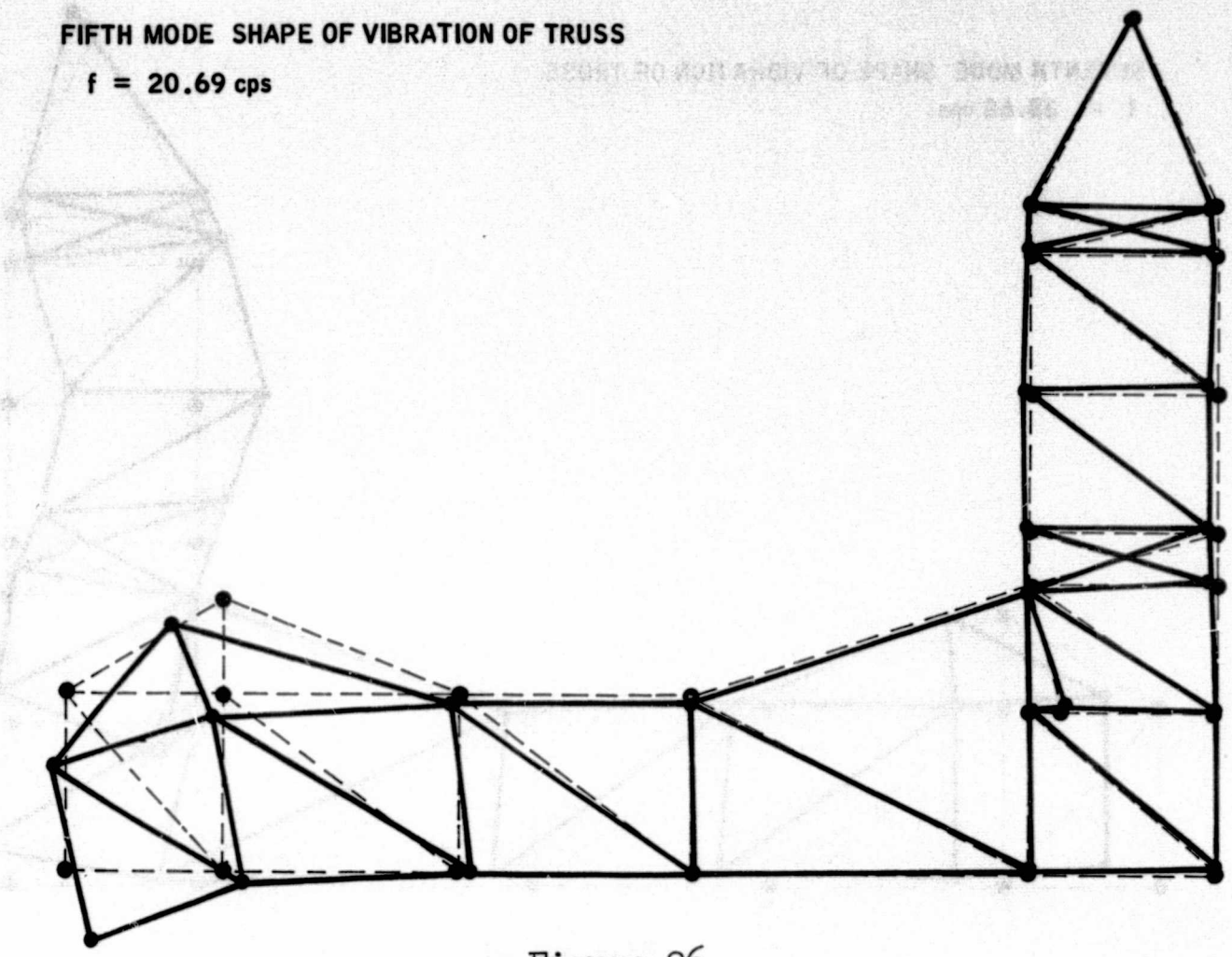

Figure 26

Fifth Mode Shape of Vibration of Truss

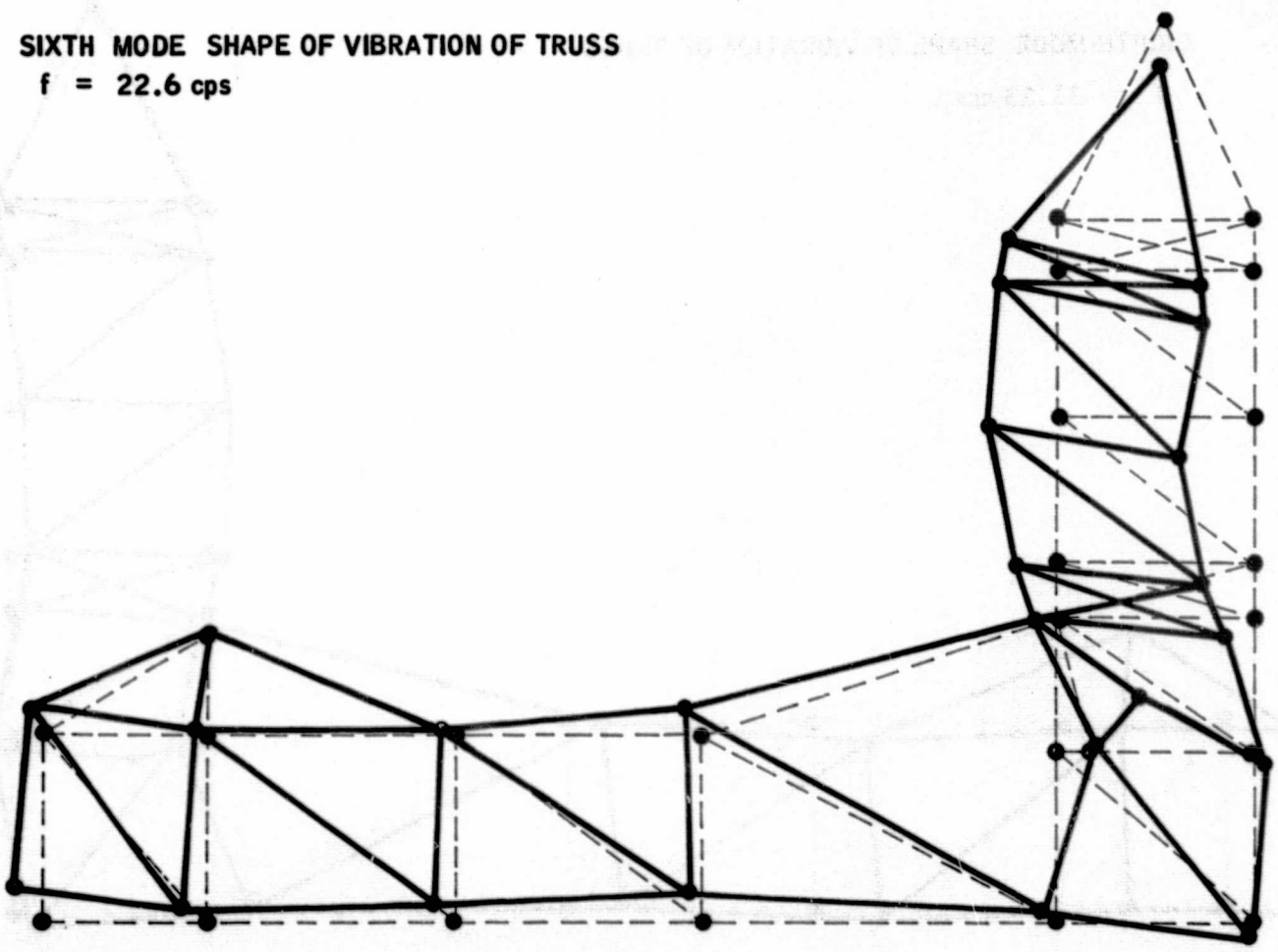

Figure 27

Sixth Mode Shape of Vibration of Truss

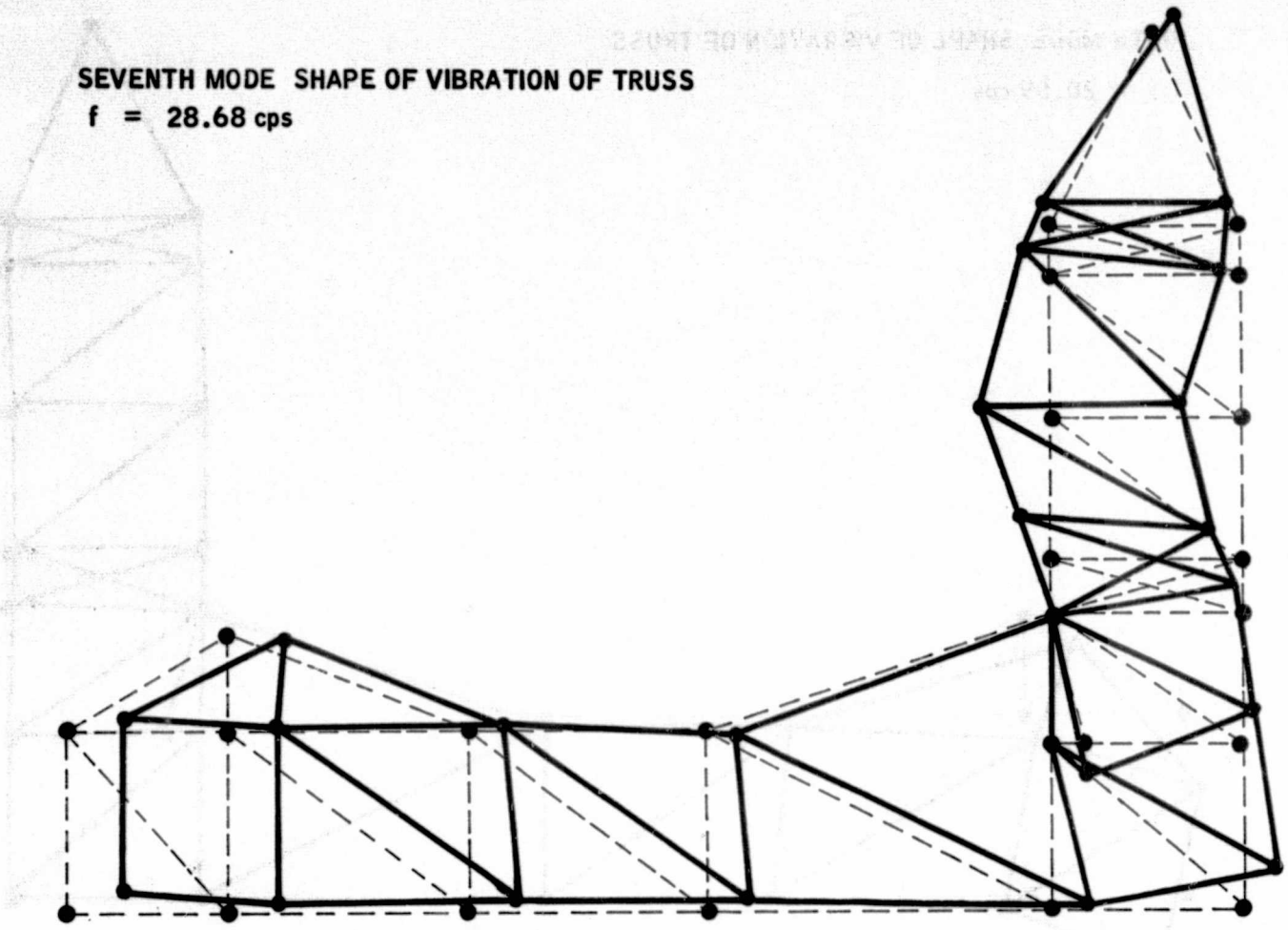

Figure 28

Seventh Mode Shape of Vibration of Truss

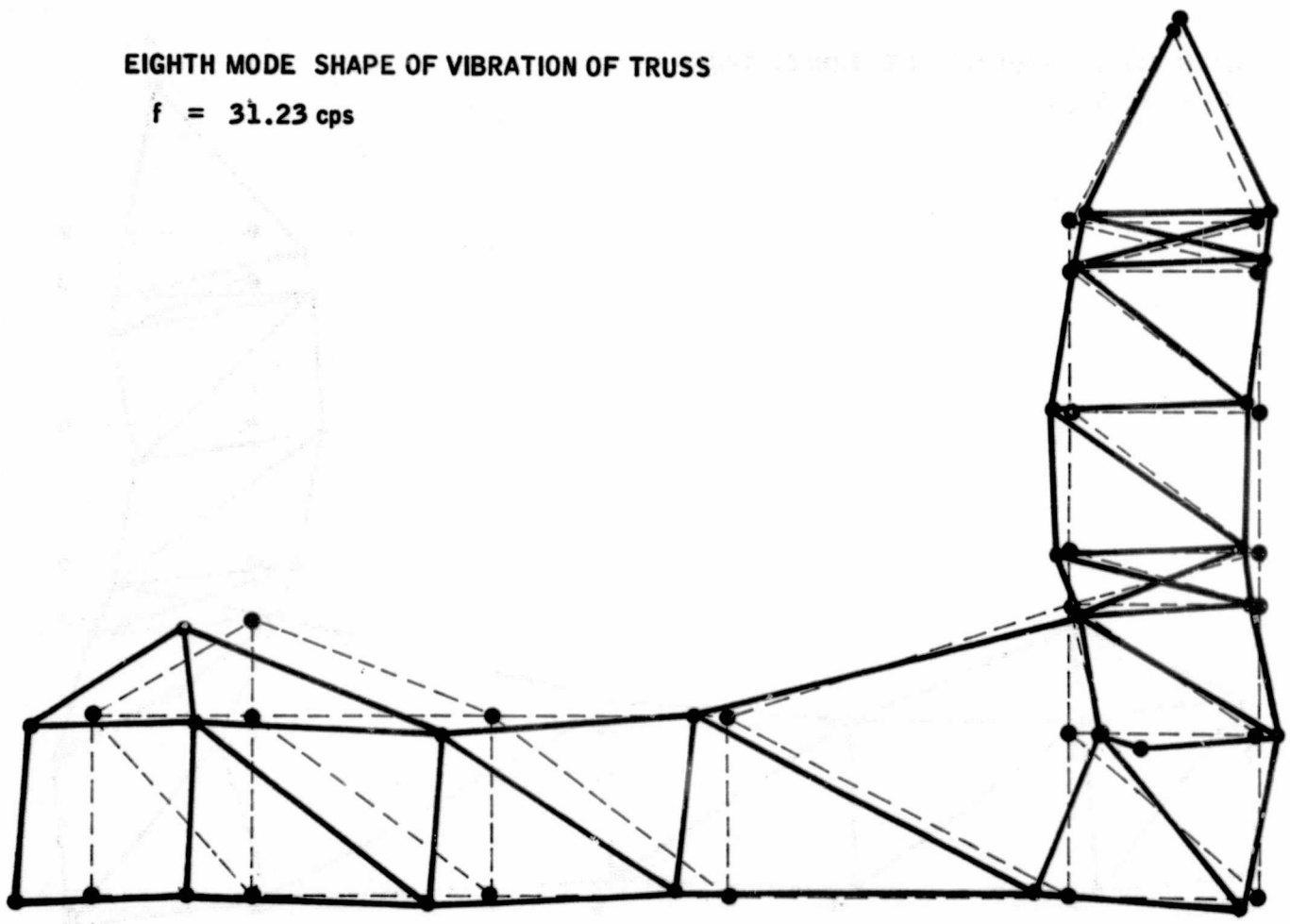

Figure 29

Eighth Mode Shape of Vibration of Truss

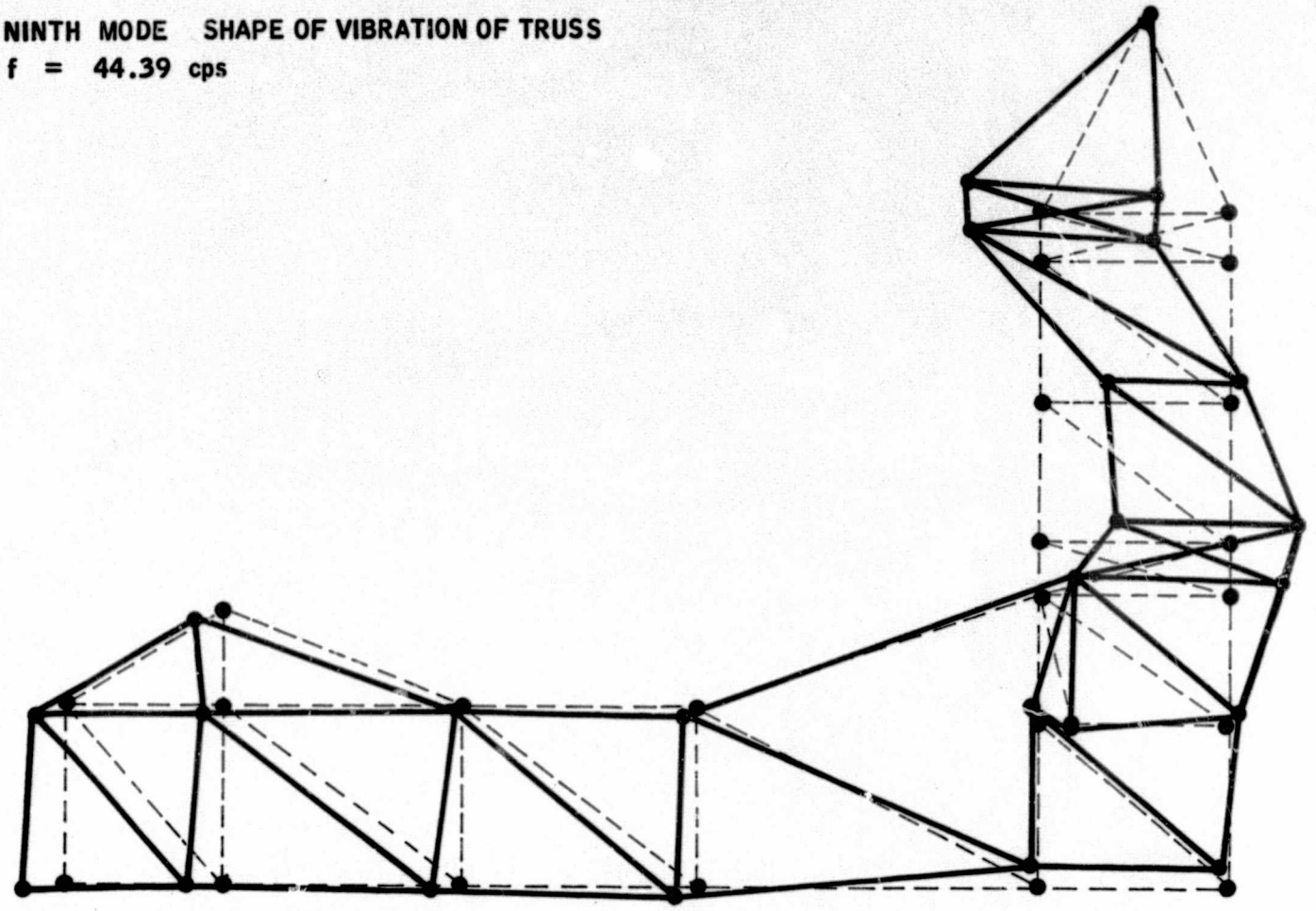

Figure 30

Ninth Mode Shape of Vibration of Truss

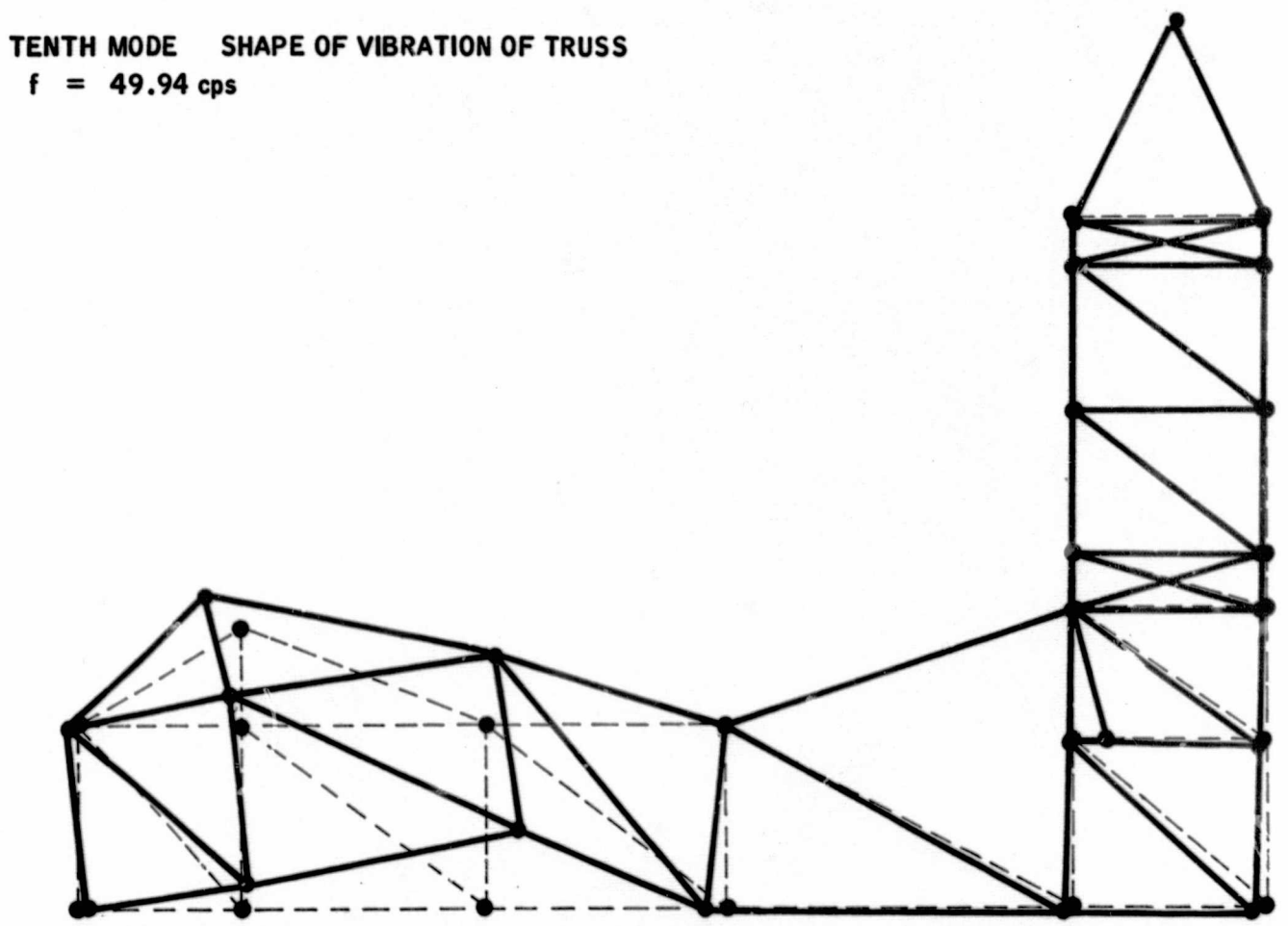

Figure 31

Tenth Mode Shape of Vibration of Truss

IV. CONCLUSIONS

The tabulated results of Tables IX and X, Subsection III-C-2-d, show the margin of safety as low as +0.05. In calculating the structural dynamic response parameters (moments and forces) of the duct, a rather conservative viscous damping of 1/2% of the critical damping and an 0.10 coefficient of sliding friction have been used (Reference 13).

In addition, the methods of predicting the forcing function profiles were overly conservative, especially for the character of loadings observed on the scale model ducts. Although extrapolation of scale model data to prototype data is not an exact solution, studies of one-eighth and one-quarter scale data indicate decreasing severity of the gas dynamics forces with increasing size. Startup pressure fluctuations which were very severe in the one-eighth scale model were less than severe in the one-quarter scale model. Flame "popping" experienced in the one-eighth scale data was considered a major source of excitation, however, this was virtually non-existent in the one-quarter scale model. Thus, it appears that in the prototype duct the environment (due to the duct geometry) will be less harsh than that predicted from the scale model tests.

Considering that the NES duct is overly designed and based on allowable ambient design normal and shear stresses of 15,000 and 8,000 psi, respectively, the combined dynamic and static environment cannot cause any stress which exceeds the allowables given above.

Although no dynamic stresses are calculated for the truss structure, the dynamic effect was included in the structural design (see Reference 14).

In this report, a complete and comprehensive approach to the dynamic problem of the NES duct and truss structure is presented. In addition, five operational computer programs (Flexibility Matrix, Eigenvalue/Eigenvector, Dynamic Response, Plane Frame Stiffness Matrix, and Torsional Flexibility Matrix) have been developed. This series of digital computer programs, together with the methods and techniques outlined in this report, should allow dynamic evaluations to proceed along with the design of any future exhaust duct or similar structure.

"Page missing from available version"

Appendix

1. Eigenvalue-Eigenvector

In the most general case, the mathematical formulation of the free vibrations of an undamped elastic structure which moves with many degrees of freedom may be described in terms of a set of algebraic equations of the form:

$$\begin{aligned}
a_{11}x_1 + a_{12}x_2 + \cdots + a_{1n}x_n &= \omega^2 M_1 x_1 \\
a_{21}x_1 + a_{22}x_2 + \cdots + a_{2n}x_n &= \omega^2 M_2 x_2 \\
&\cdots\cdots\cdots\cdots \\
a_{n1}x_1 + a_{n2}x_2 + \cdots + a_{nn}x_n &= \omega^2 M_n x_n
\end{aligned} \qquad \text{(A-1)}$$

where the a_{ij} represent constant coefficients, depending on the elasticity of the structure, and the M_j represent magnitudes of the lumped mass. The unknowns are the displacements amplitudes x_j and the natural frequency ω.

The set of equations (A-1) may be expressed in the matrix form:

$$(a - \omega_i^2 M)\, x_i = 0 \qquad \text{(A-2)}$$

This set of equations described by (A-2) is a set of algebraic, linear, homogeneous equations. A nontrivial solution is possible if and only if:

$$\left| a - \omega_i^2 M \right| = \begin{vmatrix} (a_{11} - \omega_i^2 M_1) & a_{12} & \cdots & a_{1n} \\ a_{21} & (a_{22} - \omega_i^2 M_2) & \cdots & a_{2n} \\ a_{n1} & a_{n2} & \cdots & (a_{nn} - \omega_i^2 M_n) \end{vmatrix} = 0 \qquad \text{(A-3)}$$

When this determinant is expanded, we obtain an n^{th} order equation in ω_i^2, known as the characteristic equation (or frequency equation). The roots $\omega_1, \omega_2, \cdots, \omega_n$ of the characteristic equation are known as the eigenvalues (or characteristic values). The set of values of x_i corresponding to a particular value of ω_i is known as the i^{th} eigenvector (or characteristic vector).

2. Lumped Parameter Method

A procedure that is useful in many vibration problems for finding approximations to both the natural frequencies and the mode shapes is the reduction of the system with distributed parameters to one having a finite number of degree-of-freedom. This procedure, known as the lumped parameter method, is done by lumping the parameters for each small region into an equivalent mass and elastic element interconnected by an elastic spring.

REFERENCES

1. "Design Calculations for ETS-1 Exhaust Duct", Volume III, Duct Loads and Stresses, Aetron, August 1964.

2. Tow, D., NES (ETS-1) Duct Final Loads and Stresses Profile, Unpublished Report, January 1965.

3. Bell, A. W. and Soot, H., Flexibility Matrix Program, Dynamic Science Corporation Report No. SN-51-5, July 20, 1964.

4. Brady, F. H., Graves, G. R., and Nissotti, R. M., NES (ETS-1) Duct Dynamics, Summary - Phase 4, Departments 150 and 301, Aerojet General Corporation, Azusa, 1964.

5. Bell, A. W. and Soot, H., Dynamic Response Program, Dynamic Science Corporation Report No. SN-51-6, July 30, 1964.

6. Brady, F. H., Graves, G. R., and Nissotti, R. M., NES (ETS-1) Duct Dynamics, Summary - Phase 7, Departments 150 and 260, Aerojet General Corporation, Azusa, 1964.

7. Breen, B. P., Gas Dynamics Forces on NES-1 Duct, Dynamic Science Corporation Report No. SN-51-10, October 23, 1964.

8. "NES (ETS-1) Duct Dynamic Analysis, Forced Response," Volumes I through IV, Aerojet General Corporation Computer Output, October 1964.

9. Brady, F. H. and Zukerman, A., Determination of the Forcing Function for the NES (ETS-1) Duct, Aerojet General Corporation, Azusa, March 1964.

10. "NES (ETS-1) Duct Dynamic Analysis, Forced Response, Aerojet Data," Volumes I through IV, Aerojet General Corporation Computer Output, December 1964.

11. Ball, R. E., Bell, A. W., Schjelderup, H. C., Soot, H., Torsional Vibration of ETS-1 Exhaust Duct, Dynamic Science Corporation Report No. SN35-2, December 22, 1964.

12. Bell, A. W., Schjelderup, H. C., Soot, H., In-Plane Vibration of NES-1 Truss, Dynamic Science Corporation Report No. SN35-1, December 22, 1964.

13. Discussion of Damping Coefficients Used During NES Duct Analysis, Dynamic Science Corporation Report No. SN-51-12, November 3, 1964.

14. "Design Calculations for ETS-1 Exhaust Duct", Volume I, Loads and Truss Design, Aetron, August 1964.